OPTICAL PROPERTIES AND STRUCTURE OF RARE EARTH CONTAINING GLASSES(Dissertation_全文)

AUTHOR(S):

Tanabe, Setsuhisa

OPTICAL PROPERTIES AND STRUCTURE OF RARE EARTH CONTAINING GLASSES

SETSUHISA TANABE

1992

OPTICAL PROPERTIES AND STRUCTURE OF RARE EARTH CONTAINING GLASSES

SETSUHISA TANABE

1992

CONTENTS

GENERAL INTRODUCTION

At the age of optoelectronics and for the next coming age of "photonics", we face an increasing demand for superior photonic materials to be used as a short wavelength laser, fiber amplifier, nonlinear optical glass and thin film waveguide, not simply as a conduit for transporting light but as active applications.

Glasses with new functions are now attracting a great interest in various fields. Some of them have already established their position as functional materials. The field for new glasses will be much wider especially with their transparency and other optical functions. In order to give glass some optical functions, some active components have to be added in glass. The rare earth elements, I believe, is one of the most promising key components in many new optical glasses.

From 1960's to now, a number of rare earth containing glasses have been used for applications as lasers [1], Faraday rotators[2] and optical lenses with high refractive index[3]. In these glasses, fluorescence, large effective magneton number, optical absorption and polarizability characteristics of rare earth ions are utilized.

In addition to these characteristics, rare earth elements will surely play the most important role in the photonic glasses, because of their laser oscillation capability. Fiber amplification for an efficient optical communication, and micro-waveguides used in photonic computers, and frequency upconversion of laser diode to shorter wavelength for optical data recording[4] are

some of the examples. If developed, a short wavelength laser offers a unique opportunity in a higher density in optical data storage. At present, infrared emitting laser from III-V semiconductors is being used in today's optical communications, laser printers and optical memories such as video and compact discs. In the case of optical readout memories, the storage bit density increases as the square of the spatial cut off frequency. Thus a significant technological advance is possible in the enhancement of optical readout density and printing speed if the wavelength of laser light can be altered from infrared to green or blue. A direct way to satisfy this requirement is to develop a new blue light emitting diode. However, it is difficult to achieve it at this moment. Thus an indirect way to convert infrared radiation from a current laser diode to shorter wavelength is being explored. Because of their laser oscillation capability, rare earth containing glasses are considered as a promising candidate material for this purpose.

In order to respond the state mentioned above, the characterization of optical properties of rare earth containing glasses should be done on the basis of structural viewpoints. In this respect, spectroscopic techniques capable of providing the local structure of rare earth element in glass are necessary. Mössbauer spectroscopy is one of the most powerful methods to obtain structural information[5]. Moreover, to interpret the quantum efficiency of active ions in glass, the knowledge of radiative and nonradiative properties of rare earth ions[6] is quite important, because these properties are the key to design a material with superior optical functions. For the realization of

superior and novel functions, the correlation between the optical or physical properties and the structures or composition of rare earth containing glasses has to be clarified. Without these kinds of studies, the concept of material design in the field of functional glasses would remain a posteriori.

In this thesis, I selected several important factors for the design of glass materials containing rare earths, which will make possible the development of the photonic technology in the coming age, and discussed the methodology of material design on the basis of some theories which have been strengthened by the experimental results.

In Chapter 1, general fundamental background for the theoretical research in the field is reviewed. The radiative and nonradiative relaxation of excited trivalent rare earth ions [6,7], which dominate the optical properties, such as excitation and fluorescence quantum efficiencies, are stressed. Also, the Mössbauer studies on rare earth elements are reviewed and especially, the characteristics of ^{151}Eu nucleus are pointed out [5,8].

In Chapter 2, the significant results of the ^{151}Eu Mössbauer spectroscopy[9] are shown. First, the relationship between the coordination number of trivalent europium ions in oxide crystals and the isomer shift, which is one of the most useful parameters in Mössbauer effect, is clarified. On this basis, this spectroscopy is applied to the aluminosilicate glasses, which were chosen because the basicity of glass can be changed by varying the composition. The dependence of the coordination number, which ranges from 6 to 12, on the oxide compositions is

presented and the possibility of the coordination control by the host basicity design is suggested. Also, the structure and lattice dynamic properties of rare earth aluminosilicate glasses are discussed, in which Ln^{3+} ions are found to exist as the network modifier of glass, and take a highly folded state. This group of glasses show high elastic moduli[10], and the effect of glass composition and structure on several properties are discussed[11,12].

In Chapter 3, the nonradiative decay characteristics of optically excited rare earth ions are discussed in terms of their local vibrational structure in glass. The effectiveness of phonon sideband measurements is shown with some examples. The measurements are applied to borate glasses[13,14] and fluorophosphate glasses[15]. It is shown that the local environment and vibrational properties are greatly varied with host compositions. The local glass structure surrounding rare earth ions, the energy of phonon modes coupled with the ions and also the electron-phonon coupling strength in the glass are clarified.

In Chapter 4, the proposed processes of frequency upconversion of rare earths are clarified, and upconversion phenomena of Er^{3+} ions in several glasses pumped by AlGaAs/GaAs semiconductor laser [16-18] are investigated. Mainly, the upconversion characteristics are discussed on the basis of host characters. Attention is centered on the correlation between the composition or structures of fluorophosphate glasses and the nonradiative decay rate of doped ions, which affect the lifetime of some excited levels and, of course, upconversion efficiencies[18]. The phonon sideband and Mössbauer spectroscopy succeeded in interpreting

the upconversion properties of rare earth ions on the basis of the local structure[15,18]. While most of the previous studies have been on fluoride hosts[19-21], efficient upconversion fluorescence phenomena are reported for the first time in Er^{3+} doped heavy metal oxide glasses due to their low phonon energies [16].

In Chapter 5, the analyses of upconversion mechanisms of Er^{3+}[22] and Tm^{3+}[23] ions in fluoride glasses are discussed. For the theoretical design of an efficient upconversion device with green, blue or UV radiation[24] with *LD*(laser diode) pumping, knowledge on the correlation between the controlling mechanisms and several conditions for glass becomes necessary. Characteristics of two representative mechanisms are discussed; the energy transfer and excited state absorption. The methodology for the analysis of mechanism is presented using the tunable dye laser.

REFERENCES AND PUBLICATIONS OF RELATED ARTICLES

[1] E. Snitzer, *Am. Ceram. Soc. Bull.* **52**(6), (1973) 516-525.

[2] S.G. Berger, C.B. Rubinstein, C.R. Kurkjian and A.W. Treptow, *Phys. Rev.* **133**(3A), (1964) A723-27.

[3] W. Geffcken, *Glastech. Ber.* **34**, (1961) 91-101.

[4] N. Soga and S. Tanabe, *Chemistry* **45**(11), (1990) 804-05.

[5] G.J. Perlow, in *"Chemical Application of Mössbauer Spectroscopy,"* (ed. Gol'danski and Herber, Academic Press, NY, 1968) pp.400-426.

[6] R.D. Peacock, in *"Structure and Bonding,* vol.22," (ed. J.D.Dunitz, Springer-Verlag, Berlin, 1975) pp.83-122.

[7] C.B. Layne, W.H. Lowdermilk and M.J. Weber, *Phys. Rev. B* **16**(1), (1977) 10-20.

[8] M.P. Barton and N.N. Greeenwood, in *"Mössbauer Effect Data Index,"* (ed. J.D. Stevens and V.E. Stevens, Plenum, NY, 1973) pp.395-446.

[9] S. Tanabe, K. Hirao and N. Soga, *J. Non-Cryst. Solids* **113**, (1989)

178-184.

[10] A. Makishima, Y. Tamura and T. Sakaino, *J. Am. Ceram. Soc.* **61**(5-6), (1978) 247-49.

[11] S. Tanabe, N. Soga, K. Hirao and T. Hanada, *J. Am. Ceram. Soc.* **73**(6), (1990) 1733-36.

[12] S. Tanabe, K. Hirao and N. Soga, *J. Am. Ceram. Soc.* **75**(3), (1992) 503-06.

[13] S. Tanabe, S. Todoroki, K. Hirao and N. Soga, *J. Non-Cryst. Solids* **122**, (1990) 59-65.

[14] S. Tanabe, K. Hirao, N. Soga and T. Hanada, *J. Solid State Chem.* **97**, (1992) 481-486.

[15] S. Tanabe, K. Hirao and N. Soga, *J. Non-Cryst. Solids* **142** (1992) 148-154.

[16] S. Tanabe, K. Hirao and N. Soga, *J. Non-Cryst. Solids* **122** (1990) 79-82.

[17] S. Tanabe and K. Hirao, *Bull. Ceram. Soc. Jpn.* **26**(2), (1991) 144-48.

[18] S. Tanabe, S. Yoshii, K. Hirao and N. Soga, *Phys. Rev. B* **45**(9), (1992) 4620-25.

[19] S.A. Pollack, D.B. Chang and N.L. Moise, *J. Appl. Phys.* **60**(12), (1986) 4077-86.

[20] J.P. van der Ziel, L.G. Van Uitert, W.H. Grodkiewicz and R.M. Mikulyak, *J. Appl. Phys.* **60**(12), (1986) 4262-67.

[21] D.C. Yeh, W.A. Sibley, M. Suscavage and M.G. Drexhage, *J. Appl. Phys.* **62**(1), (1987) 266-275.

[22] S. Tanabe, S. Yoshii, K. Hirao and N. Soga, *"Science and Technology of New Glasses,"* (ed. S. Sakka and N. Soga, Ceram.Soc.Jpn., 1991) pp.193-98.

[23] S. Tanabe, K. Tamai, K. Hirao and N. Soga, *Phys. Rev. B* **47**, in press.

[24] K. Hirao, S. Tanabe, S. Kishimoto, K. Tamai and N. Soga, *J. Non-Cryst. Solids* 135, (1991) 90-93.

Chapter 1.

BACKGROUND FOR RARE EARTH RESEARCH

1.1. THEORY OF RADIATIVE AND NONRADIATIVE TRANSITIONS OF TRIVALENT RARE EARTH IONS

I. Radiative Transition

Electronic transitions between $4f^n$ levels used for optical pumping and emission are predominantly of electric-dipole nature. The f-f transitions are forbidden by Laporte's rule, however, when the rare earth ion is located in a site with no centrosymmetry, the odd-order terms in the expansion of the static (or dynamic) crystal-field admix the states with higher, opposite-parity configurations, such as $4f^{n-1}5d$, into a f^n and thus the transitions become allowed. Although *ab initio* calculations of the probabilities for electric-dipole transitions are not possible, spectral intensities can be treated using the Judd-Ofelt approach[1,2], which is discussed later.

Electric-dipole transitions between states of 4f and 5d configurations are parity-allowed. The oscillator strength for f-d transitions are therefore much larger than for f-f transitions. The emission from 5d states, while it is not common, has been observed for several rare earths, such as Ce^{3+} and Eu^{2+}, for which there is a large energy gap to lower-lying 4f states[3]. To calculate the probability for 5d $\rightarrow$ 4f radiative decay by electric-dipole transitions, eigenstates and interconfigurational radial integrals are required[4].

Magnetic-dipole and electric-quadrupole transitions are allowed between states of $4f^n$ configurations and can be calculated straightforwardly, given appropriate eigenstates. Since magnetic-dipole transitions are subject to the selection rules of $|\Delta J| \leq 1$ and $\Delta S = \Delta L = 0$, they are usually only significant for intramultiplet transitions. Electric-quadrupole transitions are much less probable than dipolar processes and have not been observed for rare earth ions.

II. Judd-Ofelt Treatment

Judd[1] and Ofelt[2] have shown that calculations of f-f intensities in rare earth spectra can be made tractable by treating the excited configuration as completely degenerate. The electric-dipole line strength can then be expressed as a sum of products of "phenomenological" intensity parameters Ω_t and matrix elements of tensor operators $U^{(t)}$ connecting states of $4f^n$. The Judd-Ofelt approach is applicable to transitions between Stark levels. For transitions between J manifolds, the line strength S has the simple form,

$$S(aJ,bJ') = \sum_{t=2,4,6} \Omega_t \langle f^n aJ||U^{(t)}||f^n b'J'\rangle^2. \qquad (1)$$

The Ω_t parameters for a given ion-host combination are derived from a least squares fit of observed intensities. The validity of the Judd-Ofelt treatment has been tested for most trivalent rare earths in both crystals and solutions[5].

An attractive feature of the Judd-Ofelt approach is that once the intensity parameters are determined, they can be used to calculate the probability of transitions between any $4f^n$ levels

of interest, such as for laser action. This includes absorption and fluorescence intensities, excited state absorption, radiative lifetimes and branching ratios, and also, combined with fluorescence spectra, stimulated emission cross sections[6].

Since the Judd-Ofelt parameters are not expected to differ greatly for adjacent ions in the lanthanide series, estimate can be made using extrapolated Ω_t values[5]. This technique can provide a successful and consistent method of spectral intensities of rare earth f-f transitions in both crystals and glasses. The method predicts cross section from measurements made on even small samples.

Coefficients Ω_2, Ω_4, Ω_6 in eq.(1) involve: (a) odd harmonics in the expansion of the local crystal field, which admix opposite-parity states into the $4f^n$ configuration, thereby allowing electric-dipole transitions: (b) the energy separations of states of $4f^n$ and opposite parity configurations: (c) the interconfigurational radial integrals. These properties depend on the local environment, and large site-to-site variations in the Ω_t values may be possible in glass.

The doubly reduced matrix elements of the unit tensor operator $U^{(t)}$ are calculated in an intermediate coupling approximation. Their values for some of the Er^{3+} absorption and emission transitions are given in Table 1 [7]. The line strength in eq.(1) is related to the integrated absorbance of an electric-dipole transition by,

$$\int_{\text{band}} k(\lambda)d\lambda = \frac{8\pi^3 e^3 \bar{\lambda}\, \rho}{3hc(2J+1)n^2}\, \chi \quad S(aJ,bJ'), \qquad (2)$$

where $k(\lambda)$ is the absorption coefficient, $\bar{\lambda}$ is the mean wave-

length of the absorption band, ρ is the concentration of the rare earth ion, and the χ-terms correct the effective field at a well localized center in a medium of isotropic refractive index n and are given by $\chi_{ed}=n(n^2+2)^2/9$ for electric dipole transitions and $\chi_{md}=n^3$ for magnetic dipole transitions.

Table 1. Reduced Matrix Elements of $U^{(t)}$ for Er^{3+} ion[7]. Typical mean wavelengths $\bar{\lambda}$ are included.

[SL]J	[S'L']J'	$[U^{(2)}]^2$	$[U^{(4)}]^2$	$[U^{(6)}]^2$	$\bar{\lambda}$ (μm)
$^4I_{15/2}$	$^4I_{13/2}$ *	0.0188	0.1176	1.4617	1.50
	$^4I_{11/2}$	0.0259	0.0001	0.3994	0.98
	$^4I_{9/2}$	0.0	0.1452	0.0064	0.80
	$^4F_{9/2}$	0.0	0.5655	0.4651	0.65
	$^4S_{3/2}$	0.0	0.0	0.2285	0.54
	$^2H_{11/2}$	0.7056	0.4109	0.0870	0.52
	$^4F_{7/2}$	0.0	0.1467	0.6273	0.48
	$^4F_{5/2}$	0.0	0.0	0.2237	0.45
	$^4F_{3/2}$	0.0	0.0	0.1204	0.44
	$^2H_{9/2}$	0.0	0.078	0.17	0.41
	$^4G_{11/2}$	0.9178	0.5271	0.1197	0.38

* including magnetic dipole contribution.

From the intensity parameters obtained, the spontaneous emission probability between any initial manifold $|(S',L')J'\rangle$ and final manifold $|(\bar{S},\bar{L})\bar{J}\rangle$ is calculated by[6]

$$A[(S'L')J';(\bar{S}\bar{L})\bar{J}] = \frac{64\pi^2e^2}{3h(2J+1)}\,\chi\,S_{J'\bar{J}}. \qquad (3)$$

The induced absorption (or emission) probability, B is related to the spontaneous emission probability and is given by[8]

$$A \quad \frac{8\pi h\nu^3}{c^2} B, \tag{4}$$

where $h\nu$ is the energy separation between the states. Accordingly, the induced-emission cross section σ_p for this transition is calculated by[6]

$$\sigma_p(\lambda_p) = \frac{\lambda_p^4}{8\pi c n^2 \Delta\lambda_{eff}} A, \tag{5}$$

where λ_p is the peak fluorescence wavelength of the emission band and $\Delta\lambda_{eff}$ is the effective fluorescence linewidth, which is given as the integrated fluorescence intensity by dividing with the intensity at λ_p.

III. Nonradiative Transitions

Nonradiative transitions due to ion-phonon and ion-ion interactions affect the efficiency and performance of rare earth lasers and upconvertors, since the radiative quantum efficiency η is given with radiative and nonradiative rate by,

$$\eta = \Sigma A / (\Sigma A + W_{NR}) = \tau_f / \tau_R. \tag{6}.$$

Relaxation by phonon processes arises from the interaction of the rare earth ion with the fluctuating ligand field. In these processes, the electronic energy of the excited rare earth is transferred to vibrational energy of the host lattice[9]. Multiphonon decay rates from excited states of rare earth ions determine important properties of rare earth lasers, such as pump conversion efficiency, radiative quantum efficiency, and the lifetime of the terminal laser level. For transitions between 4f

levels, the ion-phonon interaction is characteristic of weak-coupling. Nonradiative relaxation between Stark levels, which are separated by tens to hundreds of cm^{-1}, occurs by one- or two-phonon processes and can be very fast, $\geq 10^{12} sec^{-1}$. Nonradiative relaxation between J states, which may be separated by several thousands of cm^{-1}, requires the simultaneous emission of multiple phonons to conserve energy and hence proceeds at much slower rates.

IV. Multiphonon Processes

Although several treatments for multiphonon relaxation processes for rare earth ions have been developed[10-12], calculations of rates are formidable and require information about crystal-field interactions and phonon dynamics, which are generally not available. Studies on multiphonon emission from rare earth in several different hosts have shown that the most important factor influencing the multiphonon emission rate is the energy gap to the next-lower level[13]. In these high-order processes, the detailed properties of the individual electronic states and phonon modes involved are often averaged out.

The rate of multiphonon emission for rare earths in solids is found to exhibit an approximate exponential dependence on the energy gap ΔE to the next-lower level of the form,

$$W_p = W_p(0) \exp(-\alpha \Delta E/\hbar\omega) \qquad (7).$$

The constants $W_p(0)$ and α are dependent on the host and strength of the ion-lattice coupling but not on the specific rare earth ion or electronic state. Data for the multiphonon relaxation in

several different crystals are summarized in Fig.1[13]. Experimental points correspond to different electronic states and ions. In general, the major contribution to multiphonon processes involves the highest energy vibrations, since they can conserve the energy gap in the lowest-order process[14]. For a given ΔE in Fig.1, the rates are higher as the effective phonon energy increases. The rates shown for spontaneous phonon emission; at higher temperatures, stimulated emission becomes important and rates $W_p(T)$ become faster.

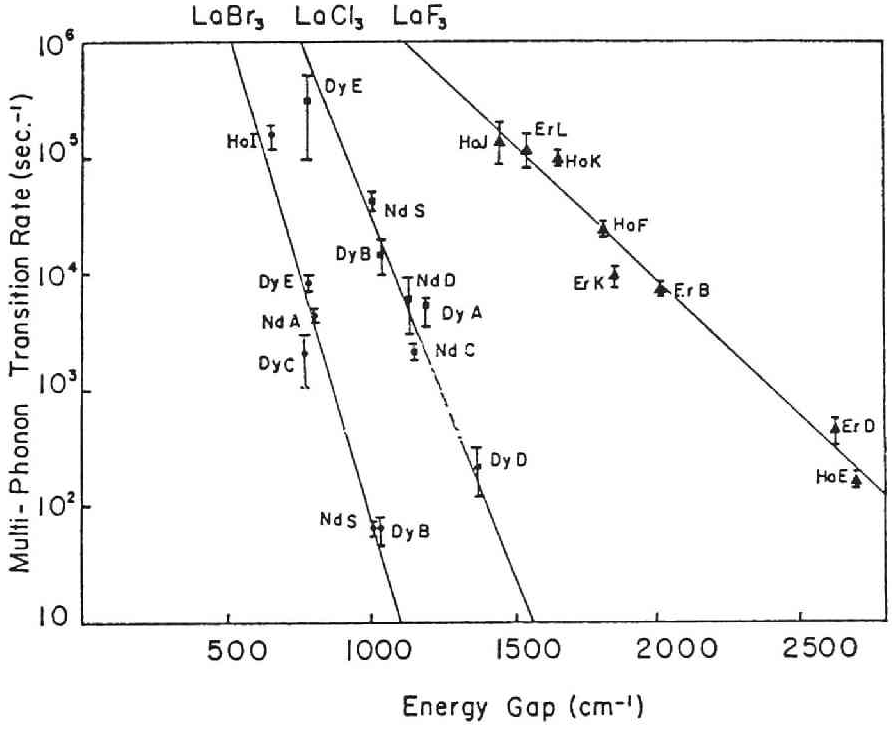

Fig.1. Multiphonon emission rates of trivalent rare earth ion energy levels in LaF_3, $LaCl_3$ and $LaBr_3$ vs. the gap to the next lower level[13].

The multiphonon emission rates for the silicate glass are much faster than for most crystals. Studies of rare earths in glass demonstrate that multiphonon relaxation is due predominantly to vibrational mode with the highest frequency which are associated with the glass network former. In both crystalline and amorphous rare earth hosts, materials having low vibrational frequencies generally have more fluorescing levels and hence more possibilities of laser action, as expected from the τ_f dependence of the quantum efficiency in eq.(6).

V. Ion-Ion Interaction

Nonradiative energy transfer between like and unlike paramagnetic ions occurs at concentrations where the ion separations become small($\leq$1~2nm) and interaction via electric multipolar or exchange forces are possible. Depending upon the ions and transitions involved, this may lead to energy migration, fluorescence quenching, and fluorescence sensitization. All of these processes are observed for rare earth ions in solids. The relative importance of the different multipolar terms, dipole-dipole, dipole-quadrupole, quadrupole-quadrupole varies with concentration due to their different range dependence. These processes are treated by Dexter[15]. Exchange coupling and the analysis of the time-dependence of ion-ion energy transfer are treated by Inokuti and Hirayama[16]. Energy transfer phenomena related to rare earth have been reviewed by Kushida[17] and Watts[18]. The rate of self-quenching for a given rare earth ion density is dependent upon the oscillator strengths and spectral match of the

two transition. If transitions are sufficiently nonresonant, self quenching is reduced. However, the energy transfer is possible even though the energy difference between pairs of transitions become large. The rate of phonon-assisted energy transfer exhibits an approximately exponential dependence on energy mismatch[11], similar to that found for multiphonon emission.

1.2. MÖSSBAUER EFFECT IN RARE EARTH ELEMENT

I. Mössbauer studies on rare earths

The Mössbauer effect has proved to be one of the most valuable tool for studying some aspects of the physics, chemistry, and magnetism of solids. Practically, every rare earth element has at least one isotope in which γ-ray transitions occur with appreciable recoil-free efficiencies, and thus suitable sources are available for Mössbauer experiments. This is a consequence of the prevalence of low-lying nuclear states near the nuclear ground state in the region of strongly deformed nuclei. In some cases, more than one transition is available in the same isotope such as ^{153}Eu. This, in some cases, permits the systematic investigation of properties throughout rare earth family of elements[19]. On the other hand, rare earth ions in solids display a variety of interesting and fundamental properties. This is also true for the chemical environment and optical properties of rare earth in amorphous solids, and measurement for these solids can throw much light on these properties, and yield information on the local structure in amorphous state which cannot be obtained in other ways.

Isomer shifts have been observed in rare earth recoil-free spectra. Particularly, large isomer shifts have been observed in europium compounds, for nuclear transitions in ^{151}Eu and ^{153}Eu. Interpretations of these shifts in terms of changes in the density of *s* wave function at nucleus have been made. The subject is

of great interest but is not yet thoroughly understood.

II. Europium

Europium has two naturally occurring isotopes, ^{151}Eu(47.82%) and ^{153}Eu (52.18%) and both can be used for Mössbauer spectroscopy. The former has one transition (21.64keV) and the latter three (83.37, 97.43 and 103.18keV)[20]. Over the past years, a lot of papers have appeared on the subject for some compounds, making europium the third most extensively studied element after iron and tin. Chemists have concentrated on the 21.6keV transition which has a reasonable natural linewidth of 1.30 mm/s and is by far the easiest of the four transitions to use. The application of Mössbauer effect in europium and other elements to problems in chemistry and solid state physics has been discussed[20] and comparison between lanthanide compounds studied by Mössbauer technique has been made[21].

The two oxidation states of europium are characterized by entirely different isomer shifts (EuF_3 taken as zero): Eu(II) -12 ± 2mm/sec and Eu(III) 0 ± 1mm/sec. Metallic alloys and band systems have shifts in the range -7 to -11mm/sec. Such a massive change of isomer shift with oxidation state can be a consequence of the shielding effect of the 4f electrons. However, the range within each oxidation state is small and this has been making it difficult to distinguish chemically or crystallographically distinct europium sites within any one oxidation state.

The 21.64keV resonance is a nuclear 7/2->5/2 magnetic dipole transition and this implies an eight-line quadrupole

pattern. However, because of the electronic configuration, only the lattice contribution to the electric field gradient is present and this, coupled with the moderately large natural linewidth of the resonance, generally results in an unresolved single-line spectrum. Occasionally the lattice contribution can be sufficient to partially resolve the peak, thereby generating an asymmetric pseudo doublet[22].

A. *Sources*

The decay scheme of ^{151}Sm nuclei which is most used as a ^{151}Eu-Mössbauer source is shown in Fig.1. along with that of ^{151}Gd[20]. The β^- emission from ^{151}Sm leads to the 21.6keV excited level of ^{151}Eu, the nuclear spin of which is 7/2. Although ^{151}Gd source can be used, the ^{151}Sm source is commonly used because of its easiness in preparation by proton bombardment, long half-life of 87 years, and simpleness of the γ-ray spectra[20]. The only desired γ-ray can be obtained with a large recoil-free fraction.

B. *Isomer shift*

For many Mössbauer active elements, the isomer shift is a valuable parameter to study the state of atoms in question. It is a measure of the electron density at the nucleus, which is affected by the valence and electronic state of the element as well as the electronegativity and the coordinating number of neighboring ligands. The isomer shift is defined as the difference in the monopolar interaction of the Z*th* nucleus between the absorber and the source, expressed by the next equation,

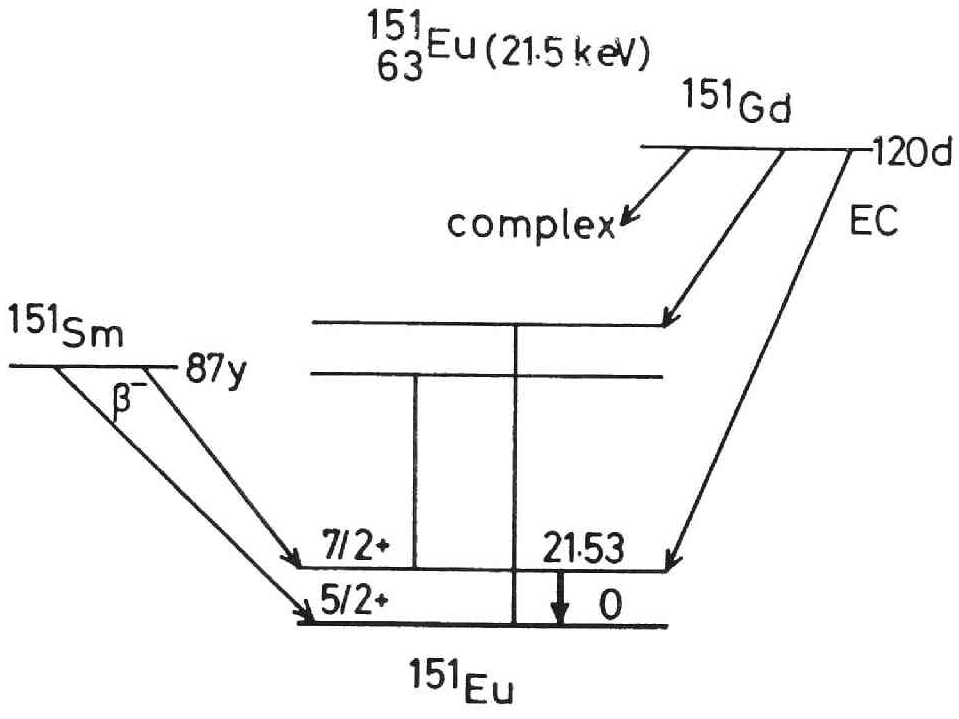

Fig.1. Decay scheme of ^{151}Sm and ^{151}Gd nuclei[22].

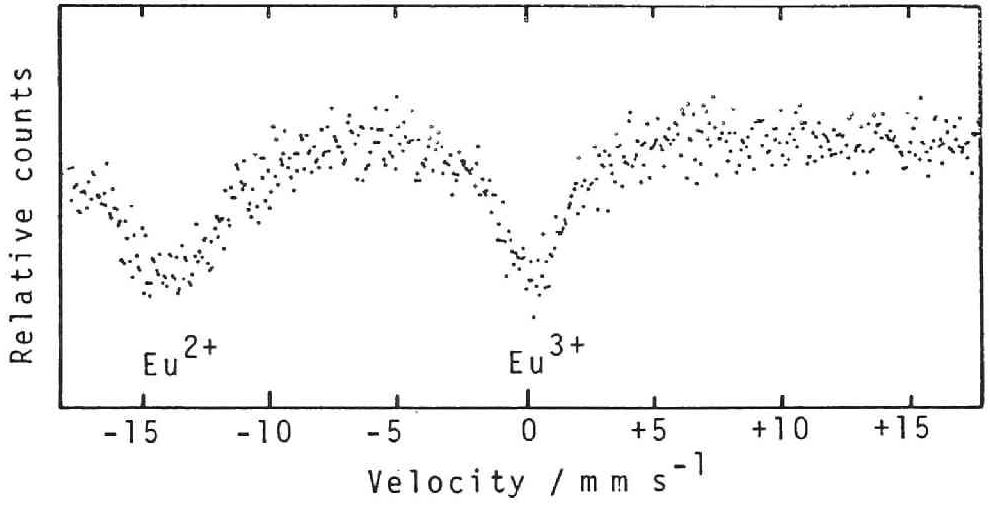

Fig.2. ^{151}Eu Mössbauer spectrum of $EuCl_2$ and $EuCl_3$.

$$IS=C(E_a-E_s)/E_\gamma=(2/5)\pi Ze^2(R_e^2-R_g^2)\{|\Psi a(0)|^2-|\Psi s(0)|^2\}. \quad (1)$$

This energy difference depends both on the difference in the electron densities at the nucleus, $|\Psi(0)|^2$ of the source and the absorber and on that in the nuclear radii, R of the excited and ground states. In the case of ^{151}Eu, R_e is larger than R_g, contrary to those of ^{57}Fe nucleus. Thus the larger the electron density of the s-orbital is, the larger the IS of ^{151}Eu becomes. The smaller IS of Eu^{2+} can be explained by the shielding effect of the $4f^7$ electrons on the s-orbitals, whereas Eu^{3+} ion has $4f^6$ configuration. Typical spectra of $EuCl_2$ and $EuCl_3$ mixture are shown in Fig.2. The difference in isomer shift between divalent and trivalent europium ions is generally more than 10 mm/sec. Increased covalency in the compounds having $4f^6$ or $4f^7$ state is considered to lead to a small increase of 6s electron density, which results in an increase of the isomer shift. This behavior has been already reported in halide compounds[23], where IS decreased with an increase of electronegativity of anion, i.e., with an increase of ionicity of Eu-X bond.

C. Quadrupole Splitting

The energy level scheme for the nuclei, the spin of which are 5/2 and 7/2 in the ground and excited state, respectively, under quadrupole interaction is expressed by the following equation.

$$Eq=e^2qQ/4I(2I-1)\ [3m_I^2-I(I+1)](1+\eta^2/3). \quad (2)$$

Assuming asymmetric parameter η to be zero, the peak shift can be calculated by the following equation,

$$\Delta E(m_{Ig},m_{Ie})=e^2qQ_e/4I_e(2I_e-1)[3m_{Ie}^2-I_e(I_e+1)-e^2qQ_g/4I_g(2I_g-1)[3m_{Ig}^2-I_g(I_g+1)]$$
$$=e^2qQ_g\{R_q[3m_{Ie}^2-I_e(I_e+1)]/4I_e(2I_e-1)-[3m_{Ig}^2-I_g(I_g+1)]/4I_g(2I_g-1)\}, \quad (3)$$

where I_g and I_e are the nuclear spin of the ground and excited states, m_I is the magnetic quantum number of each nuclear spin state, Q is the nuclear quadrupole moment which becomes non-zero for a spin larger than unity and eq is the electric field gradient at the nucleus. For the nuclei having the same spin numbers in the excited state and ground states such as ^{151}Eu and ^{127}I, the order of the peak position of each transition depends only on the ratio of the quadrupole moment Q_e/Q_g, expressed as R_q in Eq.(3). For ^{151}Eu, R_q is 1.3[24], whereas R_q is 0.896 for ^{127}I[19]. the schematic diagram of the R_q dependence of line positions is shown in Fig.3[19] and the relative positions calculated by Eq.(2) for ^{151}Eu are listed in Table 1. This order of positions of all transitions from the ground state (I_g=5/2) to the excited state (I_e=7/2) will not change under a positive electric field gradient, eq and become inverse under a negative eq. There appear eight lines due to non-zero eq and nuclear spin of each state. By calculating the center of gravity of these lines,

$\Sigma(\Delta E_i I_i)/\Sigma I_i$, where I_i is the intensity of the i*th* peak, it was found never to change, independent of the electric field gradient. So this gravity center of quadrupole peaks will correspond to their isomer shift. It is not strange that maximum position of superposed peaks usually deviates from their real isomer shift due to an asymmetric shape, which was already pointed out by Goodman et al.[7]. Thus it takes a special care to determine the

isomer shift of ^{151}Eu. It is better to adopt a least square fitting method rather than simply to check an apparent peak position.

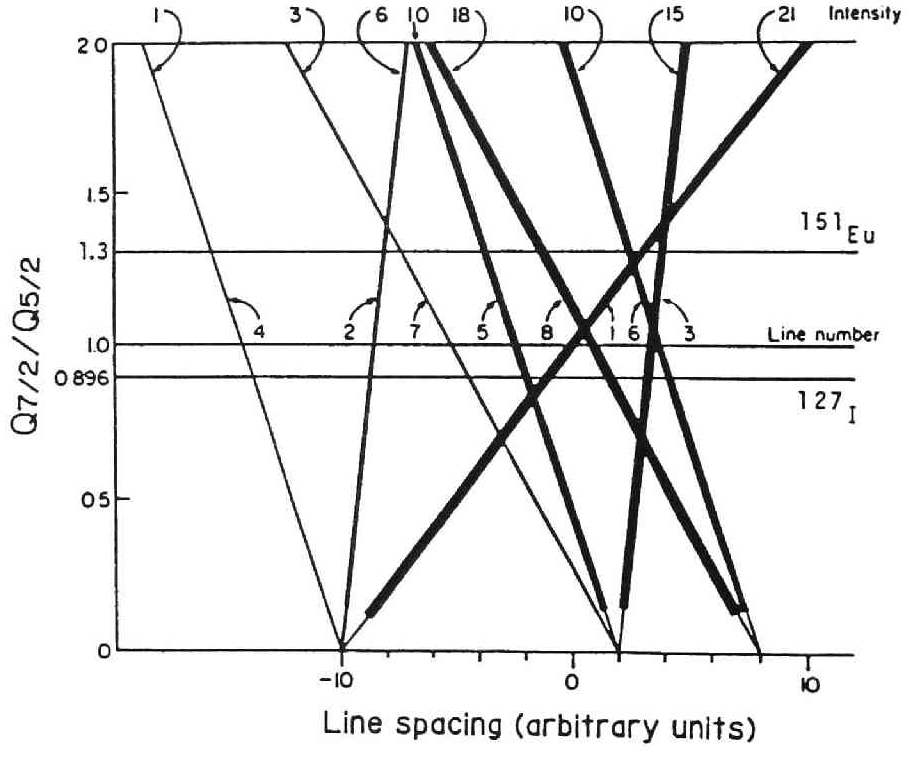

Fig.3. Plots showing the relative line positions in the ^{151}Eu Mössbauer spectrum as a function of $R_q=Q_{7/2}/Q_{5/2}$. The sign of e^2qQg is positive.

Table 1: Positions and intensities of all the peaks under quadrupole interaction.

No.	Transition $m_{Ig} \rightarrow m_{Ie}$	$\Delta Eq/e^2qQ_g$	Intensity	$\Delta EqxI$	Peak position/e^2qQ_g for Rq=1.3
1	$\pm 5/2 \rightarrow \pm 7/2$	(R-1)/4	21	21R/4-21/4	2:+0.075
2	$\pm 5/2 \rightarrow \pm 5/2$	-(R+7)/28	6	3R/14-3/2	7:-0.204
3	$\pm 3/2 \rightarrow \pm 5/2$	(5R+7)/140	15	15R/28+3/4	1:+0.096
4	$\pm 5/2 \rightarrow \pm 3/2$	-(3R+7)/28	1	-3R/28-1/4	8:-0.389
5	$\pm 3/2 \rightarrow \pm 3/2$	-(15R-7)/140	10	-15R/14+1/2	5:-0.089
6	$\pm 1/2 \rightarrow \pm 3/2$	(-15R+28)/140	10	-15R/14+2	3:+0.061
7	$\pm 3/2 \rightarrow \pm 1/2$	-(25R-7)/140	3	-15R/28+3/20	6:-0.182
8	$\pm 1/2 \rightarrow \pm 1/2$	-(25R-28)/140	18	-45R/14+18/5	4:-0.032

REFERENCES

[1] B.R. Judd, *Phys. Rev.* **127**, (1962) 750-761.

[2] G.S. Ofelt, *J. Chem. Phys.* **37**, (1962) 511-520.

[3] M.J. Weber, Solid State Commun. 12, (1973) 741-44.

[4] W.J. Manthey, Phys. Rev. B 8, (1973) 4086-98.

[5] R.D. Peacock, *"Structure and Bonding,* vol.22", (ed. J.D. Dunitz, Springer-Verlag, Berlin, 1975) pp.83-122.

[6] W.F. Krupke., *IEEE J. Quant. Electron.* **QE-10**, (1974) 450-57.

[7] M.J. Weber, *Phys. Rev.* **157**, (1967) 262-272.

[8] W.B. Fowler and D.L. Dexter, *Phys. Rev.* **128**, (1962) 2154-165.

[9] R. Orbach, in *"Optical Properties of Ions in Solids"*, (ed. B. DiBartolo, Plenum, NY, 1975) pp.355-400.

[10] L.A. Reisberg and H.W. Moos, *Phys. Rev.* **174**, (1968) 429-438.

[11] T. Miyakawa and D.L. Dexter, *Phys. Rev. B* **1**, (1970) 2961-69.

[12] F.K. Fong, S.L. Naberhuis and M.M. Miller, *J. Chem. Phys.* **56**, (1972) 4020-27.

[13] H.W. Moos, *J. Luminesc.* **1**, (1970) 106-121.

[14] C.B. Layne, W.H. Lowdermilk and M.J. Weber, *Phys. Rev. B* **16**, (1977) 10-20.

[15] D.L. Dexter, *J. Chem. Phys.* **21**, (1953) 836-850.

[16] M. Inokuti and F. Hirayama, *J. Chem. Phys.* **43**, (1965) 1978-1989.

[17] T. Kushida, *J. Phys. Soc. Jpn.* **34**, (1973) 1318-1333.

[18] R.K. Watts, in *"Optical Properties of Ions in Solids,"* (ed. B. DiBartolo, Plenum, NY, 1975) pp.307-336.

[19] C.M.P. Barton and N.N. Greenwood, in *"Mössbauer Effect Data Index"*, (ed. J.D. Stevens & V.E. Stevens, Plenum, NY, 1973) pp.395-446.

[20] G.J. Perlow, in *"Chemical Application of Mössbauer Spectroscopy"*, (ed. Goldanski and Herber, Academic Press, NY, 1968) pp.400-426.

[21] S. Ofer, I. Nowik and S.G. Cohen, in *ibid.*, pp.427-503.

[22] G.W. Dulaney and A.F. Clifford, in *"Mössbauer Effect Methodology,* vol.5", (ed. I.J. Gruverman, Plenum Press, NY, 1969) pp.65-76.

[23] G. Gerth, P. Kienle and K. Luchner, *Phys.Lett.* **27A**, (1968) 557-58.

[24] G.M. Kalvius, G.K. Shenoy, G.J. Ehnholm, T.E. Katila, O.V. Lounasmaa and P. Reibali, *Phys. Rev.* **187**, (1969) 1503-05.

[25] B.A. Goodman, N.N. Greenwood and G.E. Turner, *Chem. Phys. Lett.* **5**, (1970) 181-82.

Chapter 2.

STRUCTURE OF RARE EARTH CONTAINING OXIDES

2.1. COORDINATION NUMBER OF Eu^{3+} IN OXIDE CRYSTALS AND GLASSES BY MÖSSBAUER SPECTROSCOPY

I. INTRODUCTION

The Mössbauer effect, i.e., the recoil-free γ-ray resonant absorption in solids, has been recognized as a powerful tool to investigate the bonding character of the specific nuclei in various solids. Specifically, ^{151}Eu nucleus is one of the most suitable one among rare earth elements for this purpose because of its large recoil-free fraction, relatively sharp linewidth and long decay time of ^{151}Sm source (84 years). In the lanthanide series, Eu^{3+} ion is placed in the intermediate between light and heavy rare earths by its ionic radius and it is known to take a wide variety of coordination numbers from 6 to 12 in oxide crystals. Thus it is very interesting to investigate the coordination states of Eu^{3+} ion in various crystals and glasses also in terms of the design of a characteristic phosphor or laser. However, few Mössbauer studies have been reported for the Eu-containing glasses[1,2] in contrast to a large number of studies on ^{57}Fe-containing glasses[3-7]. In the present study, measurements were carried out at first for several mixed oxide crystals in which the coordination number of Eu^{3+} is known. Then aluminosilicate glasses containing a large amount of Eu_2O_3 were prepared and the Mössbauer parameters were determined in order to get

information about the local structure of europium ions in these glasses. Furthermore, an attempt was made to analyze the unresolved quadrupole interaction by the fitting program and the validity of the uniqueness of the solution was discussed.

II. EXPERIMENTAL

A. *Preparation of Crystals and Glasses*

Mixed oxide crystals, $Eu_3Ga_5O_{12}$ garnet, $EuBa_2Cu_3O_{7-y}$ layered perovskite, $EuAl_3(BO_3)_4$ huntite and $EuAlO_3$ perovskite were prepared by the conventional solids state reaction using reagent grade Eu_2O_3(C-type), Ga_2O_3, $BaCO_3$, CuO, Al_2O_3 and B_2O_3. They were confirmed to be single phase by X-ray diffraction with Cu $K\alpha$ line.

Glass samples were prepared by using Eu_2O_3, SiO_2 and Al_2O_3 powders. The compositions were $50SiO_2$ $(50-x)Al_2O_3 \cdot xEu_2O_3$ (x= 10, 15, 18.75, 20, 25, 30, 35, 40), $(100-x)SiO_2 \cdot xEu_2O_3$ (x = 20, 33.3, 60), $20Eu_2O_3 \cdot 80Al_2O_3$ and $30SiO_2 \cdot 20Al_2O_3 \cdot 50Eu_2O_3$. A well mixed batch was pressed and sintered at 1200°C and the sintered specimen was melted at the focus point of a bifocal gold mirror of a xenon lamp image furnace. The melt was quenched with a twin roller rotating at a rate of about 1000 rpm. The glass formation was confirmed with a polarizing microscope or XRD. The amorphous thin film obtained was ground into powder for the ^{151}Eu Mössbauer measurement.

B. *Mössbauer Effect Measurement*

^{151}Eu-Mössbauer measurement was made at room temperature by using $^{151}Sm_2O_3$ (5mCi) as a 21.6keV γ-ray source. The velocity calibration was done with the magnetic hyperfine spectrum of α-Fe by use of the 14.4keV γ-ray of ^{57}Co(Rh). The isomer shift was calculated with respect to EuF_3. The center of gravity and line width at half maximum of the peak were determined by utilizing a non-linear least-square fitting program of Lorentzian curves.

Measurements were done for C-type Eu_2O_3 (CN=6), $Eu_3Ga_5O_{12}$ garnet (CN=8), superconducting $EuBa_2Cu_3O_{7-\delta}$ (CN=8), $EuAl_3(BO_3)_4$ huntite (CN=9) and $EuAlO_3$ perovskite(CN=12) crystals as well as all the glasses prepared.

Table 1. Crystal compositions, systems and coordination numbers of Eu^{3+}.

Crystal	System	Coordination Number of Eu^{3+}
C-Eu_2O_3	Cubic	6
$Eu_3Ga_5O_{12}$	Cubic	8
$EuBa_2Cu_3O_{7-\delta}$	Orthorhombic	8
$EuAl_3(BO_3)_4$	hexagonal	9
$EuAlO_3$	Orthorhombic	12

III. RESULTS

The Mössbauer spectra of EuF_3, Eu_2O_3, $Eu_3Ga_5O_{12}$, $EuAlO_3$ crys-

tals, $50SiO_2 \cdot 25Al_2O_3$ $25Eu_2O_3$ glass and $EuCl_2$ are shown in Fig.1. No peak due to divalent Eu^{2+} ions was observed in the spectra of the glasses.

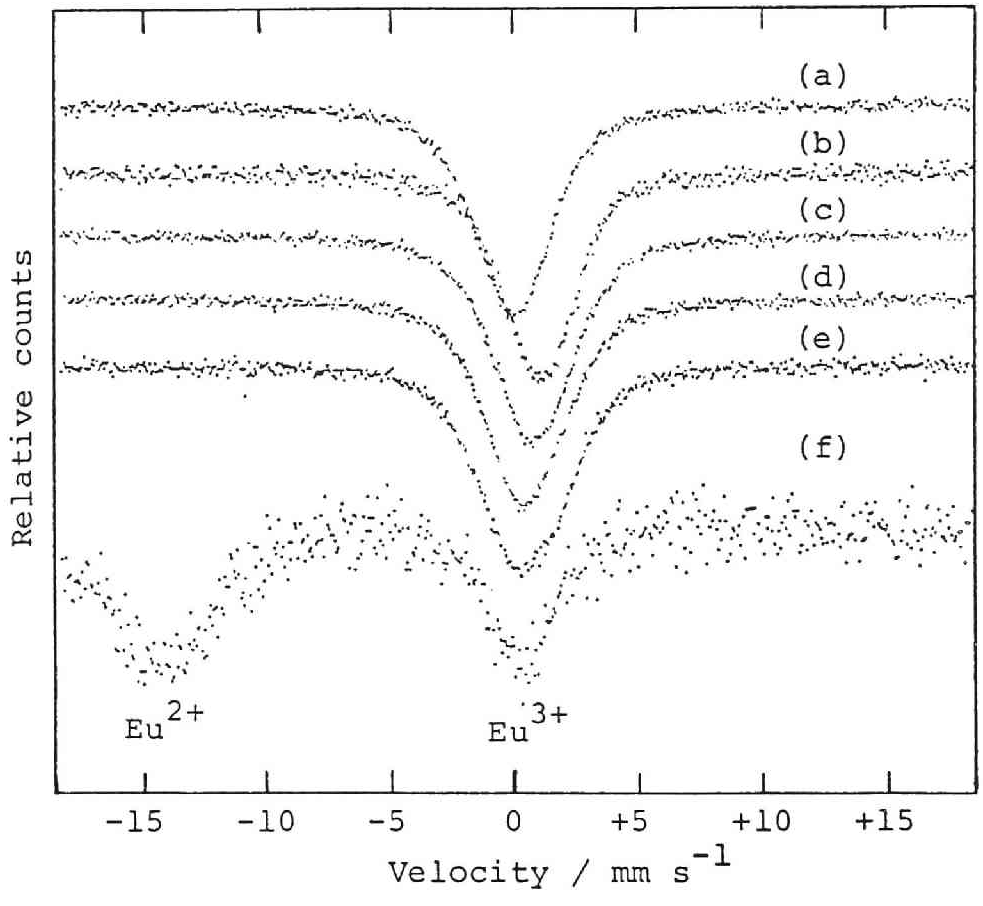

Fig.1. Mössbauer spectra of (a)EuF_3, (b)C-Eu_2O_3, (c)$Eu_3Ga_5O_{12}$, (d)$EuAlO_3$, (e)$50SiO_2 \cdot 25Al_2O_3 \cdot 25Eu_2O_3$ glass and (f)$EuCl_2$.

The isomer shift *IS* of $^{151}Eu^{3+}$ was found to decrease with an increase of the coordination number of Eu^{3+} ion in oxide crystals. The *IS* changed from 1.07 mm/sec for C-Eu_2O_3, where the CN of Eu^{3+} is 6, to 0.52 mm/sec for $EuAlO_3$ perovskite, where the CN of Eu^{3+} is 12. In the spectrum of the glass, the shoulder observed in the higher velocity side is due to the quadrupole interaction of the distorted ligand field of Eu^{3+} ions in a random network structure[8]. The compositional dependence of IS for SiO_2-Al_2O_3-Eu_2O_3 glasses is shown in Table.2.

Table 2: Composition and isomer shift of Eu^{3+} in the glasses.

SiO_2	Al_2O_3	Eu_2O_3	IS (mm/sec)
50	40	10	0.30
50	35	15	0.33
50	30	20	0.42
50	25	25	0.45
50	20	30	0.47
50	15	35	0.48
50	10	40	0.49
60	20	20	0.40
66.7	-	33.3	0.46
80	-	20	0.42
-	80	20	0.52

IV. DISCUSSION

A. *Isomer Shift and Coordination Number of $^{151}Eu^{3+}$ in Oxide Crystals*

The relationship between the isomer shift of $^{151}Eu^{3+}$ and Eu-O bond length in the crystals are plotted in Fig.2. Also shown are the coordination number of Eu^{3+} ion. The isomer shift decreases with increasing Eu-O bond length or coordination number. The similar tendency was also observed for the divalent europium chalcogenide[9]. Since the actual distance between europium ions and surrounding anions is very sensitive to the coordination number of Eu^{3+} ion, the results shown in Fig.2. indicates that the *IS* parameter can be used as a measure of coordination number in oxide solids having unknown structures such as amorphous states. It has been shown that for glasses containing the Fe^{3+}, the *IS* of ^{57}Fe is a measure of coordination number, i.e., more covalent Fe^{3+} ions in the tetrahedral site show smaller *IS* and more ionic Fe^{3+} ions in the octahedral site show larger *IS* value[3,4]. These are explained by the contribution of 4s-electron density to $|\Psi(0)|^2$[10]. Thus the IS is a measure to identify the Fe^{3+} ions present in tetrahedral or octahedral sites[3]. The opposite tendency in the dependence of *IS* on covalency or coordination number for Fe^{3+} ions from that of Eu^{3+} ions is due to the negative sign of $(R_e^2-R_g^2)$ in Eq.(1) in Chapter 1.2 for ^{57}Fe nucleus[11]. On the other hand, the larger the 6s-electron density, the larger becomes the *IS* of ^{151}Eu. Thus the decreased *IS* observed with increased CN is ascribed to the elongated bond length, i.e., the reduced covalency in the

Eu-O bond.

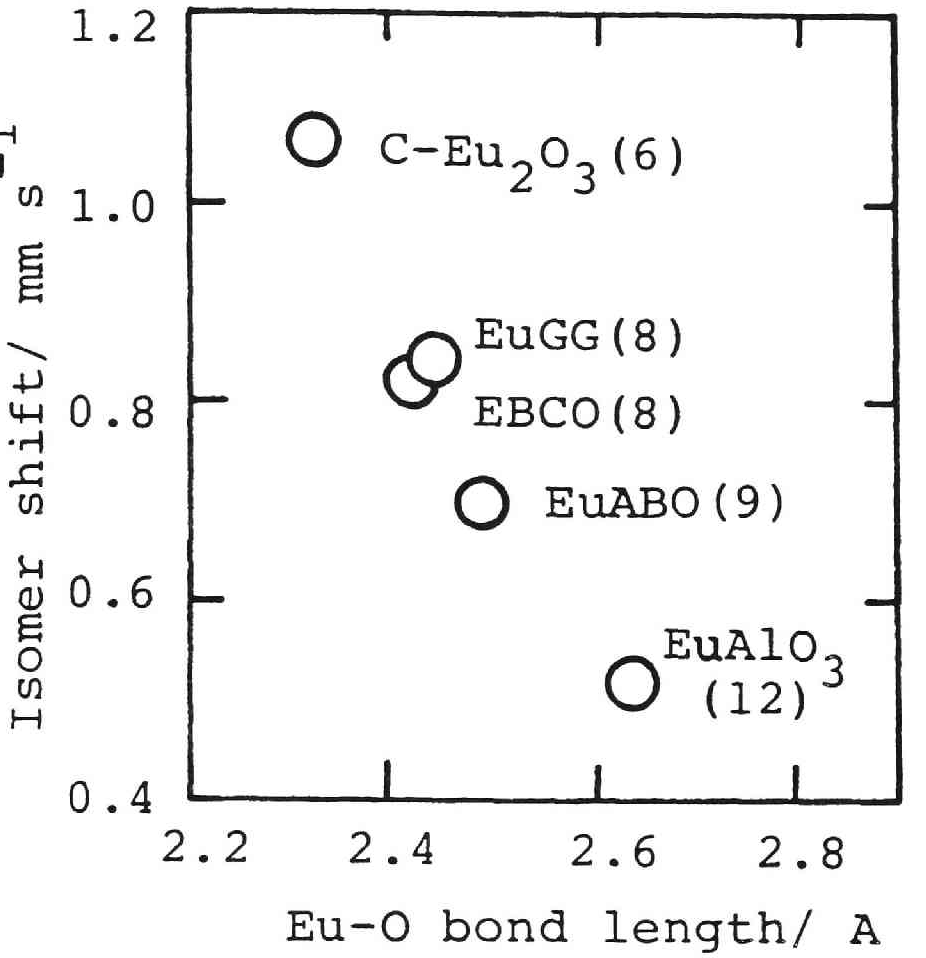

Fig.2. Relationship between the isomer shift and Eu-O bond length in oxide crystals. The coordination number of Eu^{3+} ions is shown in parentheses.

B. *State of Eu^{3+} Ions in Aluminosilicate Glasses*

No absorption peak due to Eu^{2+} ion was observed in all the glasses, although Eu^{2+} is known to be the most stable among all the divalent rare earth ions[12]. The isomer shift of Eu^{3+} ion with respect to EuF_3 was 0.46 mm/sec, indicating a strong ionic character of Eu-O bonds and high coordination states as seen from the relationship in Fig.2. The small *IS* value is attributed to a small electron density at the nucleus. Thus it can be considered that the degree of electron donation by the surrounding oxide ions is not so strong in this system, which is due to the low effective negative charge on oxygen ions caused by the larger polarizing ability of Si^{4+} and Al^{3+} ions. In order to explain the compositional variation of *IS*, the optical basicity concept by Duffy and Ingram[13] was adopted. As already referred, the electron donating ability of oxygen depends upon the negative charge on oxygen. This electron donating power depends upon the oxidation number of the constituent cations, z and its basicity moderating parameter, γ, which is empirically related to the electronegativity, x by the next equation[14].

$$\gamma_i = 1.36(x_i - 0.26) \qquad (1)$$

The optical basicity Λ can be calculated by using the next equation[13,14],

$$\Lambda_{cal} = \Sigma(z_i r_i / 2\gamma_i), \qquad (2)$$

where r_i denotes the atomic ratio of cation i with respect to the total number of oxide ions. The results of CNDO molecular orbital calculation[15] have indicated a simple relationship that the optical basicity value is directly proportional to the negative charge born by the oxygen atoms of the oxy-anion groups. In the

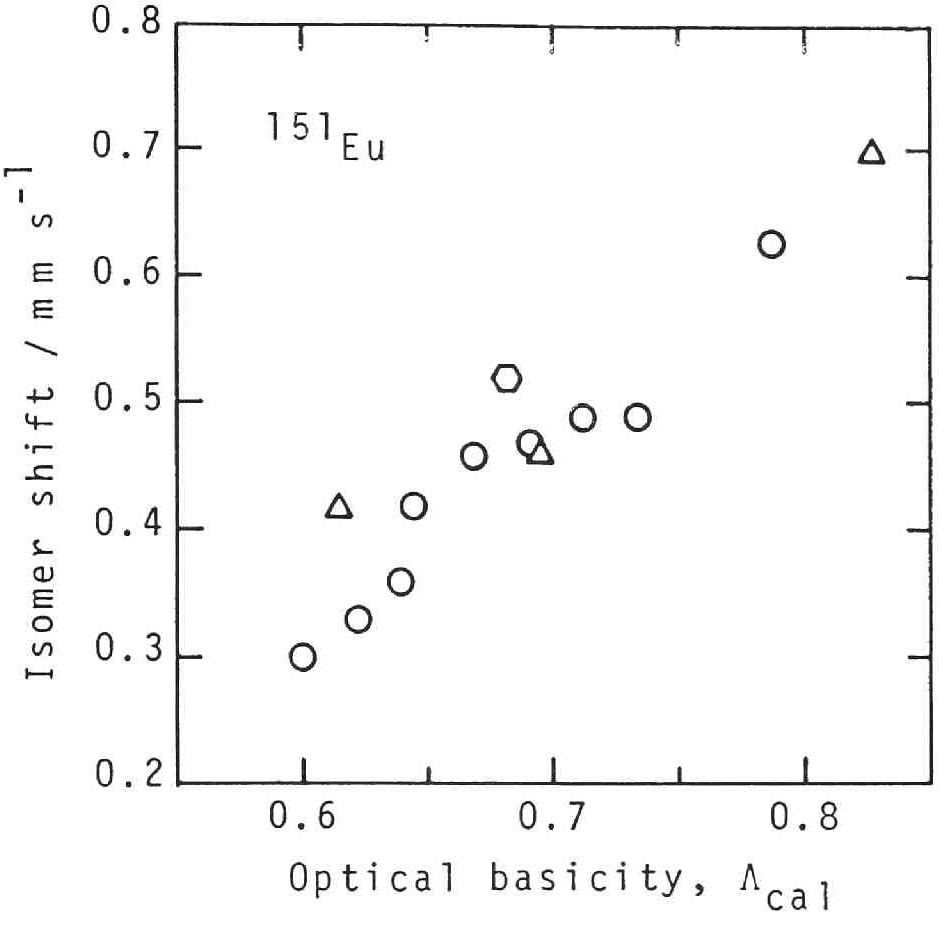

Fig.3. Relationship between the isomer shift of Eu^{3+} ion and the theoretical optical basicity of glass; ○: SiO_2-Al_2O_3-Eu_2O_3, ⬡: Al_2O_3-Eu_2O_3, △: SiO_2-Eu_2O_3.

present case, γ_{Si}, γ_{Al}, and γ_{Eu} were assumed to be 2.09, 1.65 and 1.02, respectively, although γ is strictly a function of CN of the cation. In this study, the dependence of γ on CN is negligibly small compared with the compositional change of Λ.

The isomer shift of Eu^{3+} in the present SiO_2-Al_2O_3-Eu_2O_3 glasses is plotted as a function of calculated optical basicity in Fig.3. The linear correlation suggests that the electron density of 6s orbital of Eu^{3+} ions is affected by the electron donating ability of oxide ions in the glass. Generally, the CN of Al^{3+} and Mg^{2+} in glasses is affected by the donor property of oxygen, which is explained by the optical basicity concept in a sense that the negative charge on oxygen atoms compensate the positive charge of the central cation. This effect has been investigated with the data of Al or Mg $K\alpha_{1,2}$ emission[16,17]. According to the absolute values of *IS* compared with those of crystals, the CN varies from 8 to 12 depending on Λ. The lower *IS* is due to the larger ionicity of Eu-O bonds and the higher CN of Eu^{3+} ions owing to the large γ of Si^{4+} and Al^{3+} ions. The assumption of high CN in low basicity matrix seems to be correct when the ionic radius ratio is taken into account. One of the important factors controlling the CN of cation in ionic solids is the radius ratio of cation to anion, r_c/r_a. For Eu^{3+} ion in oxides, the ratio is calculated to be 0.89 with the ionic radii reported by Shannon[18]. This value is large enough to take eight folded state where this ratio is usually more than 0.732. Thus it can be difficult for Eu^{3+} ions in low basicity matrix to take a CN less than 8. For the cation with r_c/r_a ratio of unity, CN of 12 will be predominant. Thus if there are no charge compensating cations which makes nonbridging oxygen such as alkaline metal ions in silicate glasses, the electron density on oxygen atoms become small. This will lead to a small effective ionic radius of O^{2-} resulting in a higher $r_{Eu^{3+}}/r_{O^{2-}}$ value near unity. On the

other hand, in the Eu_2O_3-doped silicate glass containing Na^+ and Ba^{2+} ions, the *IS* was reported to be close to Eu_2O_3[1], indicating a basic environment of Eu^{3+} in those glasses. This difference may be ascribed to the presence of basic oxides such as BaO and Na_2O, which are considered to make nonbridging oxygen ions in the silicate glass and also enhance the local basicity. On the other hand, in aluminosilicate glasses without any basic oxides, Eu^{3+} ions take higher CN more than 8 and thus, trivalent rare earth ions are present as a network modifier in these glasses.

C. *Analysis of quadrupole interaction*

As the fitting of the measured spectra by a single Lorentzian led to a systematic misfit in the shape of the real peaks, the resolution of the lineshape was tried into eight line quadrupole splittings for the 5/2 → 7/2 transition. The deviation of the peak shape from a single Lorentzian, which can be ascribed to the quadrupole interaction, was not resolved with enough precision. The analysis was not impossible and yielded a better fit to the real peak, but the uniqueness of the solution by fitting seems to include some uncertainty because of a large linewidth of all components. One example of the resolution is shown in Fig.4. The linewidth of one component was 2.02 mm/sec and e^2qQ_g was -9.2 mm/sec. A larger linewidth than the natural line width of 1.31 mm/sec is mostly due to the site-to-site variation in the glass. The very large e^2qQ_g which is about twice as large as that of Eu_2O_3 crystals(-5.2~-4.0 mm/sec[19]) can be due to asymmetric lattice contribution to the electric field gradient. Similarly,

an asymmetric ligand field around Eu^{3+} ion will cause a large quadrupole splitting in glasses. A slight shoulder at the higher velocity side almost corresponds to the 1/2→1/2 transition, which has the second largest intensity among the eight components. This indicates that the sign of *eq* is negative. The shoulder peak is not due to an independent single component because such a deconvolution would result in the *IS* of 1.58 mm/sec, which means much higher covalency than nitrides. This would also result in the main peak with the *IS* of -0.16 mm/sec, which shows much higher ionicity than that of fluorides. The

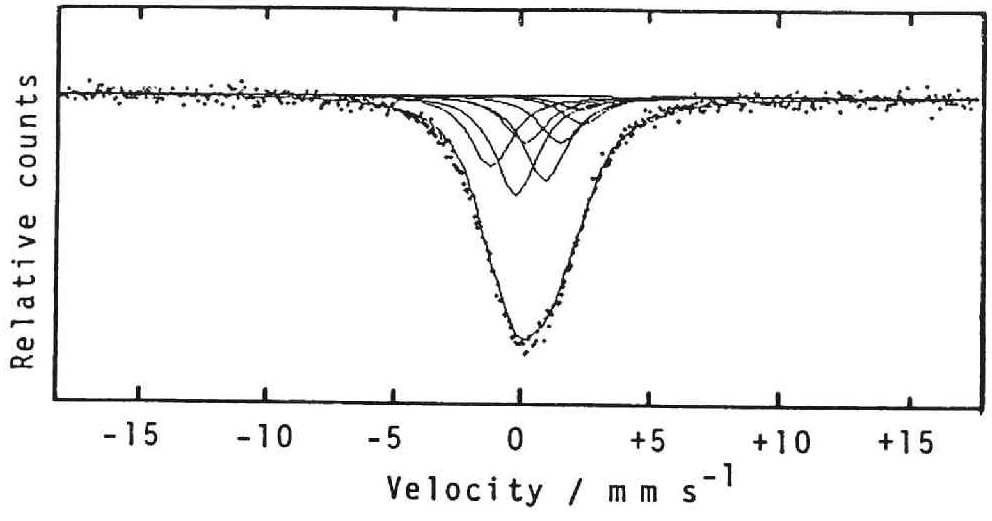

Fig.4. Example of the spectral analysis of glass. The sign of e^2qQ_g is assumed to be negative.

negative eq has also been observed more clearly for $Eu_2Ti_2O_7$ crystal[20]. In the case of glasses, the linewidth of one component is unknown. Consequently, when eqQ_g is not so large compared with the linewidth, the solution of the fitting may converge either in a small eq with a broad linewidth or in a large eq with a sharp linewidth, in the range where no apparent deviation nor unexpected fine structure appears. Thus it can be concluded that the uniqueness of the quadrupole solution for the glass is controversial unless the shape of the peak is clearly asymmetric or shows some shoulders which indicates the sign of eq.

V. CONCLUSIONS

Mössbauer effect measurements were made on ^{151}Eu in various oxide crystals and glasses. It was found that the isomer shift of ^{151}Eu nucleus in crystals varied with the Eu-O bond length or coordination number of Eu^{3+} ion in oxide. The IS decreased with elongated Eu-O bond length with an increase of coordination number. In aluminosilicate glasses, the compositional dependence of the isomer shift was systematically explained by the optical basicity concept. The CN of Eu^{3+} ion was found to change from 8 to 12 in these glasses. The analysis of eight-line quadrupole splittings due to $5/2 \rightarrow 7/2$ transition in the nuclear spin was also tried by the least square fitting, but no successful results were obtained.

2.2. Structure and Physical Properties of Europium Aluminosilicate Glasses by Means of Lattice Dynamic Measurement

I. Introduction

Few studies have been carried out on the structure of rare earth containing oxide glasses partly because of few spectroscopic techniques applicable to identify the chemical states of rare earth elements. For their high elastic moduli, hardness and high refractive index, these glasses are receiving an interest. In this study, the Eu_2O_3-containing glass system was chosen as a representative of the rare earth aluminosilicate glasses because the atomic number and ionic radius of Eu^{3+} ion are in the middle of the lanthanide series and also because the ^{151}Eu Mössbauer spectroscopy is a powerful technique to investigate the coordination states of Eu^{3+} ions. The applicability of Mössbauer spectroscopy to the study of glass structure has been shown by several authors[1-5], however, most of the studies were on ^{57}Fe nuclei. In this study, the relationship between the coordination number and the isomer shift of Eu^{3+} ions[21], reported in the former section, were applied to discuss the state of Eu^{3+} ions in the aluminosilicate glasses. Also the density, molar volume, sound velocity and elastic moduli were measured and their compositional dependence was discussed.

II. Experimental Procedure

(1) Sample Preparation

An image furnace apparatus(designed by *NEC Nichiden kikai KK.*, Fig.1) was used to obtain glass samples. By using reagent grade powders of SiO_2(Wako Pure Chemical Industries Ltd.), Al_2O_3 (Hayashi Pure Chemical Industries, Ltd., 99.9%), and Eu_2O_3 (Mitsuwa Pure Chemicals, 99.9%), batch compositions expressed as $50SiO_2 \cdot (50-x)Al_2O_3 \cdot xEu_2O_3$ in mol%, where x is 10, 15, 18.75, 20, 25, 30, 35 and 40, were fully mixed in an alumina mortar for about 50min. and pressed into a stick with a rubber press. A pressed compact was sintered at 1200 °C for 15 hours and the sintered specimen was melted at the focus point of the bifocal gold mirror by the Xe-lamp which is placed at another focus point. The melt was quenched by a twin-roller rotating at about 1000 rpm or air-cooled on a stainless steel in order to examine the glass-forming tendency.

(2) Physical Property Measurement

The density was measured by Archimedes' method by using kerosine as a medium and silica glass as a standard. The molar volume was calculated by the density measured and the molar weight. The measurements of sound velocities were carried out on the samples which formed a glass by the air cooling. After cutting the bulk sample precisely into a cube of 3 mm size, the sound velocities of shear and longitudinal wave, V_s, V_l were measured by the cube resonance technique described elsewhere[22]. The shear modulus G, bulk modulus K, and Young's modulus E were calculated by the following equations.

$$G=\rho V_s^2 \quad (1)$$

$$K=\rho (V_l^2-4V_s^2/3) \quad (2)$$

$$E=\rho V_s^2(3V_l^2-4V_s^2)/3(V_l^2-V_s^2) \quad (3)$$

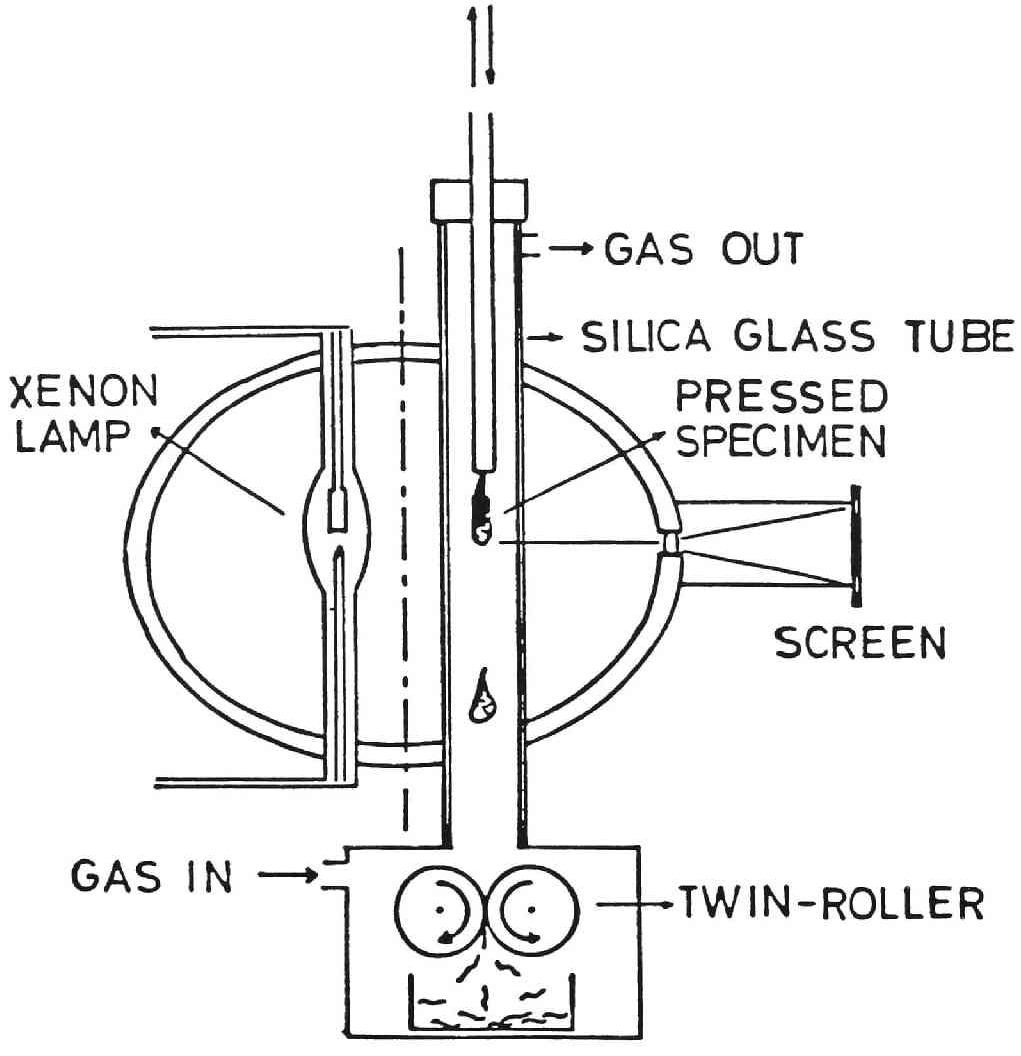

Fig.1: Image furnace apparatus.

(3) Spectroscopic measurement

The ^{151}Eu Mössbauer effect was measured with a $^{151}Sm_2O_3$ source (5mCi) using a driving unit in the velocity range of $\pm$18 mm/sec. The velocity calibration was done with the spectrum of hyperfine splitting of α-Fe by a $^{57}Co(Rh)$ source and the isomer shift was calculated by using the spectrum of EuF_3 as a standard. The position and linewidth of each spectrum were determined with a least-square fitting program, Lorentzian curves being assumed.

The Al$K\alpha$ band emission was measured by an X-ray probe microanalyzer(ARL EMX-SM, Shimadzu-Seisakusho, Kyoto, Japan). The peak position was determined by the midpoint of the half maximum and the chemical shift, $\Delta\lambda$ was represented by the difference between the wavelength of X-ray emission spectrum of the sample and that of Al-metal.

III.Results

(1) Glass-Forming Region

The glass-forming regions of $50SiO_2$ $(50-x)Al_2O_3 \cdot xEu_2O_3$ by the air cooling and by the twin-roller quenching are represented by a white circle in Fig.2(a) and (b), respectively. By the air-cooling method, an X-ray amorphous was obtained in the composition range where the Eu_2O_3 content, x was 15~30 mol%. By the twin-roller quenching method, an amorphous was obtained in the range where x is 10~40.

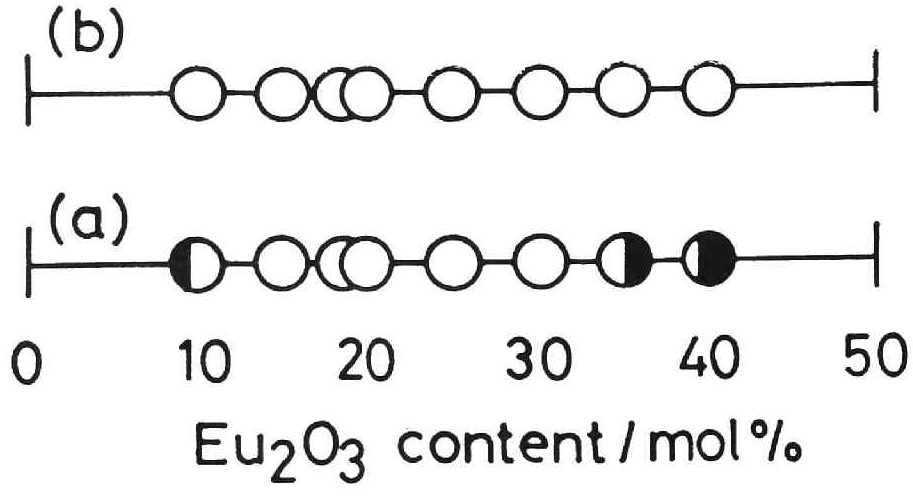

Fig.2: Glass forming regions of $50SiO_2 \cdot (50-x)Al_2O_3 \cdot xEu_2O_3$ system (a) Air cooling and (b) Twin-roller quenching.

(2) Physical Properties

(2.1) Density

The results of density measurement for the present amorphous samples are shown in Fig.3 as a function of Eu_2O_3 content. It can be seen that the density increases continuously with increasing Eu_2O_3 content.

(2.2) Sound velocity

The sound velocity of shear wave, V_s and that of longitudinal wave, V_l are plotted as a function of Eu_2O_3 content in Fig.4. The value plotted by a black circle is that of an amorphous $50SiO_2 \cdot 50Al_2O_3$ (x=0) thin film prepared by the rf-sputtering[23]. Both velocities decreased with increasing Eu_2O_3 content.

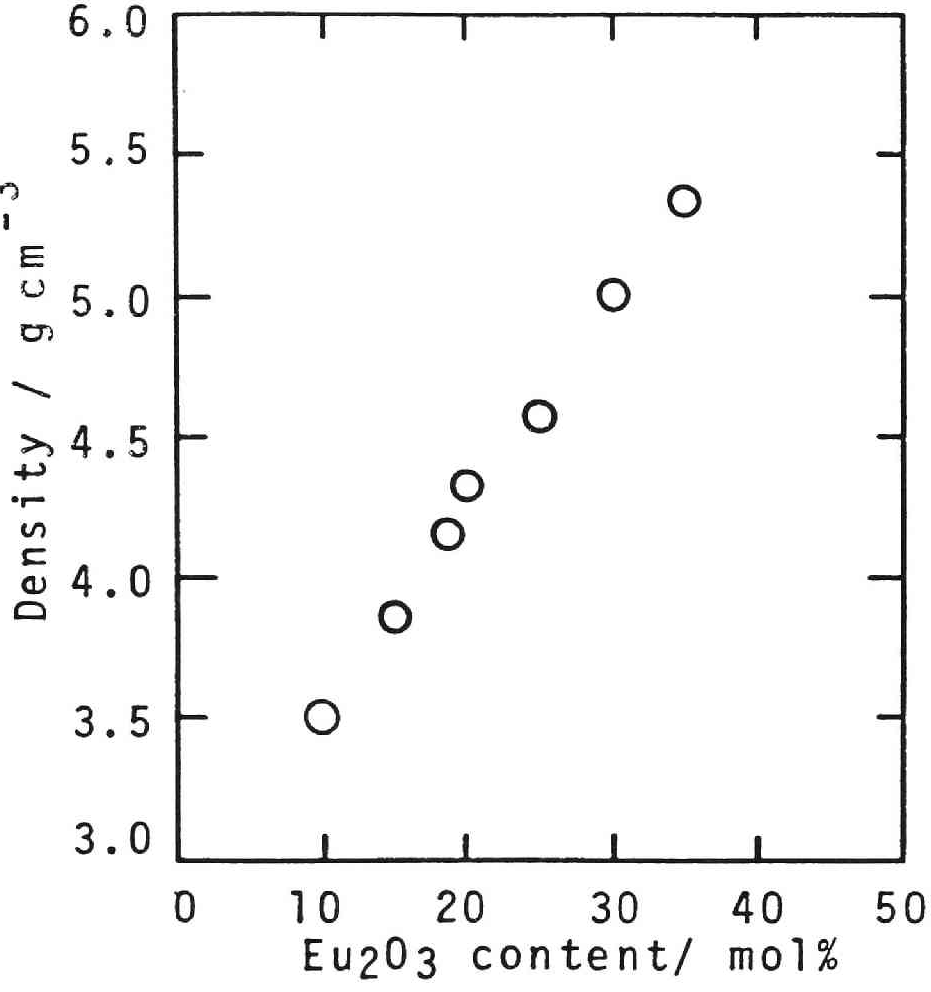

Fig.3: Density of glasses as a function of Eu_2O_3 content.

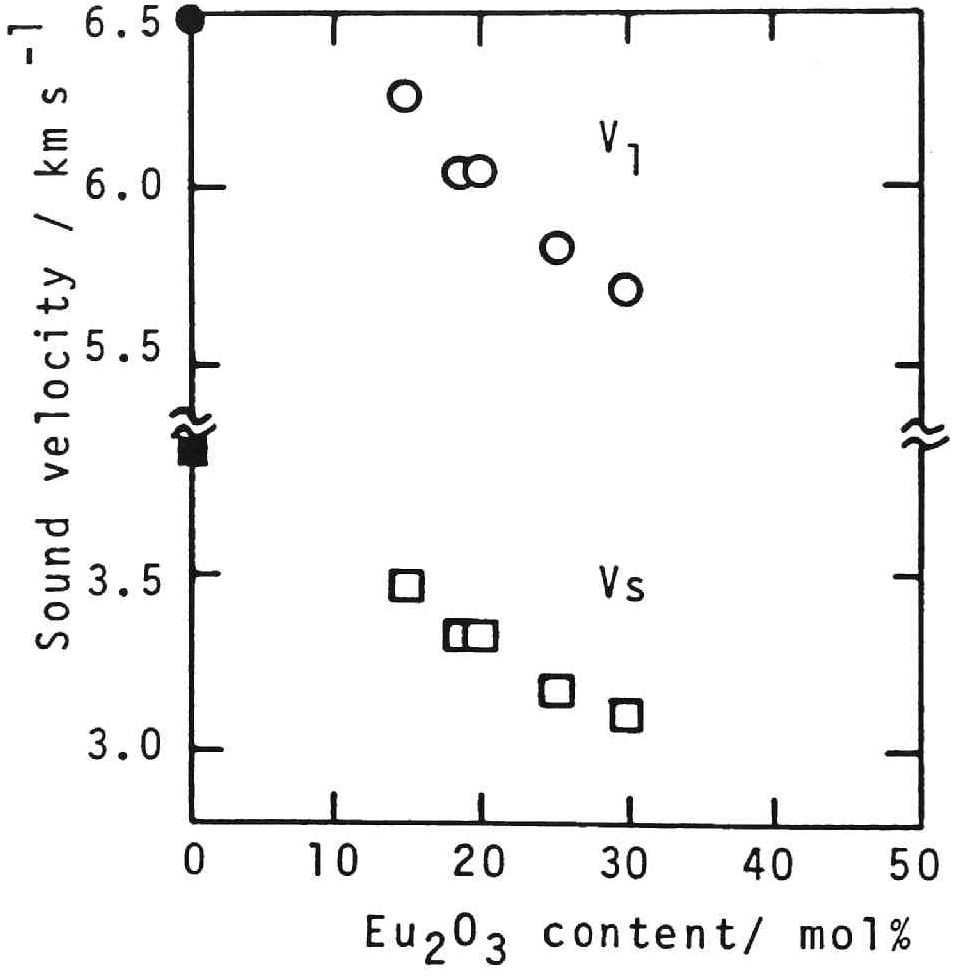

Fig.4: Sound velocities of Glasses as a function of Eu_2O_3 content.

(2.3) Elastic Moduli

The results of Young's and bulk moduli of the present glasses are plotted as a function of Eu_2O_3 content in Fig.5 and 6, respectively. The Young's modulus of these glasses ranged from 117 to 125 GPa, which is very high for oxide glasses and almost comparable to the highest value of the SiO_2-Al_2O_3-Y_2O_3 system[24]. Both moduli did not show a large dependence on Eu_2O_3 content in the composition range of x=15~30.

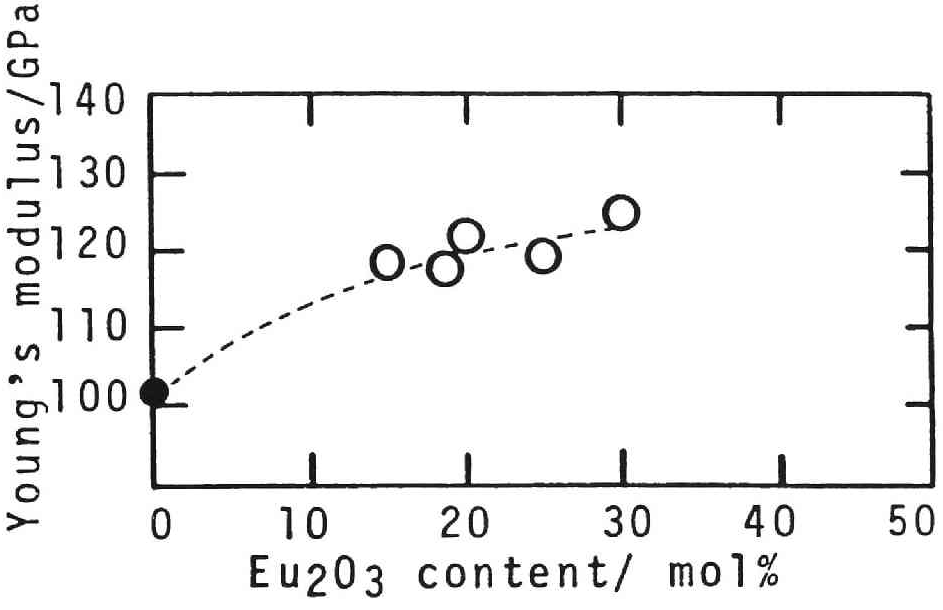

Fig.5: Young's modulus of glasses as a function of x.

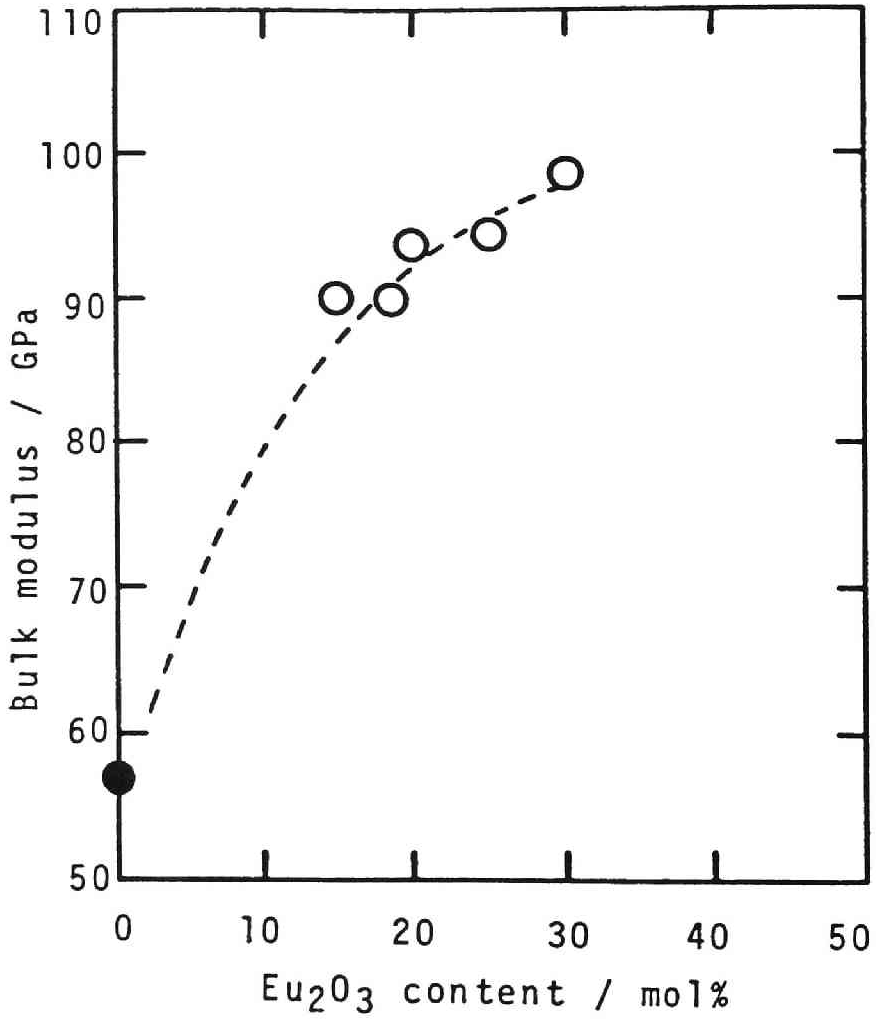

Fig.6: Bulk modulus of glasses as a function of x.

(3) Mössbauer Effect

No peak due to divalent Eu^{2+} ions was observed in the spectra of the glasses. It is known that the isomer shift IS of $^{151}Eu^{3+}$ decrease with an increase of the coordination number in oxide crystals[21]. The IS changed from 1.07 mm/sec for C-Eu_2O_3, where the CN of Eu^{3+} is 6, to 0.52 mm/sec for $EuAlO_3$ perovskite, where the CN of Eu^{3+} is 12. The shoulder observed in the higher velocity side in the spectrum of the glass is due to the quadrupole interaction of the distorted ligand field of Eu^{3+} ions in a random network structure. The compositional dependence of IS for the glasses is shown in Fig.7. The IS increased with increasing Eu_2O_3 content, but all the values were less than that for $EuAlO_3$ perovskite crystal.

(4) AlKα Emission

The compositional dependence of the chemical shift of Al*Kα* emission band is shown in Fig.8. The chemical shift of the standard crystals are also shown for α-Al_2O_3 (CN=6), mullite (CN=4.8) and K-feldspar (CN=4). The values for all the glasses were close to that of mullite, indicating that the average coordination number of Al^{3+} ions is almost five in the whole range of compositions.

IV. Discussion

(1) Coordination States of Europium

It has been shown that the isomer shift of ^{151}Eu nuclei is

a good parameter to get the information about the coordination number of Eu^{3+} ions. As shown in Fig.7, all the values of IS for the present glasses were smaller than that of $EuAlO_3$ perovskite

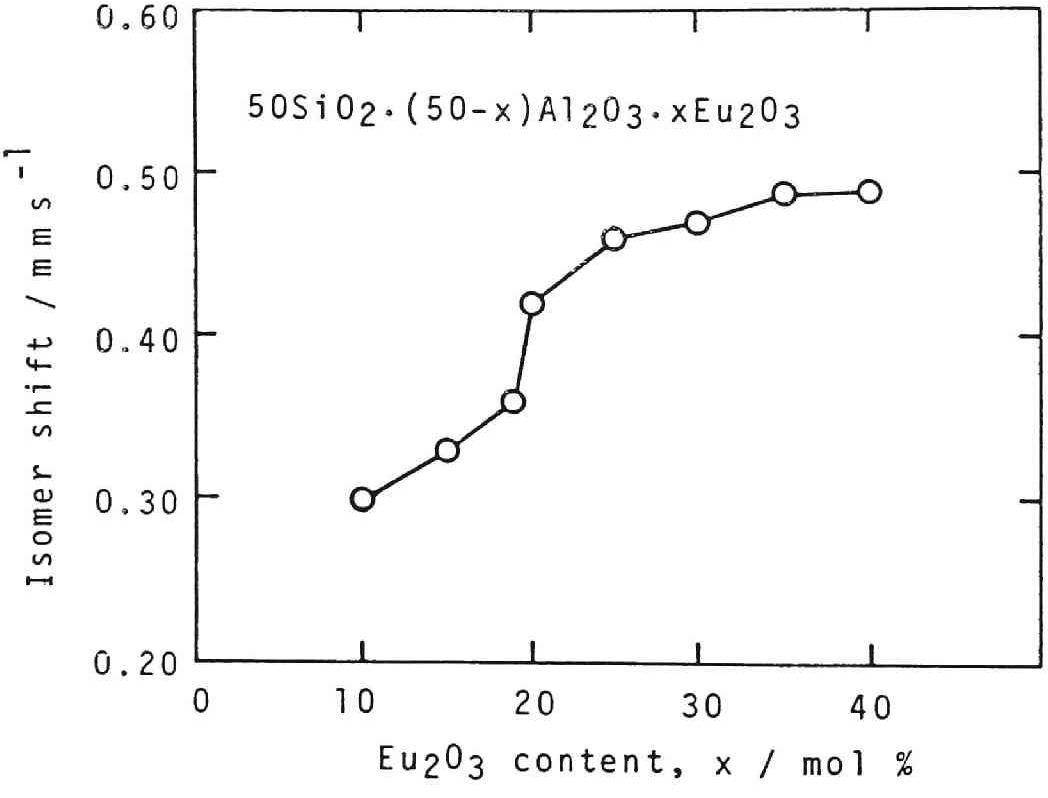

Fig.7: Isomer shift of ^{151}Eu for glasses as a function of x.

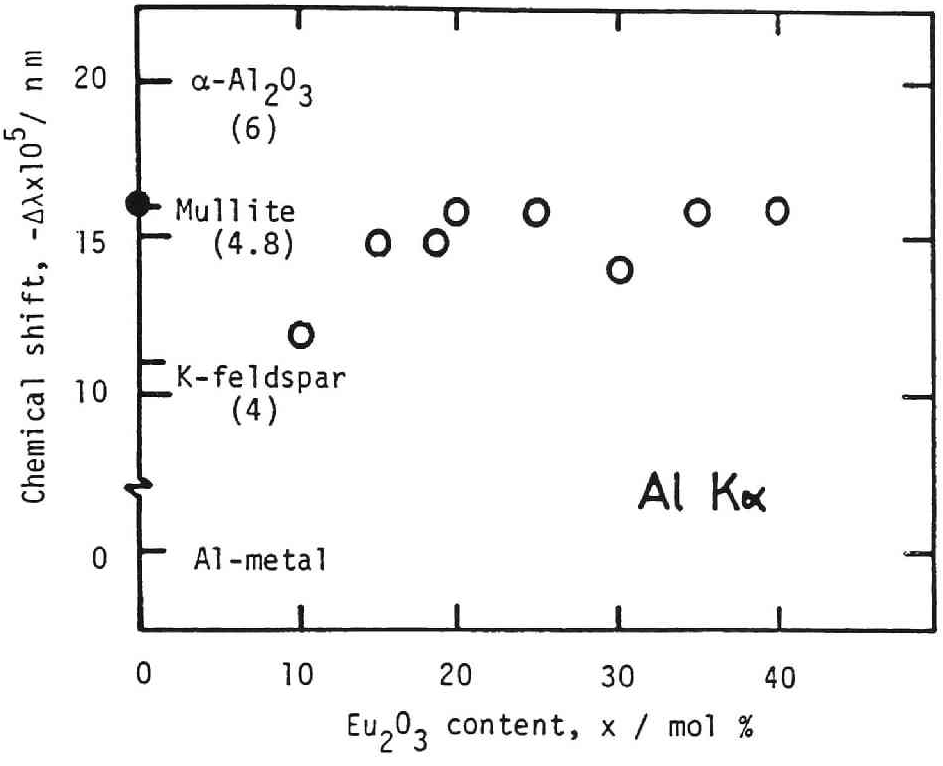

Fig.8: Chemical shift of Al$K\alpha$ emission as a function of x.

crystal (IS = 0.52 mm/sec) where the CN of Eu^{3+} ions is 12. From the crystallographical point of view, it is difficult to take CN more than twelve because the ionic radius of O^{2-} is larger than that of Eu^{3+} ion. Thus, this small IS is not due to a higher CN of Eu^{3+} than twelve.

The isomer shift, IS of the Mössbauer nuclei can be ex-

pressed by the next equation,

$$IS=C(R_e^2-R_g^2)(|\Psi a(0)|^2 - |\Psi s(0)|^2) \quad (4)$$

where R_e, R_g denote the nuclear radii of excited and ground states, $|\Psi a(0)|^2$ and $|\Psi s(0)|^2$ are the electron density at the nucleus of the absorber and of the source, respectively and C is a constant characteristic of the species. As the nuclear radius of ^{151}Eu in the excited state R_e is larger than that in the ground state R_g, a smaller isomer shift indicates a smaller electron density of *6s*-orbital[25], which may be ascribed to the elongated bond length of Eu-O due to the large coordination number of Eu^{3+} ions or the reduced covalency of Eu-O bond. Such an increase in ionicity is probably brought in by the higher polarizing ability of Al^{3+} ions coexisting in the glass. With increasing Al_2O_3 content, the effective charge density on oxygen ions becomes small, because the electron polarizing ability of Al^{3+} ions is stronger than that of Eu^{3+} ions. In this case, the electron donor ability of O^{2-} ions to Eu^{3+} ion becomes small, which leads to a decrease of overlap integral of *2p*-orbital and *6s*-orbital of Eu^{3+} ion. Thus the electron density at the nucleus of Eu^{3+} ion decreases, which resulted in a decrease of IS for ^{151}Eu.

(2) Change of Packing State of Glass with Eu^{3+} Ions

As shown in Fig.3, the density increased monotonously with increasing Eu_2O_3 content, which is attributable to the much larger atomic weight of Eu^{3+} ions than other kinds of ions in the glass. From these data, the compositional dependence of the

molar volume was calculated and the results are shown in Fig.9. Also shown is the expected slope calculated based on the assumption that the molar volume is the sum of the fractional molar volume of staring oxide crystals in which the CN of Al^{3+} and Eu^{3+} ions were six. The molar volume used for the calculation were 25.57 $cm^3 \cdot mol^{-1}$ for $V(\alpha\text{-}Al_2O_3)$ and 48.29 $cm^3 \cdot mol^{-1}$ for $V(C\text{-}Eu_2O_3)$. The actual change in molar volume for the glasses was much smaller than that expected from the above assumption. This discrepancy arose from the assumption that the CN of Eu^{3+} and Al^{3+} ions in the glass are the same as those in crystal. However, as described in the previous section, Eu^{3+} and Al^{3+} ions have the CN of 12 and 5, respectively. The molar volume for a fictitious 12-folded Eu_2O_3 crystal, $V(Eu_2O_3\{12\})$, may be estimated from the molar volume of $EuAlO_3$ or $EuGaO_3$ perovskite and $\alpha\text{-}Al_2O_3$ or $\alpha\text{-}Ga_2O_3$ as follows.

$$V(Eu_2O_3\{12\})=2V(EuAlO_3\{12,6\})-V(\alpha\text{-}Al_2O_3\{6\})=36.82 \quad (5)$$

$$V(Eu_2O_3\{12\})=2V(EuGaO_3\{12,6\})-v(\alpha\text{-}Ga_2O_3\{6\})=39.00 \quad (6)$$

Although the $V(Eu_2O_3\{12\})$ was slightly different depending upon the kind of crystals, $38(\pm 1)$ $cm^3 \cdot mol^{-1}$ was taken as a probable value. By taking the molar volume of 29.69 $cm^3 \cdot mol^{-1}$ for the 5-folded $\gamma\text{-}Al_2O_3\{4,6\}$, the change in molar volume due to the simple substitution of the 5-folded Al^{3+} by the 12-folded Eu^{3+} was calculated and the slope of the change in molar volume with Eu_2O_3 content was obtained. As shown in Fig.10, this slope fits almost perfectly with the obtained data. This result supports the conclusion of Mössbauer measurements that the CN of Eu^{3+} ions in the present glass is 12.

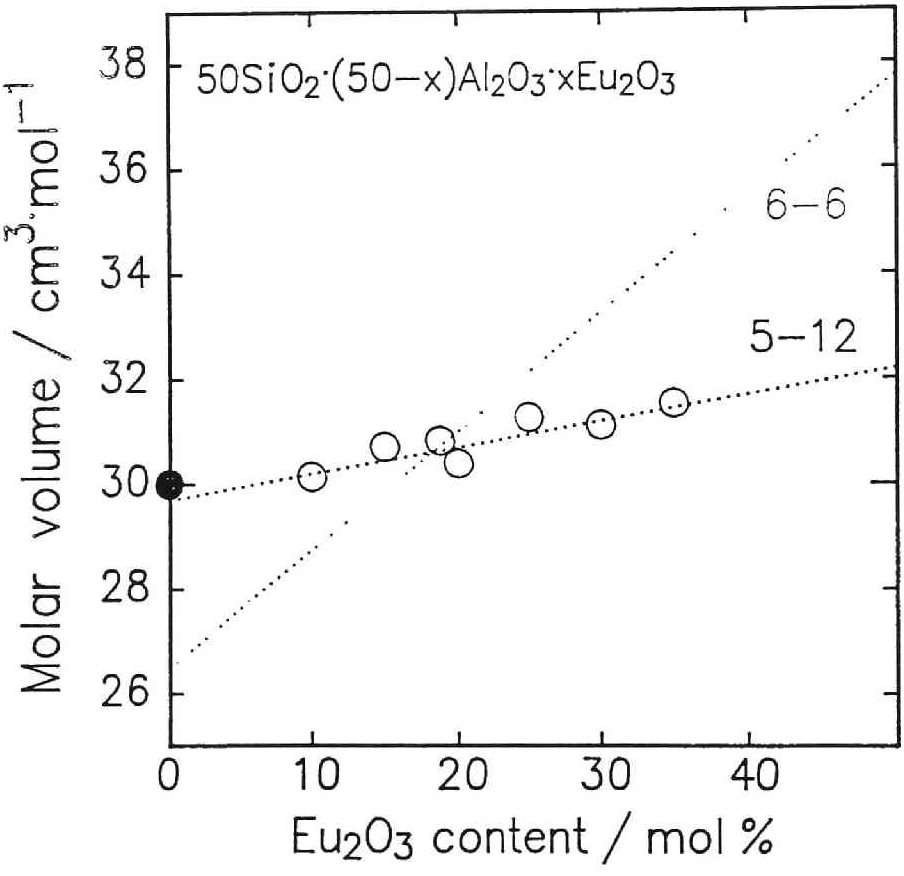

Fig.9: Molar volume of glasses as a function of x.

(3) High Elastic Moduli of Eu_2O_3 Containing Glass

Although the vibrational frequencies or the sound velocities of the present glasses decreased with increasing Eu_2O_3 content,

the elastic moduli increased with Eu_2O_3 content, because of more rapid increase in the density. This result indicates that the packing density of these glasses increased by the substitution of Al^{3+} ions with larger Eu^{3+} ions because of the higher CN of Eu^{3+} ions as described in the previous section. If both Eu^{3+} and Al^{3+} ions were to take the same coordination number, the Young's modulus of glass should decrease with increasing Eu_2O_3 content, because the elastic moduli of Al_2O_3 (E=400 GPa) is much higher than that of Eu_2O_3 (E=150 GPa)[26,27]. It has been pointed out that the elastic moduli of an oxide glass can be increased enormously by introducing highly coordinated ions. The introduction of 5-folded Al^{3+} ions to SiO_2 glass raised the Young's modulus of SiO_2 (E = 72 GPa) to 102 GPa for $50SiO_2 \cdot 50Al_2O_3$ [23] in spite of the fact that the single bond strength of Al-O is lower than that of Si-O. In the present glass system, the Young's modulus was found to be increased by introduction of higher-folded Eu^{3+} ions compared with that of $50SiO_2 \cdot 50Al_2O_3$. Among trivalent cations, the role of rare-earth elements is always considered as a network modifier unlike Al^{3+} ion. This tendency is caused by a small field strength and large ionicity. For this reason of taking a high CN state, the addition of rare earth elements in glass is advantageous to attain high elastic moduli.

V. Conclusions

The SiO_2-Al_2O_3-Eu_2O_3 glasses were prepared for the compositions of $50SiO_2$ $(50-x)Al_2O_3 \cdot xEu_2O_3$ and their density, sound velocity and elastic moduli were measured. Also the chemical

shift of Al$K\alpha$ band emission spectra and the isomer shift of ^{151}Eu by Mössbauer effect were obtained in order to determine the coordination states of aluminum and europium ions in these glasses. It was found that the coordination number of Eu^{3+} ions was twelve, while the average coordination number of Al^{3+} ions was almost five in these glasses. By introducing Eu_2O_3, the packing of constituent ions was strongly enhanced and the elastic moduli increased in this system. The compositional dependence of the molar volume and elastic moduli were explained by these states of high CN for Eu^{3+} and low CN for Al^{3+} ions compared with those in the corresponding M_2O_3 crystals.

REFERENCES

[1] M.F. Taragin and J.C. Eisenstein, *Phys. Rev. B* **2**, (1970) 3490-94.

[2] J.M.D. Coey, A. McEvoy and M.W. Shafer, *J. Non-Cryst. Solids* **43**, (1981) 387-392.

[3] C.R. Kurkjian and D.N.E. Buchanan, *Phys. Chem. Glasses* **5**, (1964) 63-70.

[4] C.R. Kurkjian, *J. Non-Cryst. Solids* **3**, (1970) 157-194.

[5] S. Tanabe, K. Hirao and N. Soga, *J. Non-Cryst. Solids* **100**, (1988) 388-393.

[6] K. Hirao, N. Soga and M. Kunugi, *J. Am. Ceram. Soc.* **62**, (1979) 109-10.

[7] T. Nishida, T. Shiotsuki and Y. Takashima, *J. Non-Cryst. Solids* **43**, (1981) 115-122.

[8] T. Komatsu and N. Soga, *J. Appl. Phys.* **51**, (1980) 601-06.

[9] O. Berkooz, *J. Phys. Chem. Solids* **30**, (1969) 1763-67.

[10] L.R. Walker, G.K. Wertheim and V. Jaccarino, *Phys. Rev. Lett.* **6**, (1961) 98-101.

[11] G.J. Perlow, in *"Chemical Application of Mössbauer Spectroscopy,"* (ed. Gol'danski and Herber, Academic Press, NY, 1968) pp.400-426.

[12] M.W. Shafer and J.C. Suits, *J. Am. Ceram. Soc.* **49**, (1966) 261-64.

[13] J.A. Duffy and M.D. Ingram, *J. Non-Cryst. Solids* **21**, (1976) 373-410.

[14] J.A. Duffy and M.D. Ingram, *J. Inorg. Nucl. Chem.* **37**, (1975) 1203-06.

[15] J.H. Binks and J.A. Duffy, *J. Non-Cryst. Solids* **37**, (1980) 387-400.

[16] S. Sakka, *Bull. Inst. Chem. Res. Kyoto Univ.* **49**, (1971) 349-367.

[17] H. Kawazoe, *J. Non-Cryst. Solids* **42**, (1980) 281-84.

[18] R.D. Shannon, *Acta. Crystallogr.* **A32**, (1976) 751.

[19] P. Glentworth, A.L. Nichols, N.R. Large and R.J. Bullock, *J. Chem. Soc. Dalton Trans.* (1973) 546-550.

[20] G.W. Dulaney and A.F. Clifford, *"Mössbauer Effect Methodology, vol.5"*, (ed. J.Gruverman, Plenum, NY, 1969) pp.65-76.

[21] S. Tanabe, K. Hirao and N. Soga, *J. Non-Cryst. Solids* **113**, (1989) 178-184.

[22] T. Goto and N. Soga, *Yogyo-kyokai-shi* **91**, (1983) 34-41.

[23] T. Hanada, Y. Bessyo and N. Soga, *J. Non-Cryst. Solids* **113**, (1989) 213-220.

[24] A. Makishima, Y. Tamura and T. Sakaino, *J. Am. Ceram. Soc.* **61**, (1978) 247-49.

[25] G. Gerth, P. Kienle and K. Luchner, *Phys. Lett.* **27A**, (1968) 557-58.

[26] N. Soga and O.L. Anderson, *J. Am. Ceram. Soc.* **49**, (1966) 318-320.

[27] K.K. Phani and S.K. Nyogi, *J. Am. Ceram. Soc.* **70**, (1987) C-362-66.

Chapter 3.

LOCAL STRUCTURE AND NONRADIATIVE RELAXATION OF RARE EARTH IONS IN GLASSES

3.1. Phonon Sideband of Trivalent Rare Earth Ions in Glasses

A. *Multiphonon Decay as a Nonradiative Process*

The most important factor among nonradiative decay process is that of giving the energy, which corresponds to the energy gap between the levels, to the vibrational energy of the host[1]. In general, since the energy gaps of the rare earth electronic levels are about several 1000 cm^{-1}, and the highest frequencies of the oxide hosts are about several or at most fifteen $100cm^{-1}$, this process becomes multiphonon decay process, creating multiple phonons. The rate of this process can be given by[2],

$$W_p = W_0 \exp(-\alpha \Delta E) \cdot [n(T)+1]^p \qquad (1)$$

$$\alpha = (\hbar\omega)^{-1}\{\ln(p/g)-1\} \qquad (2)$$

$$p \simeq \Delta E/\hbar\omega \qquad (3)$$

where ΔE is the energy gap and W_0 is the parameter corresponding to the decay rate at zero energy gap and zero phonon emission. Here, α and p are given by eq.(2) and (3), respectively, where $\hbar\omega$ is the phonon energy, p is the number of phonons emitted, and g is the electron-phonon coupling strength. By the phonon sideband measurement, $h\omega$ and g can be determined experimentally and thus it is possible to calculate the value of W_p/W_0. From these

equations, it can be seen that the larger the phonon energy $\hbar\omega$, and electron phonon coupling strength g, the larger becomes the nonradiative decay rate W_p when W_0 is constant. Generally, in multiphonon decay process, the most important role is played by the phonons with the highest frequency, which reflects the conservation of the energy gap in the lowest order process. The quantum efficiency of a level depends on the nonradiative contribution, which is a function of the energy gap to the next lower level. For Eu^{3+} ions in oxide hosts, as $\hbar\omega$ and g are large compared with fluoride hosts, the emissions from the upper $^5D_1$ or $^5D_2$ level are suppressed due to their small energy gap[3].

B. *Phonon Sideband in Glass*

The most representative example is that of Eu^{3+} ions, for which the phonon sideband can be clearly seen in the excitation spectra of $^5D_0 \rightarrow {}^7F_2$ emission. The phonon energy distributions were obtained in the sideband spectra associated with $^5D_2 \leftarrow {}^7F_0$ transition and are shown for several oxide glasses in Fig.1. The obtained phonon energy almost corresponds to that of the stretching vibrational mode of the cation-centered oxygen polyhedra studied by the infrared absorption or Raman scattering spectroscopies[4]. The mean free path of the phonons in amorphous structure is, in general, the order of the bond length between adjacent atoms, so these polyhedra are considered to directly coordinate to rare earth ion and contribute to its multiphonon decay[4]. In the glass chemistry, constituents of glass are usually divided into two categories; network formers and network

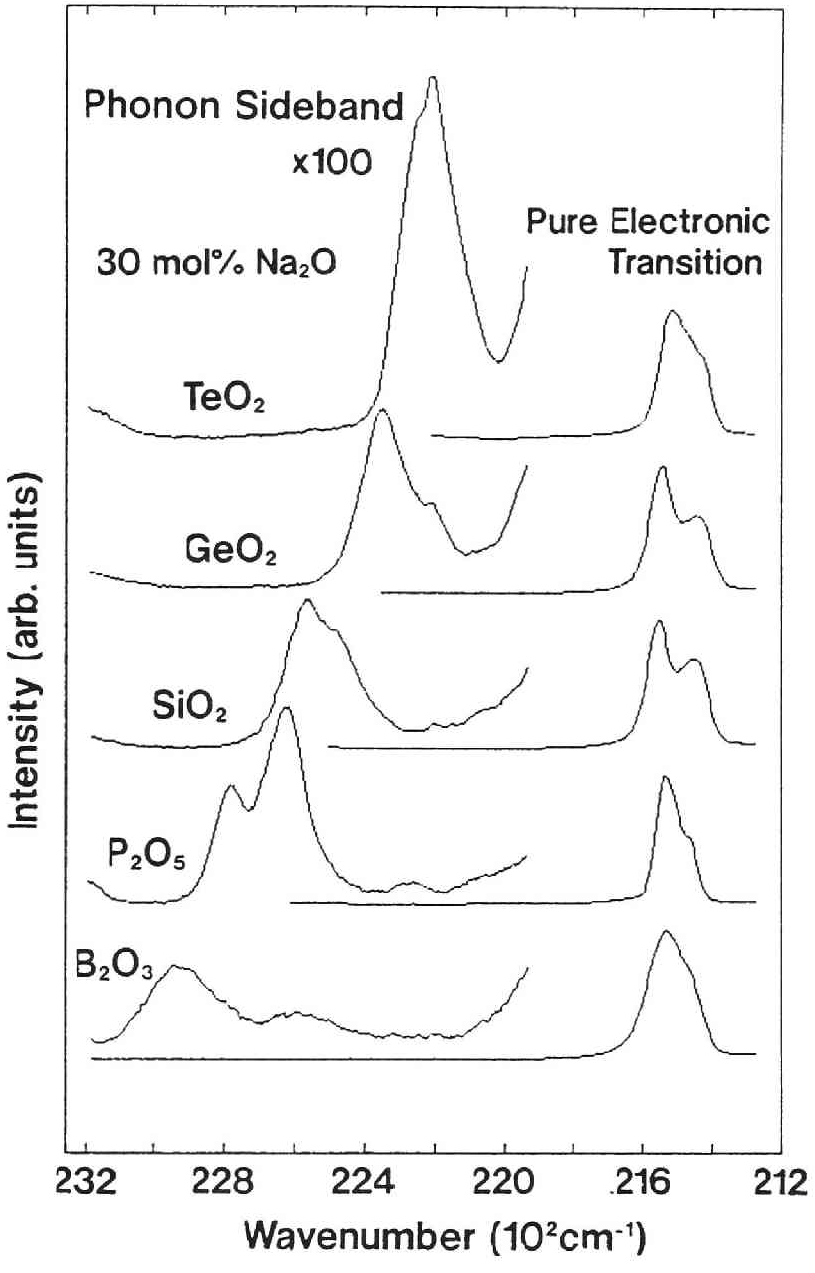

FIG.1. Excitation spectra of Eu^{3+} ions in several oxide glasses, $70M_xO_y \cdot 30Na_2O \cdot 1Eu_2O_3$(M = B, P, Si, Ge, Te). The phonon sideband appears at higher energy side of the pure electronic $^5D_2 \leftarrow ^7F_0$ transition.

modifiers. Network formers are considered to form the glass structure through an interconnection of network polyhedra. Network modifiers, on the other hand, usually break the periodicity by taking up interstitial spaces between polyhedra of network formers. These natures are due to the difference in ionic sizes and bonding characters. Usually recognized for network formers are a moderately high covalency of M-O bond with a large single bond strength and a low coordination state of M ion. Both features contribute to the higher frequency of stretching vibration detectable in IR or Raman spectra. Accordingly, the phonon mode with the highest frequency in oxide glasses generally corresponds to the stretching vibration of network formers. Therefore, to gain longer lifetime or higher quantum efficiency of the excited levels with a small energy gap by suppressing the nonradiative loss, it is disadvantageous to select conventional oxide glasses as a host of rare earth ions.

In addition to the oxide systems, the highest frequency mode can contribute to the multiphonon relaxation of rare earth ions also in mixed anion systems. Direct evidence for the preferential coupling of the oxide ions to rare earth ion was confirmed for fluorophosphate glasses by the increased isomer shift in ^{151}Eu Mössbauer spectroscopy and the phonon sideband, in which the coupling of $P\text{-}O^-$ stretching vibration is shown. This is revealed in Chap. 3.4.

3.2. PHONON SIDEBAND AND LOCAL STRUCTURE OF Eu^{3+} IN BORATE GLASSES

I. INTRODUCTION

The knowledge of the local structure around rare earth ions in oxide glasses is important not only in interpreting their optical properties but also in designing new types of glasses. For example, the relationship between local structure and fluorescence properties of oxide glasses containing rare earth ions has been investigated widely from the viewpoint of making new laser glasses or phosphors[5-7]. For Eu^{3+} ions, as the energy gap of $^5D_0$-^7F_J (J=0~6) is much larger than those of $^5D_{J+1}$-^5D_J (J=0~3), the multiphonon relaxation process is predominant between the ^5D_J levels and radiative emission occurs mainly from the $^5D_0$ level in most oxide hosts of higher phonon energy. Also, the phonon sideband (PSB) can be clearly observed in the higher energy side of $^5D_2 \leftarrow ^7F_0$ transition, and thus Eu^{3+} ion can become a good probe[8]. In Fig.1 shown is an example for $50SiO_2$ $25Al_2O_3 \cdot 25La_2O_3 \cdot 1Eu_2O_3$ glass. Certainly, the PSB is clearly observed around 445 nm, due to Si-O-Al stretching vibration coupled with Eu^{3+} ion in the glass[9]. These bridging oxygen atoms in Si-O-Al bonds can be considered to coordinate Eu^{3+} ion, which was found to take coordination number higher than eight in the glass by ^{151}Eu Mössbauer spectroscopy[10]. Thus it is interesting to investigate the local structure around rare earth ions in glasses by the phonon sideband spectra. Among several oxide glasses, it is known phenomenologically that the Eu^{3+}-doped

borate glasses, where the coordination number of boron atom changes from 3 to 4 with alkali content[11], show the corresponding change of the fluorescence spectra of the $^5D_0 \rightarrow {}^7F_0$ transition[5]. Namely, the inhomogeneous linewidth of fluorescence spectrum varies with the amount of Na_2O, having the maximum value around 20 mol% Na_2O, although the resonant homogeneous linewidth excited by a dye-laser shows a monotonous dependence on them.

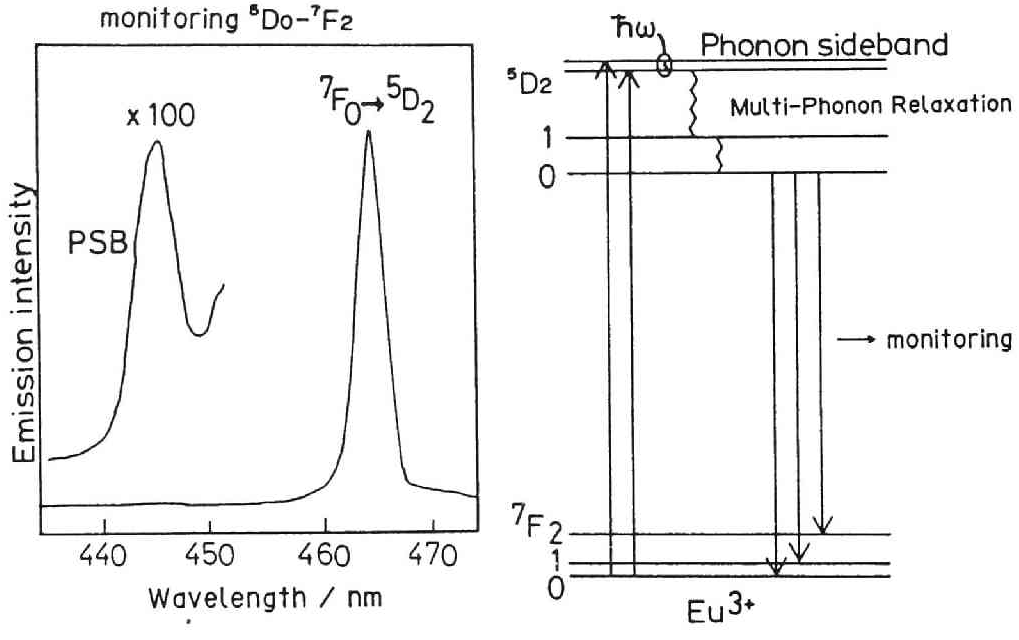

Fig.1: Energy level and phonon sideband of Eu^{3+} ion in $50SiO_2 \cdot 25Al_2O_3 \cdot 25La_2O_3 \cdot 1Eu_2O_3$ glass.

However, few information on the local structure of borate glass has been obtained about the ligand of the doped fluorescent ions, while the structure of undoped alkali borate glasses has been well established by NMR[12,13] and Raman spectroscopy[14]. In addition, it is necessary to know the short range ligand structure of fluorescent ions in order to predict the nonradiative decay rate due to the multiphonon relaxation[2] as well as its mechanism.

Therefore in this study, the excitation spectra for the B_2O_3-Na_2O glasses containing 1 mol% of Eu_2O_3 were measured. Especially, the phonon sideband associated with the $^5D_2 \leftarrow ^7F_0$ transition was investigated precisely in order to get the information about the compositional dependence of the phonon energy and electron-phonon coupling strength relating with the nonradiative decay of Eu^{3+} ions. From these studies, it is possible to know the local structure around Eu^{3+} ions in glasses[9,10], which cannot be detected by the usual IR absorption or Raman scattering method, which are for the bulk measurement.

II. EXPERIMENTAL

The excitation spectra of the glass samples were measured with Hitachi-850 Fluorescence Spectrophotometer, monitoring the $^5D_0 \rightarrow ^7F_2$ emission at 612 nm as a fixed wavelength. The phonon sideband associated with the $^5D_2 \leftarrow ^7F_0$ transition was multiplied by a factor of 100 in the wavelength range of 430~450 nm. The spectra obtained were analyzed by the least-square fitting program, Gaussian curves being assumed. From these analysis, the

electron-phonon coupling strength can be evaluated as the ratio of integrated intensity of the phonon sideband to that of the pure electronic transition[12]. Also, the phonon energy can be obtained from the energy difference between two peak positions.

III. RESULTS

The excitation spectrum of glass specimen(x=20) was shown in Fig.2, where the emission intensity of $^5D_0 \rightarrow {}^7F_2$ at 612 nm was taken as the ordinate. The pure electronic transition of $^5D_2 \leftarrow {}^7F_0$ can be seen around 465 nm, the line shape of which was almost

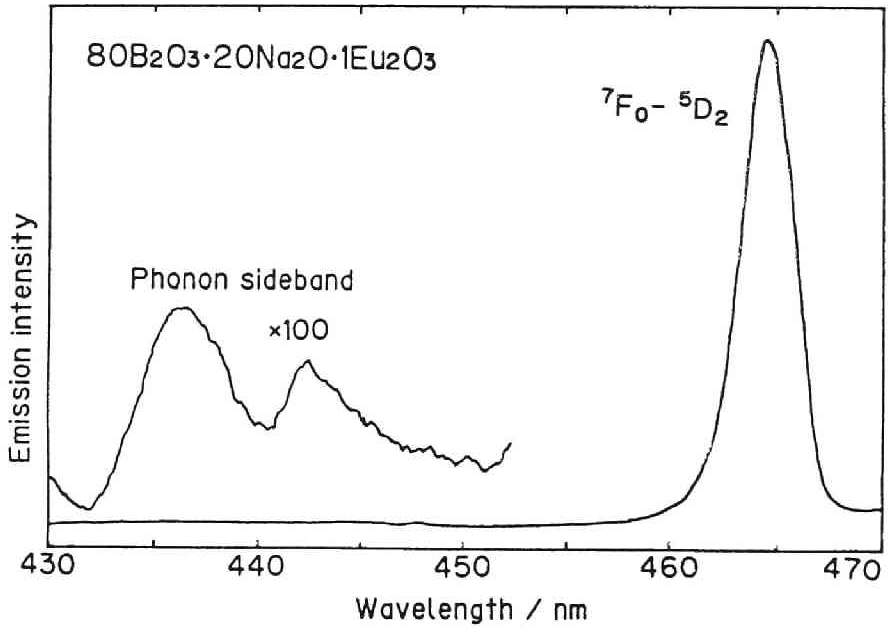

Fig.2: Excitation spectrum of $80B_2O_3 \cdot 20Na_2O \cdot 1Eu_2O_3$ glass.

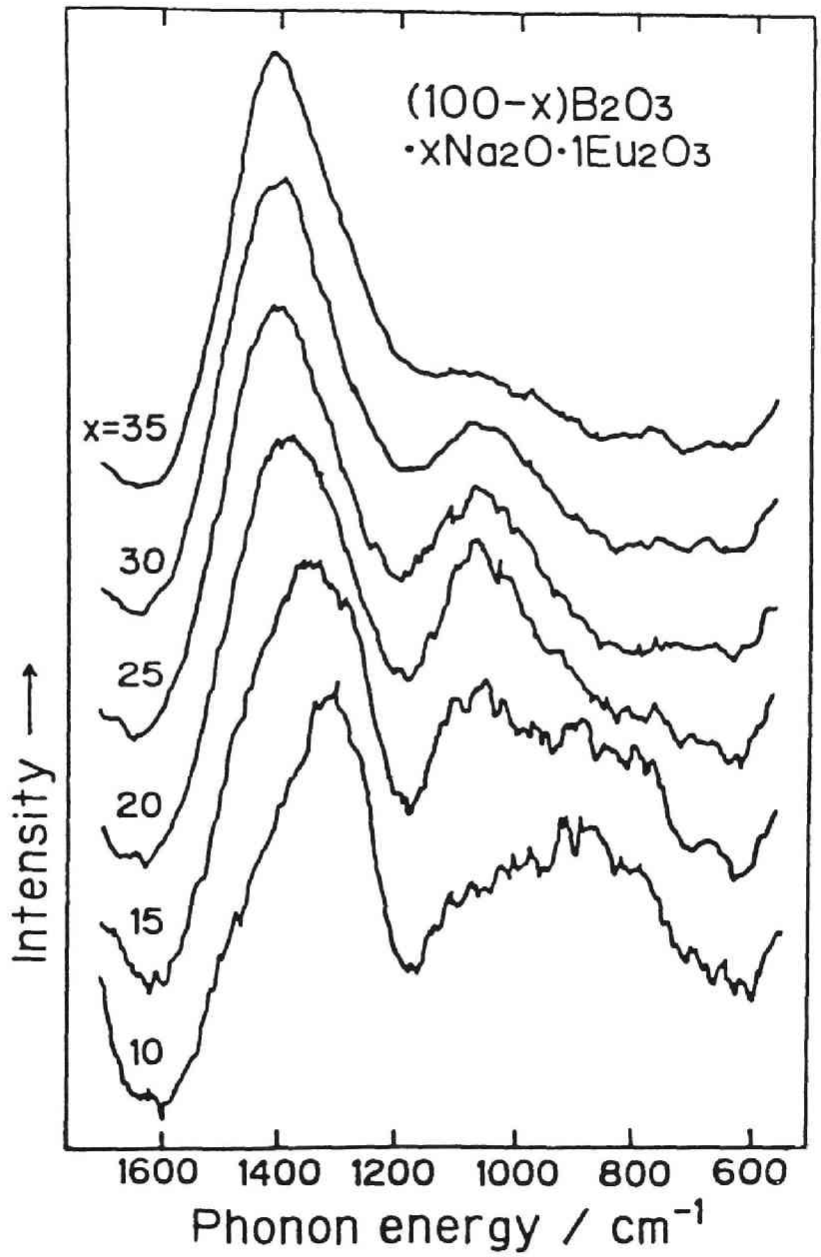

Fig.3: Compositional variation of phonon sideband of Eu^{3+} ion for $(100-x)B_2O_3 \cdot xNa_2O \cdot 1Eu_2O_3$ glasses.

symmetrical singlet and not so changed with Na_2O content. The phonon sideband is observed around 435~450 nm, which is multiplied by 100 times. It can be seen that the shape and position of PSB in Fig.2 were quite different from those for the $50SiO_2 \cdot 25Al_2O_3 \cdot 25La_2O_3 \cdot 1Eu_2O_3$ glass shown in Fig.1. That is, the phonon energy varied in the range of 600~1600 cm^{-1} and the spectrum was composed of several bands in borate glasses, while the peak was almost singlet at 910 cm^{-1} in the lanthanum aluminosilicate glass. The compositional variation of the PSB for the $(100-x)B_2O_3 \cdot xNa_2O \cdot 1Eu_2O_3$ glasses is shown in Fig.3, where the abscissa is converted to the phonon energy in wavenumber with respect to the center of gravity of the pure electronic transition for simplicity in comparison. The largest band around 1400 cm^{-1} shifted to a higher frequency side with increasing Na_2O content, while the weak broad bands in the lower wavenumber side became small with changing their line shape and apparent peak positions.

IV. DISCUSSION

A. *Phonon energy*

In order to make an assignment for each sideband to the corresponding vibrational mode, the bands of IR and Raman spectra were employed. In IR spectra of borate glasses, the bands of BO_3 stretching mode are present at the highest frequency, ranging from 1350~1400 cm^{-1} to 1420~1550 cm^{-1}. The former is assigned to B-O vibrational mode inside the various borate rings and the latter to nonbridging $B-O^-$ bonds, respectively[13]. Table 1 shows the assignment of these bands[13,16]. Their characteristic

bands listed in Table 1 were taken into account and the frequency was used as the initial value of the fitting. The analytical results of the phonon sideband for the present glasses (x=10, 35) are shown in Fig.4. It is clear that the largest band is composed of two peaks. The smaller band at higher energy side is considered to correspond to the $B-O^-$ mode and the larger band at lower energy side to the B-O mode. It is known that the $B-O^-$ nonbridging oxygen can not exist in Eu^{3+}-undoped alkali borate glasses where the alkali content is less than 29 mol%[16].

Table 1: Assignments of bands present in spectra.

Peak position/cm^{-1}	Assignment	Spectroscopy
1420-1550	$B-O^-$ bond	IR
1350-1400	B-O bond	IR
1120	diborate group	Raman
1050	tetraborate group	IR
900-1000	diborate group	IR
880	tetraborate group	IR
805	boroxol ring	Raman
770	tetraborate group	Raman
690-770	B-O-B bending	IR

However, the peak due to the $B-O^-$ mode can be seen in the (a)x=10 sample. Thus the $B-O^-$ bonds are coupled with Eu^{3+} in the doped glasses. Therefore, by analyzing the PSB in this study, it was suggested that the $B-O^-$ bonds were present only around Eu^{3+} ions

in Eu^{3+}-doped alkali borate glasses and contributed to its nonradiative decay. The compositional variation of electron-phonon

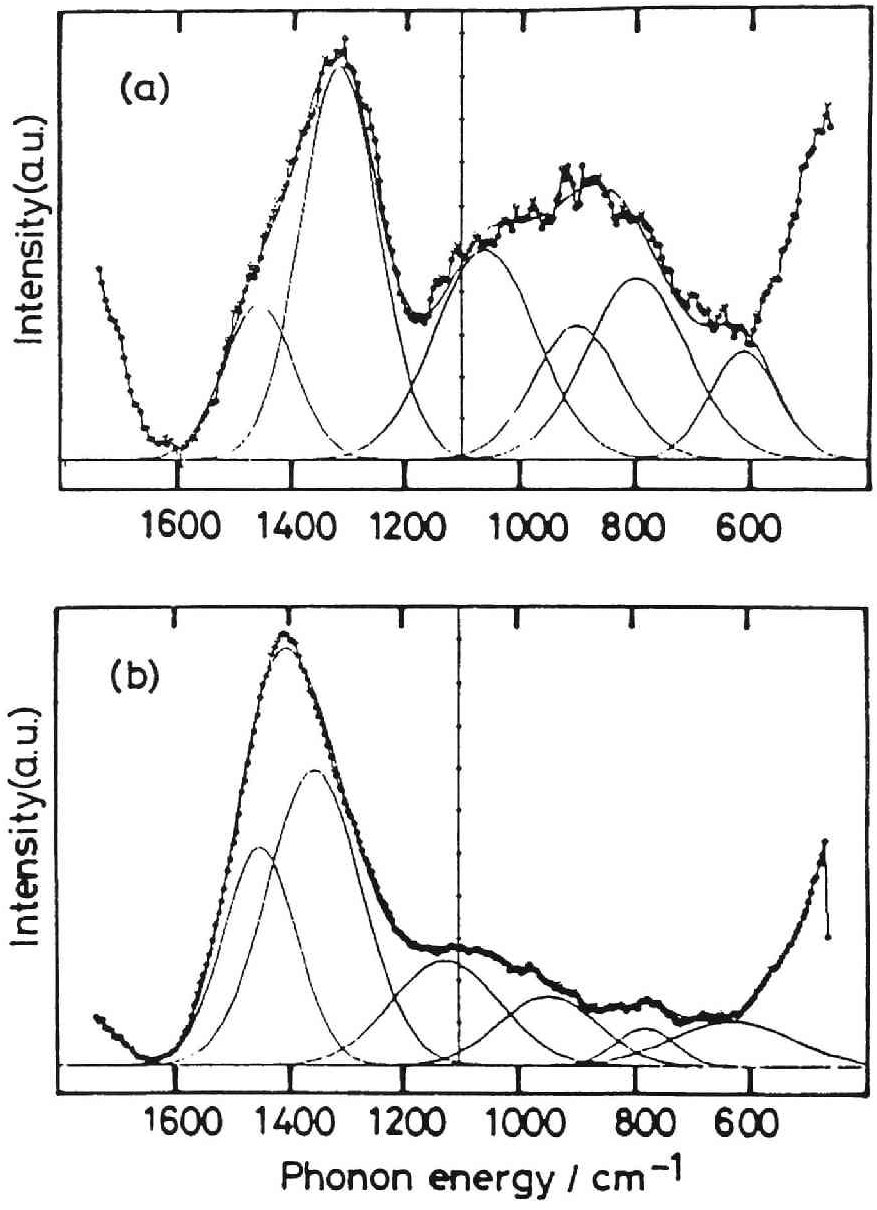

Fig.4: Examples of analysis of phonon sideband of Eu^{3+} ion for (a)$90B_2O_3 \cdot 10Na_2O \cdot 1Eu_2O_3$ and (b)$65B_2O_3 \cdot 35Na_2O \cdot 1Eu_2O_3$ glasses.

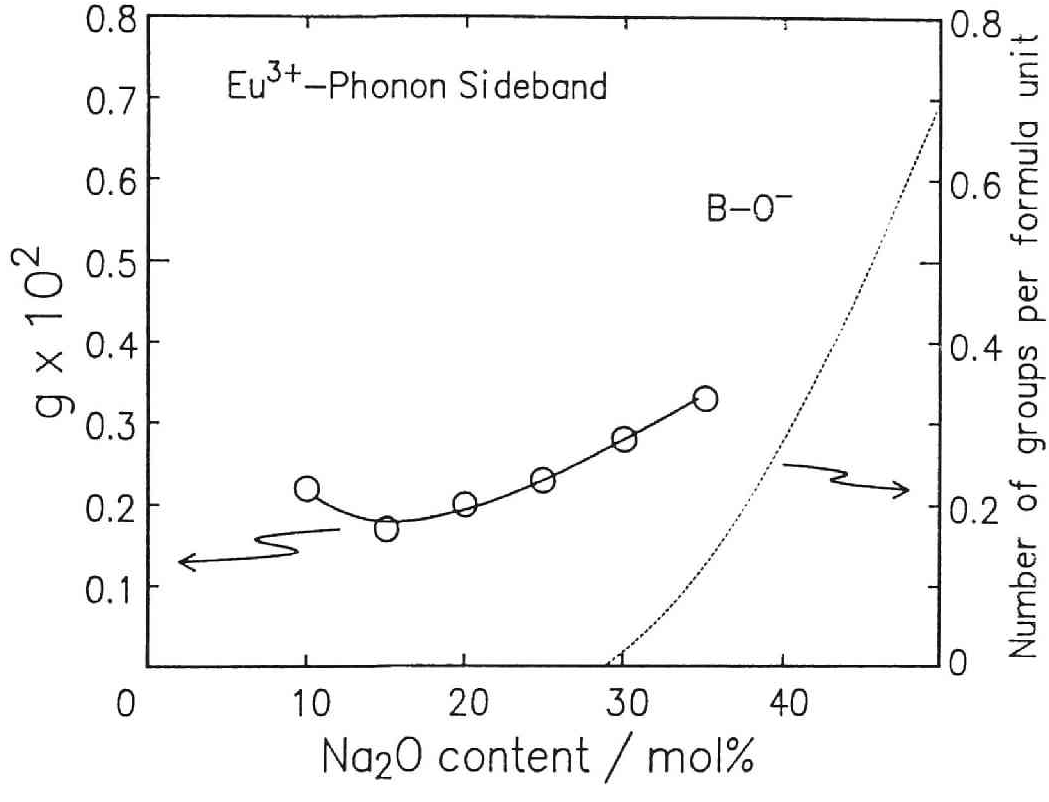

Fig.5: Electron-phonon coupling strength of $B\text{-}O^-$ stretching modes as a function of Na_2O content.

coupling strength of $B\text{-}O^-$ bonds is plotted in Fig.5. The increase of g in larger x region shows that the contribution of

$B\text{-}O^-$ bond is enhanced by the nonbridging oxygen which drastically increase in number at more than 29 mol% Na_2O. A larger g value of $B\text{-}O^-$ at x=10 indicates that the $B\text{-}O^-$ bonds formed by an introduction of Eu_2O_3 itself dominantly coordinate instead of a large number of boroxol rings. In addition to the $B\text{-}O^-$ bonds, there existed several peaks due to other vibrational modes. The compositional variation of various borate groups present in B_2O_3-Na_2O glasses has been already reported [13,16] and according to the references, both boroxol rings and tetraborate groups exist mainly at x=0~20, while tetraborate and diborate groups exist at x=20~35. It is shown that not only IR-active modes but also Raman-active one could be revealed in the PSB spectra. For example, the band of 805 cm^{-1} assigned to the boroxol rings, which is Raman-active but completely IR-inactive, could be clearly detected in the phonon sideband spectra for glass samples of x=10 and 15. The band of 1120 cm^{-1} assigned to the diborate groups[13], which is weakly Raman-active, could be also observed in the phonon sideband spectra for x=25~35. On the other hand, the band of B-O vibrational mode in borate rings around 1350 cm^{-1}, which is Raman-inactive but IR-active, could be also detected. Therefore, it can be concluded that by using the PSB spectra, even either IR-inactive or Raman-inactive modes can be detected simultaneously. Also, this fact is a clear evidence that the multiphonon relaxation can occur by means of both kinds of optical phonons.

B. *Electron-Phonon Coupling Strength*

In Fig.6, the electron-phonon coupling strengths obtained by

the integrated intensity of PSB of the present glasses are shown as a function of Na_2O content. The total value of g decreased rapidly around 15 mol% with increasing Na_2O content. It may be correlated with the structural change of the glass. As the wavenumber of vibrational modes are characteristic to the kind of borate groups, it was possible to assign some bands to one of the borate group. In Fig.7, the electron-phonon coupling strength of several modes obtained from the analyses of phonon sideband spectra was plotted for boroxol rings, tetraborate and diborate groups as a function of Na_2O content. Also shown by the dashed line is the number of each group per formula unit in the undoped glasses[17]. It can be seen that the coupling strength, g of each mode is related to the fraction of groups present in the glass. The boroxol rings existed in the range of $x<20$ and the diborate groups appeared at $x>20$. The values of them were changing almost consistently with their number of groups per formula unit. However, the g of the tetraborate groups did not correspond to the real fraction. For example, in the lower x region, in spite of a number of boroxol rings much more than that of the tetraborate groups, the electron-phonon coupling strength of the former is smaller than that of the latter. In order to explain this discrepancy, the feasibility of coordination to Eu^{3+} should be taken into account. One interpretation is due to the different affinity to Eu^{3+} ion between two groups. In fact, since the largest peak of tetraborate group at 1050 cm^{-1} is assigned to BO_4 stretching vibration[13], it is probable that the BO_4^- of negative charge can preferentially coordinate to Eu^{3+} ion to neutralize its positive charge. On the other hand, the boroxol ring

does not have the formal negative charge and thereby it has less tendency of coordination to Eu^{3+} ions. The site preference of Eu^{3+} in glasses is considered to be influenced by the chemical affinity of structural unit and its fraction present in glass.

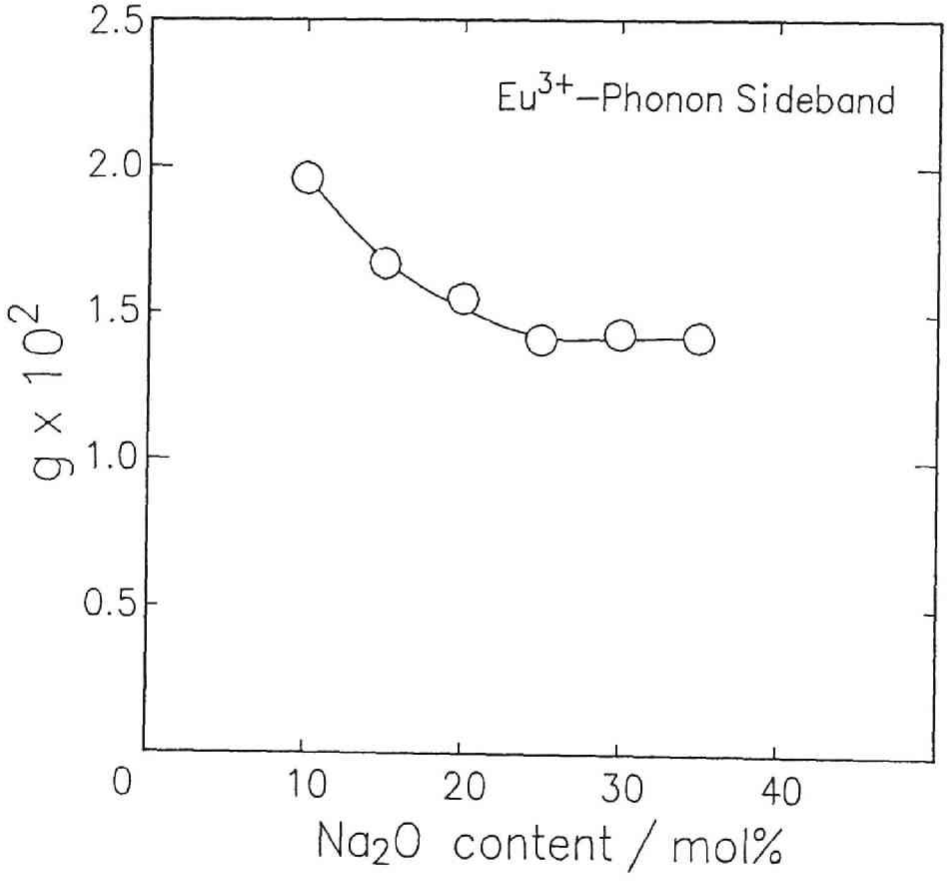

Fig.6: Electron-phonon coupling strength of total vibrational modes as a function of Na_2O content.

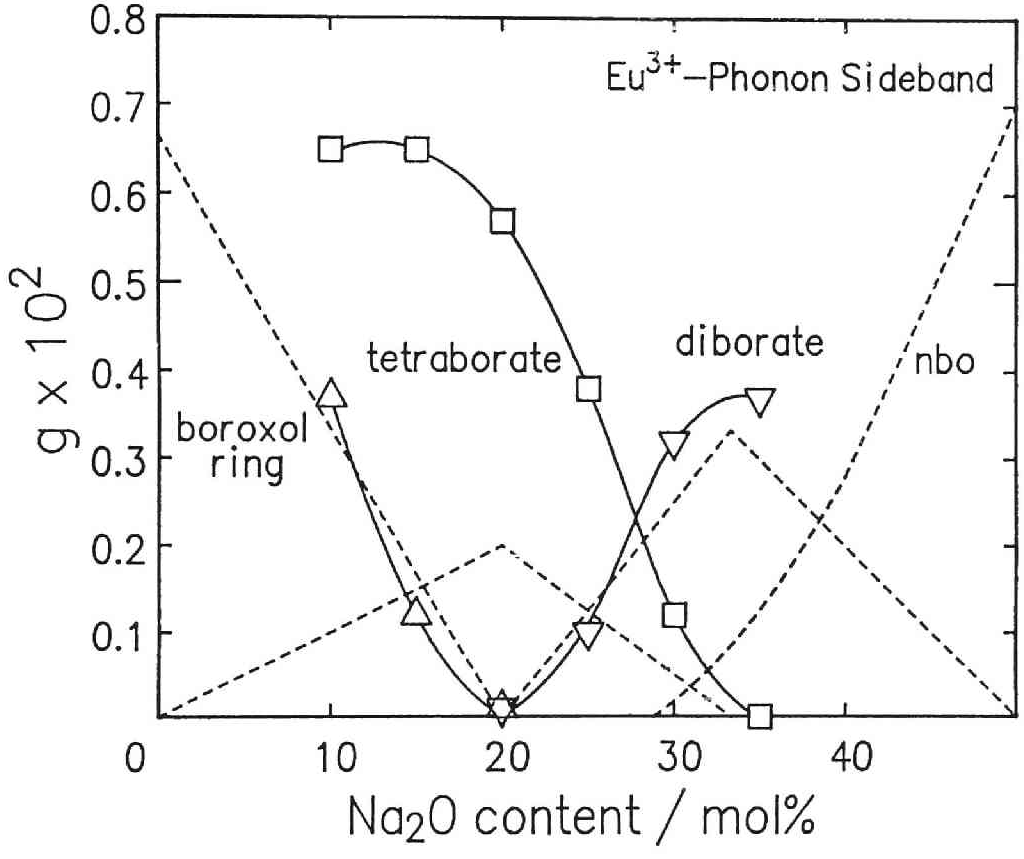

Fig.7: Compositional variation of electron-phonon coupling strength of borate groups: The dashed lines show the number of groups per formula unit[17].

Thus, the *g* value can be a measure of the chemical affinity to Eu^{3+} ions in borate glasses, because the fraction of each structural unit has already been well established[18] and can not be

so different as a whole by 1 mol% doping. The g of tetraborate groups is constantly larger than that of boroxol rings in the range of x=10~20, where the number of tetraborate groups increases with increasing Na_2O content. Around 15 mol% Na_2O, the g of tetraborate groups begins to decrease and in the larger x region than 20 mol%, it becomes small and the diborate group begins to appear instead. However, since $B\text{-}O^-$ bonds are also formed in this compositional range and they have a strong tendency of coordination to Eu^{3+} ion, it can be said that the electron-phonon coupling strength of diborate groups can not become so large compared with the actual number of diborate groups in the glass. Thus, Eu^{3+} ions can preferentially select a certain stable site of negative charge rather than be randomly distributed in the average matrix.

V. CONCLUSIONS

The phonon sideband (PSB) of Eu^{3+} associated with the $^5D_2 \leftarrow {}^7F_0$ transition was investigated for the B_2O_3-Na_2O glasses doped with 1 mol% Eu_2O_3. It was found that the phonon mode coupled with Eu^{3+} ions in the glasses, assigned to those in IR or Raman spectra, was almost consisting of $B\text{-}O^-$ or B-O stretching vibration of BO_3 units and vibrations of BO_4^- units in tetra- and diborate groups. The results showed that $B\text{-}O^-$ bonds present around Eu^{3+} ion, which has the highest phonon energy, contributed to the nonradiative decay due to the multiphonon relaxation of Eu^{3+} ions even in alkali-poor borate glasses. Moreover, the electron-phonon coupling strength of each borate group was found to be influenced not only by its fraction present in glasses but

also by the site selectivity of Eu^{3+} ion to them. This discrepancy could be interpreted in terms of the different chemical affinity of groups and site-preference of Eu^{3+} ion. Among borate groups, the tetraborate groups had the tendency to dominantly coordinate Eu^{3+} ion compared with other groups, such as boroxol rings and diborate groups.

3.3. PREPARATION AND OPTICAL PROPERTIES OF SINGLE CRYSTALLINE AND AMORPHOUS HUNTITE $EuAl_3(BO_3)_4$

I. INTRODUCTION

Self-concentration quenching by ion-ion interaction reduces the efficiency of most rare earth based luminescent materials because the nonradiative decay process occurs due to the electric-dipole coupling between rare earth ions[19]. Thus, in most glass systems doped with luminescent ions such as Nd-doped oxide glasses, the maximum content of Nd^{3+} ions is usually limited to much less than ~5 mol%. On the other hand, in some kinds of phosphate glasses, a large amount of rare earth ions can be doped as a main component of glass composition without the concentration quenching such as $Eu(PO_3)_3$[19]. The rare earth aluminoborate crystal, $LnAl_3(BO_3)_4$ [20,21] is a highly concentrated rare earth crystal in stoichiometry along with $Ln_3Al_5O_{12}$[22], $Li_6Ln(BO_3)_3$ [23,24] and $LnMgB_5O_{10}$[25]. This crystal structure is isomorphous with huntite $CaMg_3(CO_3)_4$ [26]. Among the rare earth huntite groups, $NdAl_3(BO_3)_4$ is known as a minilaser device (NAB) utilizing the fluorescence of the $^4F_{3/2} \rightarrow {}^4I_{11/2}$ transition of Nd^{3+} ion[27]. In addition to the benefit of unusual weak self-concentration quenching in these crystal groups, the possibility of glass formation in this system is of interest, because it contains a large amount of network-forming compounds such as B_2O_3 and Al_2O_3. Thus it is attractive to investigate the fluorescence property of the glassy state, which is surely expected to accom-

pany the structural change, under the same composition as that of crystal.

In the present section, a single crystal of $EuAl_3(BO_3)_4$ huntite was prepared by the usual flux method and its fluorescence property was examined. In this structure, the $^5D_0 \rightarrow {}^7F_0$ transition of Eu^{3+} ion is forbidden due to the site symmetry of D_{3h}[22]. In order to investigate the effect of glass formation on the structure and fluorescence property, an amorphous thin film was also prepared by the twin-roller quenching method. The coordination numbers of Eu^{3+} and Al^{3+} ions were also investigated by the ^{151}Eu Mössbauer and Al$K\alpha$ emission spectra, respectively.

II. EXPERIMENTAL

A single crystal was obtained by using the Li_2O-B_2O_3 flux method, which was reported for $NdAl_3(BO_3)_4$ elsewhere[28]. The composition shown in Table 1 was melted in a platinum crucible at 1200 °C for 2h and the melt was slowly cooled at a rate of 10 K/h down to 500 °C. The solid obtained was etched with 0.1N HCl aqueous solution to avoid the lithium borate flux. The X-ray diffraction analysis was carried out to confirm the formation of a pure phase in the powder form.

The glassification of this crystal was conducted by using the twin-roller super cooling method. The rollers rotate themselves at a rate of about 1000 rpm. The glassy phase was confirmed by XRD. The glass transition temperature, T_g was determined by differential thermal analysis(TG-DTA 8112-BH, *Rigaku Denki Co. Ltd.*, Tokyo, Japan) in a powder form with a heating

rate of 10 °C/min.

Table 1: Compositional ratio of flux

Source	Ratio
Eu_2O_3	1
Al_2O_3	3
Li_2CO_3	2
B_2O_3	6.44

Fluorescence and excitation spectra of the crystalline and amorphous sample were measured with a *Hitachi-850* Fluorescence Spectrophotometer. The excitation source was a Xe-lamp and the wavelength was 394 nm, which corresponds to the Eu^{3+}: $^5L_6 \leftarrow ^7F_0$ transition.

The ^{151}Eu Mössbauer measurement was carried out by using $^{151}Sm_2O_3$ (5mCi) as a 21.6 keV γ-ray source. The velocity calibration was done with the spectrum of α-Fe by the $^{57}Co(Rh)$ source, and the isomer shift was determined with respect to that of EuF_3. In order to investigate the coordination number of Al^{3+} ions accompanied with the structural change, the chemical shift of Al$K\alpha$ emission was determined with X-ray probe microanalyzer (*Model ARL EMX-SM, Shimadzu-Seisakusho*, Kyoto, Japan). The chemical shift was calculated in wavelength with respect to that of the emission peak for metallic Al.

III. RESULTS AND DISCUSSION

The photograph of the single crystal obtained is shown in Fig.1. The crystals obtained were hexagonal rod in shape and pinkish in color with transparency. From XRD, no impurity phase was observed and all the peaks could be assigned to $EuAl_3(BO_3)_4$ huntite crystal. The DTA curve is shown in Fig.2. The glass transition was clearly observed around 730 °C as an endothermal step and crystallization temperature, T_{cr} of the first exothermal peak was 830 °C. This value of T_g is much higher than that of other borate glasses, which is probably due to the absence of a monovalent network modifier such as alkali-metal ions.

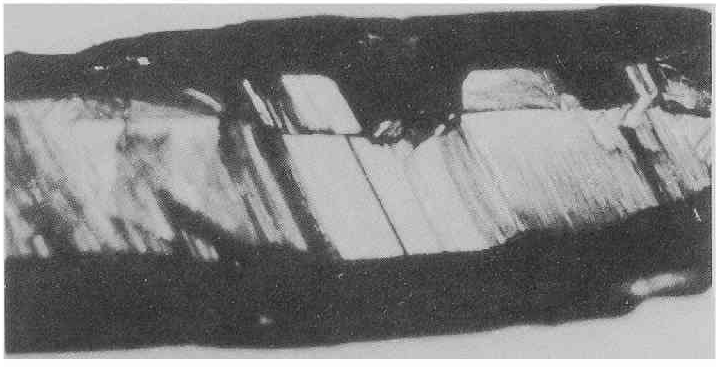

Fig.1: $EuAl_3(BO_3)_4$ single crystal prepared by the flux method.

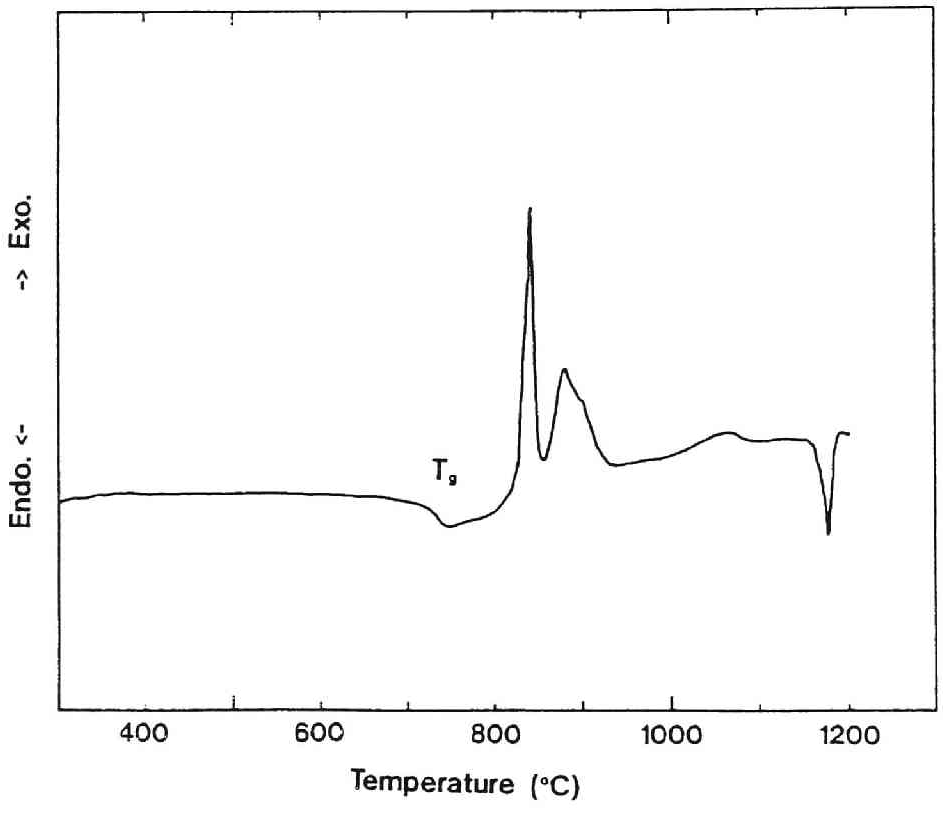

Fig.2: DTA curve of amorphous sample.

Fluorescence spectra of the crystalline and amorphous sample are shown in Fig.3. For the crystal sample, the spectrum was the same as that reported elsewhere[21]. The $^5D_0 \rightarrow {}^7F_0$ transition around 580 nm was not observed, since this transition is forbidden for Eu^{3+} ions at D_{3h} symmetry as in $EuAl_3(BO_3)_4$[21] and $YAl_3(BO_3)_4:Eu^{3+}$ huntite structures[29]. On the other hand, this

emission line was clearly observed for the glass sample. This phenomenon can be ascribed to the change in the site symmetry of each Eu^{3+} site from crystalline to glassy state. The splitting of $^7F_1$ and $^7F_2$ states became large due to the crystal field Stark splitting but the fine structure could not be clearly observed because of site-to-site variation characteristic of the amorphous state.

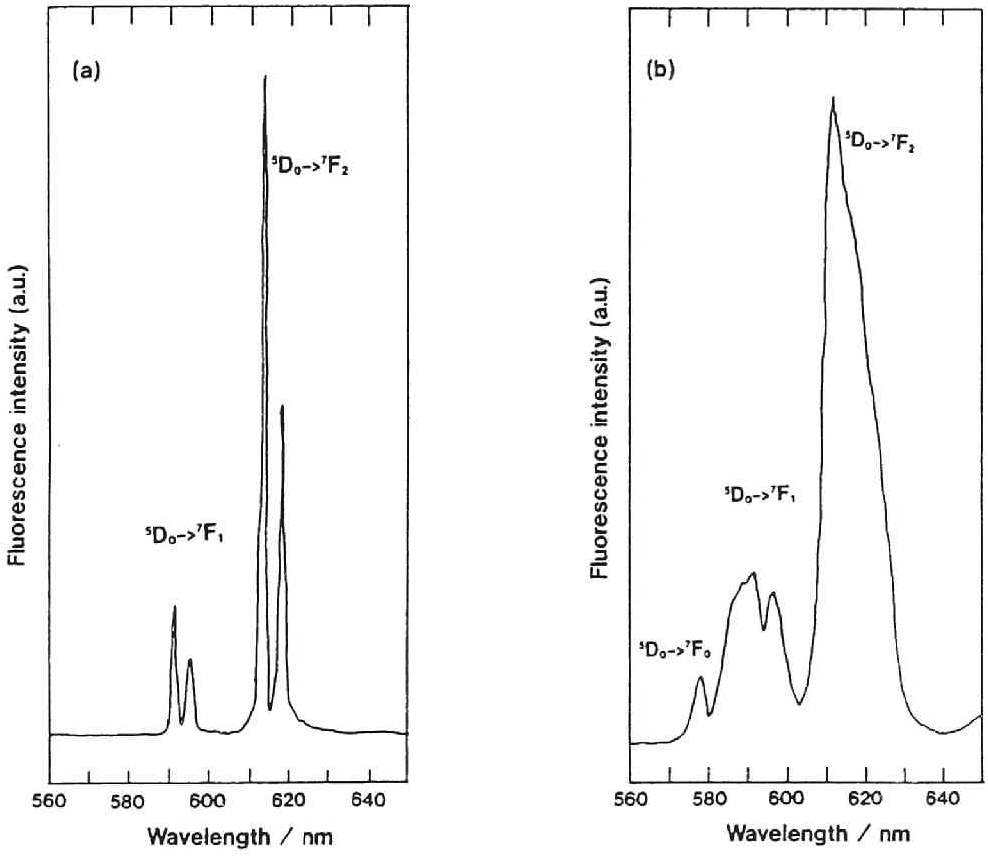

Fig.3: Fluorescence spectra of (a)crystal and (b) amorphous sample.

In Fig.4, the ^{151}Eu Mössbauer spectra of crystalline and glass samples are shown. From Fig.4, it can be seen that no Eu^{2+} ion (IS ~ -12 mm/sec) was formed and the linewidth of the absorption peak due to Eu^{3+} ions became large for the glass sample. This line broadening can be due to the formation of site variation and to the increase of the electric field gradient at ^{151}Eu nuclei in a random glass structure. The isomer shift, IS of Eu^{3+} ions in the glass sample was 0.30 mm/sec, while that of huntite crystal was 0.70 mm/sec. According to the previous study concerning about the relationship between IS and coordination numbers (CN=6,8,9,12) of Eu^{3+} ion in various oxide crystals[10], IS of Eu^{3+} ion can be a measure of the coordination number. For example, the IS of C-Eu_2O_3 (CN=6) was 1.07 mm/sec and that of $EuAlO_3$ (CN=12) was 0.52 mm/sec. Thus, it is suggested that the coordination number of Eu^{3+} ions in glass sample increases up to 12.

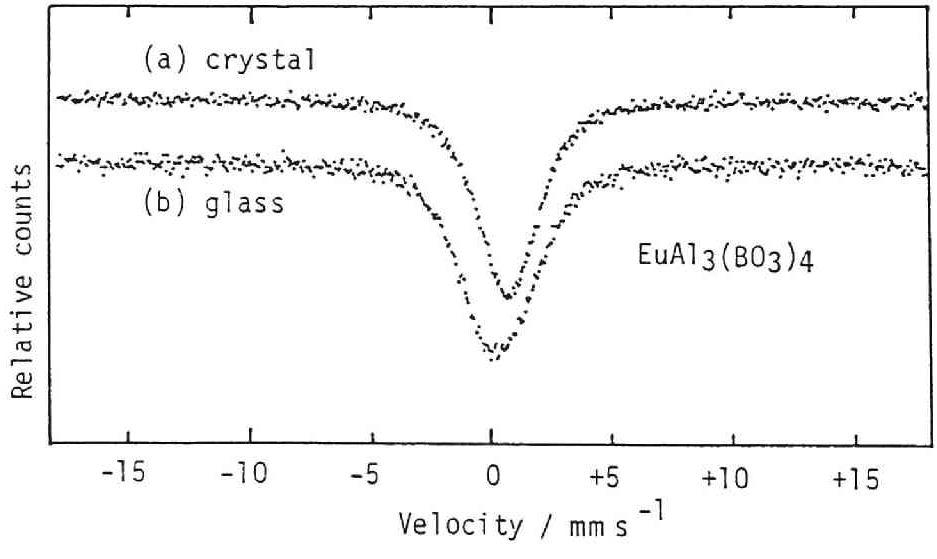

Fig.4: The ^{151}Eu Mössbauer spectra of (a)crystal and (b) amorphous sample.

The results of Al$K\alpha$ emission are shown in Table 2 together with the chemical shifts of α-Al_2O_3, amorphous-Al_2O_3 and mullite crystal. It can be seen that the chemical shift of the single crystal corresponds to that of the six-folded state, while that of the glass sample to that of the mullite crystal, where the average coordination number of Al^{3+} ions is 4.8. The change of the chemical shift in the same composition was -11×10^{-5} nm. This change in chemical shift is much larger than that for Al_2O_3 (-3×10^{-5} nm) in which the average coordination number of Al^{3+} changed from 6 to 5 with amorphous formation by rf-sputtering [30]. Therefore, the coordination number of most Al^{3+} ions in the present system is considered to decrease from 6 to 4 by glassification. These four-folded Al^{3+} ions probably contribute to the network formation along with B^{3+}, while the Eu^{3+} ions work as the network modifier, taking higher-folded states.

Table 2: Chemical shift of Al Kα emission.

Sample	Coordination Number	Chemical shift (10^{-5}nm)
$EuAl_3(BO_3)_4$		
crystal	6	27
amorphous	?	16
α-Al_2O_3	6	20
v-Al_2O_3*	5	17
Mullite	4.8(3tet.+ 2oct.)	16
K-feldspar	4	11

*: Prepared by rf-sputtering[30].

The excitation spectra of the crystal and glass are shown in Fig.5(a) and (b), respectively. At higher energy side of the $^5D_2 \leftarrow {}^7F_0$ electronic transition, the phonon sideband[31] can be observed. The phonon energy, which can be obtained as the energy difference between those peaks, was 1290 cm^{-1} for the crystal. This energy is exactly equal to that of the stretching vibration of BO_3^{3-} orthoborate group[14]. This high energy phonon reduces the fluorescence lifetime by a rapid multiphonon decay process as in the $NdAl_3(BO_3)_4$[21]. By glassification, although the highest energy phonon did not change drastically, the electron-phonon coupling strength, which is the intensity ratio of the phonon sideband to that of pure electronic transition, decreased drastically from $5x10^{-2}$ to $6x10^{-3}$. In the glass, the chemical bonding with the highest phonon energy is considered to be still ^{3}B-O, although the CN change of some B atoms might occur from 3 to 4 accompanied with the CN change of Al^{3+} and Eu^{3+}. However, it is plausible that the network modifying Eu^{3+} is placed near the nonbridging oxygen of ^{3}B-O$^-$. Therefore, the phonon energy coupled with the multiphonon relaxation can be still about 1300cm^{-1} of ^{3}B-O rather than ^{4}B-O with lower phonon energy (~ 1100 cm^{-1}). As mentioned above, the electron-phonon coupling strength changed with structural change. This can be ascribed to two reasons. One is the decrease in the number of three-folded boron atoms, which generates a decrease of the number of the ^{3}B-O bond. Another is the decrease of the mean free path of the phonon in amorphous structures. Further study is needed to clarify the structure of this amorphous as well as the electron-phonon coupling of rare earth ions.

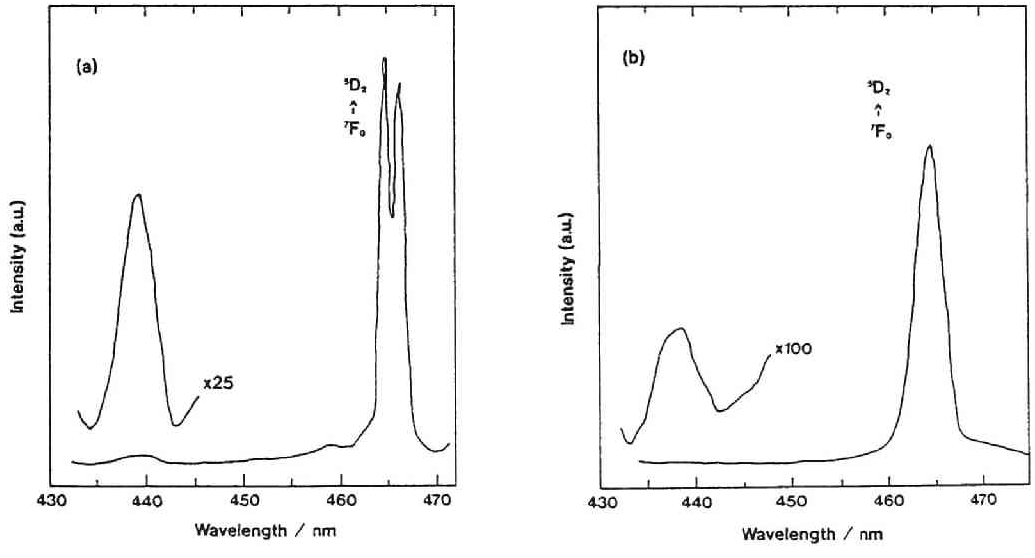

Fig.5: Excitation spectra of Eu^{3+}:$^5D_0 \rightarrow {}^7F_2$ emission: (a)crystal and (b)amorphous sample. The phonon sideband associated with $^5D_2 \leftarrow {}^7F_0$ electronic transition is observed at higher energy side.

V. CONCLUSIONS

A single crystal and an amorphous solid of $EuAl_3(BO_3)_4$ were prepared and their fluorescence properties were compared each other. It was found that the $^5D_0 \rightarrow {}^7F_0$ transition in the amorphous state, which is forbidden for Eu^{3+} ions at D_{3h} symmetry in the huntite crystal structure, was allowed and a decrease of the ligand field symmetry around Eu^{3+} ion was suggested with the glass formation. The results of ^{151}Eu Mössbauer effect and Al$K\alpha$ emission spectroscopy showed that the coordination number of Eu^{3+} ions increased from 9 to 12 and that of Al^{3+} ions almost decreased from 6 to 4 by glassification. The increase of the linewidth of both the fluorescence and Mössbauer spectra could be attributed to the site variation and ligand asymmetry of Eu^{3+} ions in the glass of this system.

3.4. LOCAL STRUCTURE AND NONRADIATIVE DECAY OF Eu^{3+} IONS IN FLUOROPHOSPHATE GLASSES

I. INTRODUCTION

The local structures of rare earth ions in fluoride glasses are of great research interest for new phosphors and lasers[32-34]. One of the superior points of the fluoride hosts to the oxide hosts is their lower phonon energies, which lead to the reduction of nonradiative loss due to multiphonon relaxation[35]. However, in oxide systems, the highest energy phonons of network former can play the major role in the multiphonon relaxation because they can conserve the energy gap in the lowest-order process[1]. The material research for new functional glass devices is very important objectives in the field of optoelectronics. For laser applications, the fluorophosphate glasses are attractive in terms of their small refractive index nonlinearity[36]. One of the main interests from the viewpoint of material design of oxyfluoride optical device is in the coordination states and multiphonon relaxation mechanisms of fluorescent ions in the mixed-anion host. In this section, an AlF_3-based fluoride glass was chosen as a host and the effect of substitution for $AlPO_4$ on the fluorescence properties of Eu^{3+} ion was investigated. Since it is known that the probability of the multiphonon process is dominated by the lattice phonon[4], the phonon sideband associated with Eu^{3+}: $^5D_2 \leftarrow {}^7F_0$ transition was measured to get the information about the phonon modes coupled with rare earth ions. Also, compositional variations of ^{151}Eu Mössbauer parameters were

obtained to investigate the state of anion coordination to rare earth ions.

II. EXPERIMENTAL

The compositions of the glasses are expressed by (50-x-y) $AlF_3 \cdot xAlPO_4 \cdot yEuF_3 \cdot 30CaF_2$ $20BaF_2$. This system was selected because the fluoride melt with the composition of $50AlF_3 \cdot 30CaF_2$ $20BaF_2$ can be vitrified by pressing it with two iron plates in the absence of BeF_2 or ZrF_4[37,38]. Furthermore, the glass-forming ability is not suppressed by addition of substantial amounts of LnF_3 and $AlPO_4$.

Glasses were prepared by using reagent grade AlF_3, $AlPO_4$, EuF_3, CaF_2 and BaF_2. For pure fluoride glasses, a small amount of $NH_4F \cdot HF$ was also added to the batch. The batch materials were well mixed in an alumina mortar and was melted in a platinum crucible with a cover at 900~1100 ˚C. The melt was poured on a stainless steel plate and was pressed with another plate.

The fluorescence and excitation spectra were measured with a Hitachi-850 Fluorescence Spectrophotometer. A Xe-lamp were used as the excitation source of fluorescence measurement, in which the 394nm-band due to $^5L_6 \leftarrow {}^7F_0$ transition was excited. In the excitation spectra of Eu^{3+}, the $^5D_0 \rightarrow {}^7F_2$ emission at 613nm was monitored. The phonon sideband associated with the pure electronic $^5D_2 \leftarrow {}^7F_0$ transition was multiplied by 100 times to investigate the phonon mode contributing to multiphonon relaxation.

The ^{151}Eu Mössbauer measurement was carried out at room temperature with $^{151}Sm_2O_3$ (50 mCi) as a 21.6keV γ-ray source.

The velocity calibration was done with the spectrum of magnetic splitting of α-Fe by a $^{57}Co/Rh$ source and the isomer shift was determined with respect to EuF_3. All the spectra were analyzed with a least-square fitting program of Lorentzian curves.

III. RESULTS

A. ^{151}Eu-Mössbauer spectroscopy

A typical ^{151}Eu-Mössbauer spectrum of a glass ($25AlF_3 \cdot 20AlPO_4 \cdot 5EuF_3 \cdot 30CaF_2 \cdot 20BaF_2$) is shown in Fig.1. The peak due to Eu^{2+} ions, which should be seen around -14 mm/sec[39], was scarcely observed in almost all samples except for the (x,y) = (0,1) glass. Even in this sample, the fraction of Eu^{2+} among all

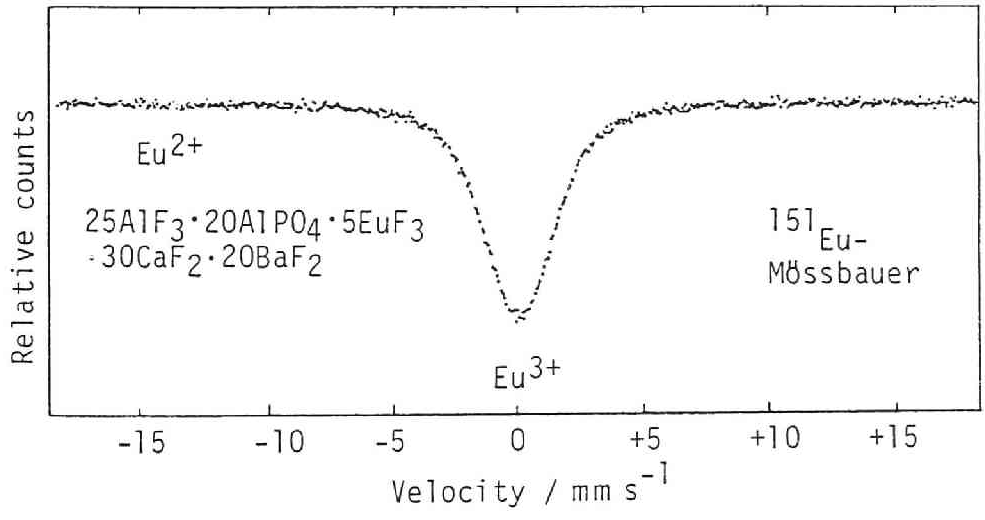

Fig.1. The ^{151}Eu-Mössbauer spectrum of $25AlF_3 \cdot 20AlPO_4 \cdot 5EuF_3 \cdot 30CaF_2 \cdot 20BaF_2$ glass.

the europium ions was at most one percent on the assumption of the equal recoil-free fractions. The compositional dependence of the isomer shift *IS* of Eu^{3+} in fluorophosphate glasses (y=5) is shown in Fig.2. Although the *IS* of fluoride glass(x=0) was lower

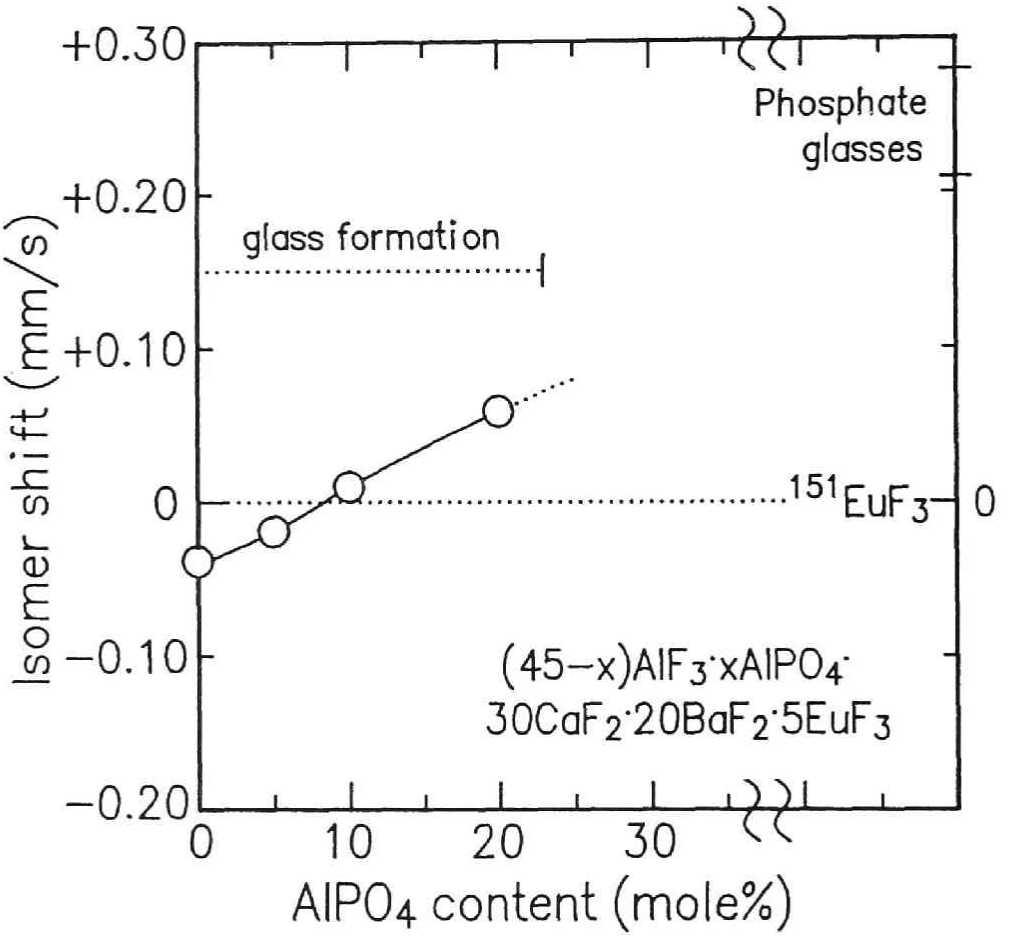

Fig.2. Compositional dependence of the isomer shift of $^{151}Eu^{3+}$ ions in $(45-x)AlF_3 \cdot xAlPO_4 \cdot 5EuF_3 \cdot 30CaF_2 \cdot 20BaF_2$ glasses.

than that of EuF_3, the IS increased with increasing $AlPO_4$ content and becomes positive above 10 mol% $AlPO_4$. Homogeneous glass was not obtained for the x=25 composition. The full-width at half-maximum (FWHM) of the Mössbauer peak is also plotted in Fig.3.

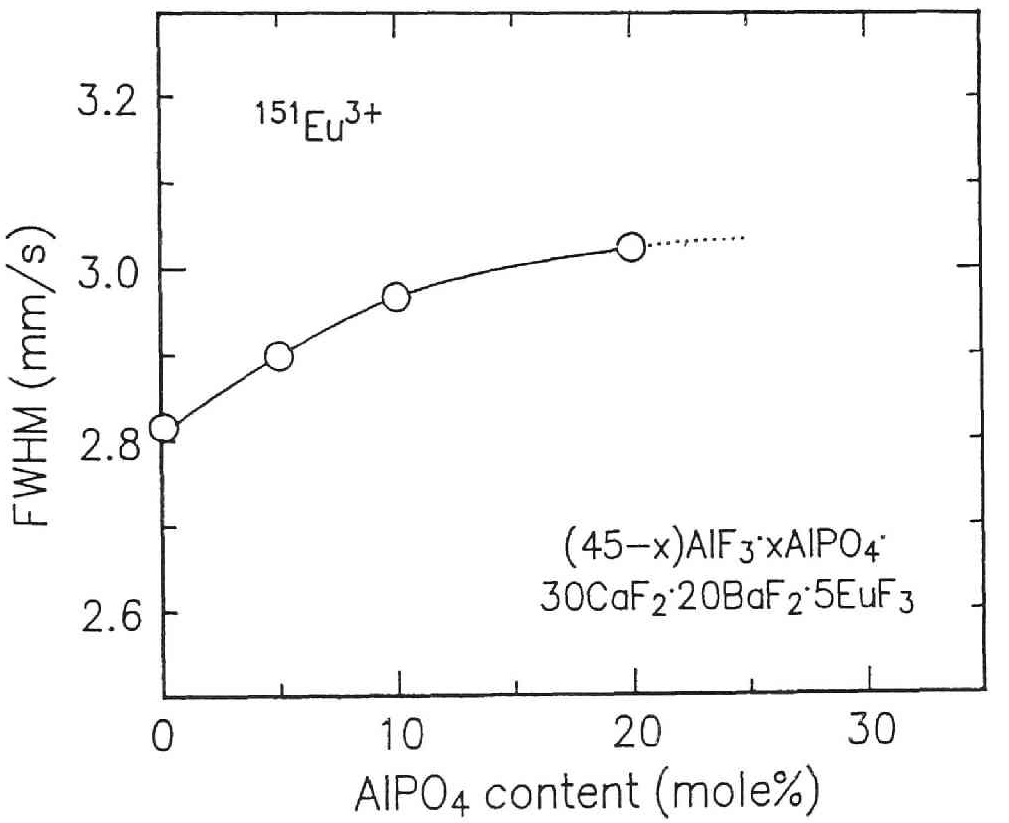

Fig.3. Compositional dependence of the full-width at half-maximum for the Eu^{3+} in the Mössbauer spectra of (45-x)AlF_3·x$AlPO_4$·5EuF_3·30CaF_2·20BaF_2 glasses.

It gradually increases with increasing $AlPO_4$ content. In Fig.4, the variation of IS with the EuF_3 content is plotted. The *IS* of these fluoride glasses are lower than that of EuF_3(0 mm/sec) and increases slightly with increasing EuF_3 content.

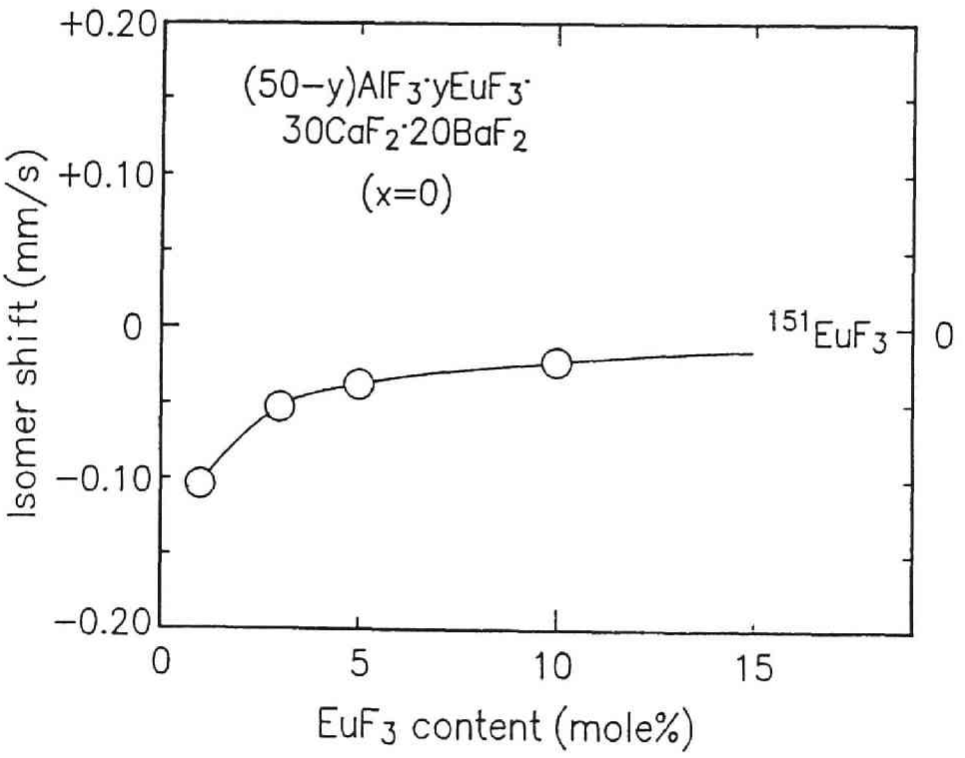

Fig.4. Compositional dependence of the isomer shift of $^{151}Eu^{3+}$ ions in $(50-y)AlF_3 \cdot yEuF_3 \cdot 30CaF_2 \cdot 20BaF_2$ glasses.

B. Fluorescence spectra

The fluorescence spectra of $(49-x)AlF_3 \cdot xAlPO_4$ $1EuF_3 \cdot 30CaF_2 \cdot 20BaF_2$ (y=1) glasses are shown in Fig.5. The absolute intensity was not obtained in this study and thus the ordinate is normalized with the height of the magnetic dipole ${}^5D_0 \rightarrow {}^7F_1$ transition[40]. The emission lines due to the transitions from ${}^5D_2$ and ${}^5D_1$ to ${}^7F_J$ levels can be clearly seen around 450~560 nm for the x=0 sample. However, the intensity of these lines decreases

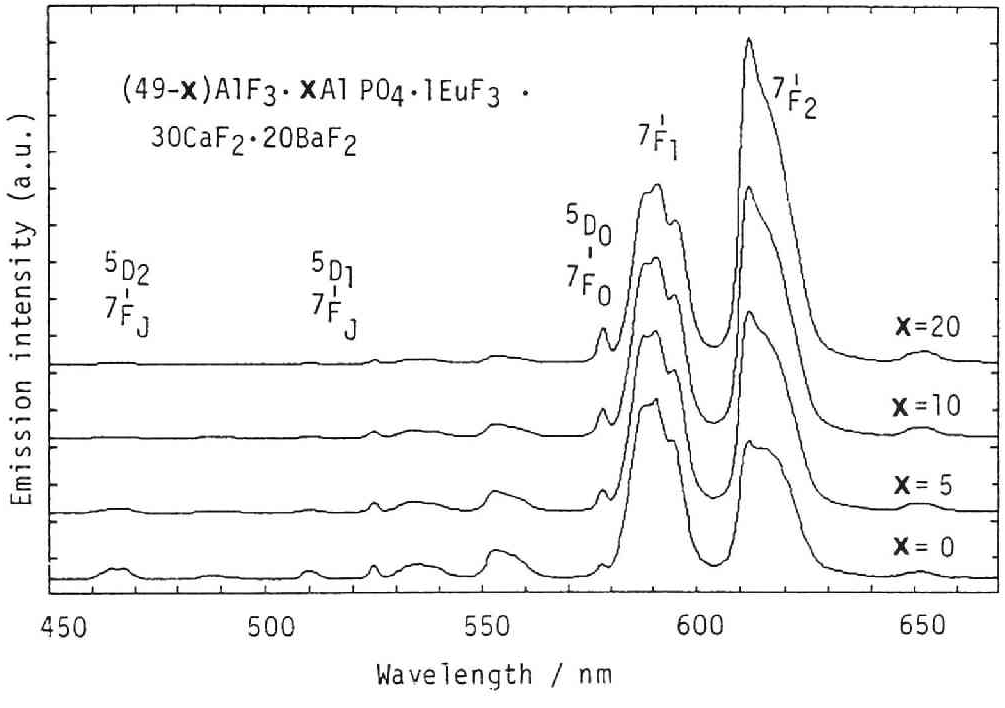

Fig.5. UV-excited fluorescence spectra of Eu^{3+} ions in $(49-x)AlF_3 \cdot xAlPO_4 \cdot 1EuF_3 \cdot 30CaF_2 \cdot 20BaF_2$ glasses(λ_{ex}=394nm).

with an increase of $AlPO_4$ content. On the other hand, among emission lines from $^5D_0$ to ^7F_J levels observed in the range of 570~670 nm, the intensity ratio of $^7F_2$ to $^7F_1$ increases with an increase of x. The similar tendency could be observed for the y=5 series, which is shown in Fig.6. In these samples, the intensity of emission lines from higher ^5D_J, (J'>0) levels is smaller than that for the y=1 series.

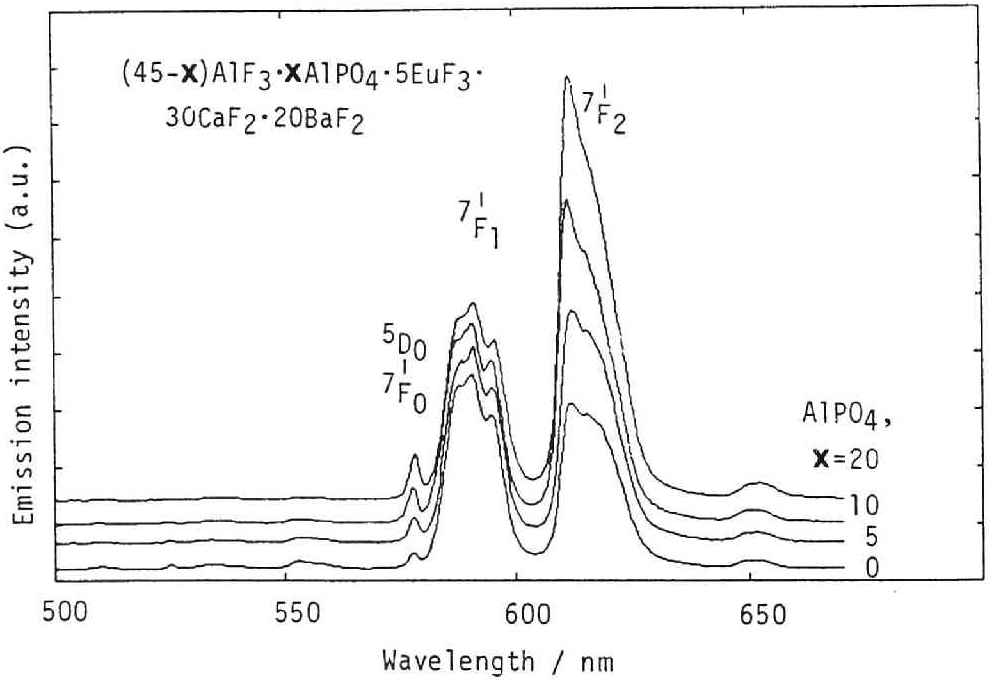

Fig.6. UV-excited fluorescence spectra of Eu^{3+} ions in (45-x)AlF_3 ·x$AlPO_4$·5EuF_3·30CaF_2·20BaF_2 glasses(λ_{ex}=394nm).

C. Phonon sideband spectra

The excitation spectra of Eu^{3+}:$^5D_0 \rightarrow {}^7F_2$ emission for the y=1 and y=5 series are shown in Figs.7 and 8 for various $AlPO_4$ contents x, respectively. The peak due to $^5D_2 \leftarrow {}^7F_0$ transition can be seen around 464 nm, and the shape of the peak was almost symmetric and unchanged with the composition. Each spectrum is multiplied by 100 times and superposed on its original one. Clearly, a peak around 442 nm and a shoulder around 451 nm are observed in both figures. As there is no peak due to pure elec-

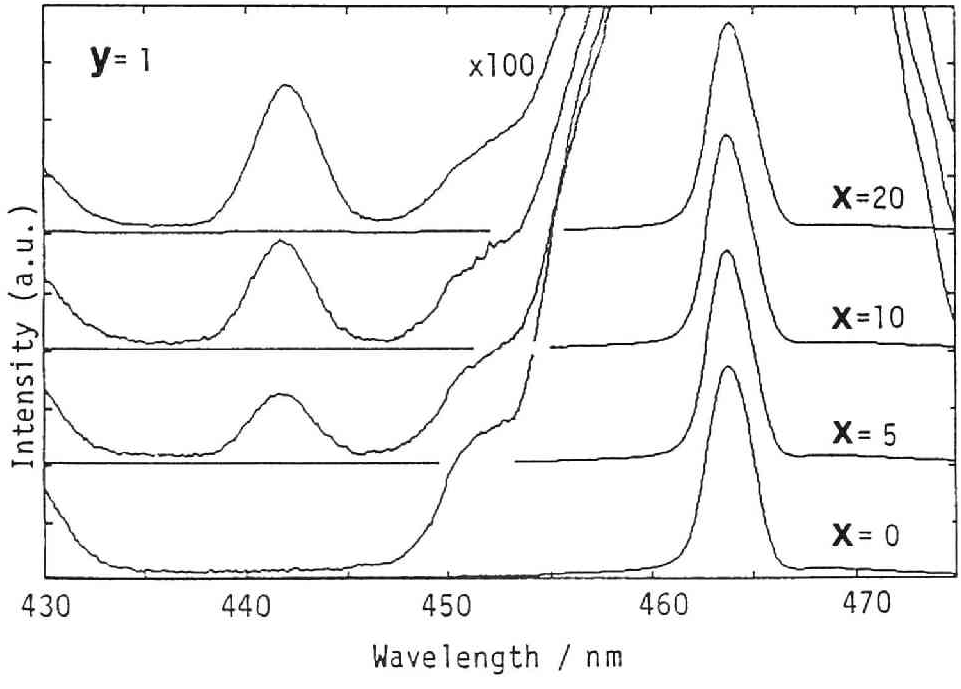

Fig.7. Excitation spectra of Eu^{3+} ions in $(50-x-y)AlF_3 \cdot xAlPO_4 \cdot yEuF_3 \cdot 30CaF_2 \cdot 20BaF_2$ glasses of y=1. Phonon sideband can be observed in the higher energy side of $^5D_2 \leftarrow {}^7F_0$ transition.

tronic transitions of Eu^{3+} in this energy range, these bands are identified as the phonon sideband associated with the $^5D_2 \leftarrow {}^7F_0$ transition of Eu^{3+}[4]. The peak around 442 nm cannot be found for x=0 sample and its intensity increased with an increase of $AlPO_4$ content. On the other hand, the shoulder around 451 nm was clearly observed for x=0, and its intensity decreased with increasing $AlPO_4$ content. The situation occurs both for the y=1 and y=5 series. The intensity of the 442 nm peak seems to be saturated at 20 mole% $AlPO_4$.

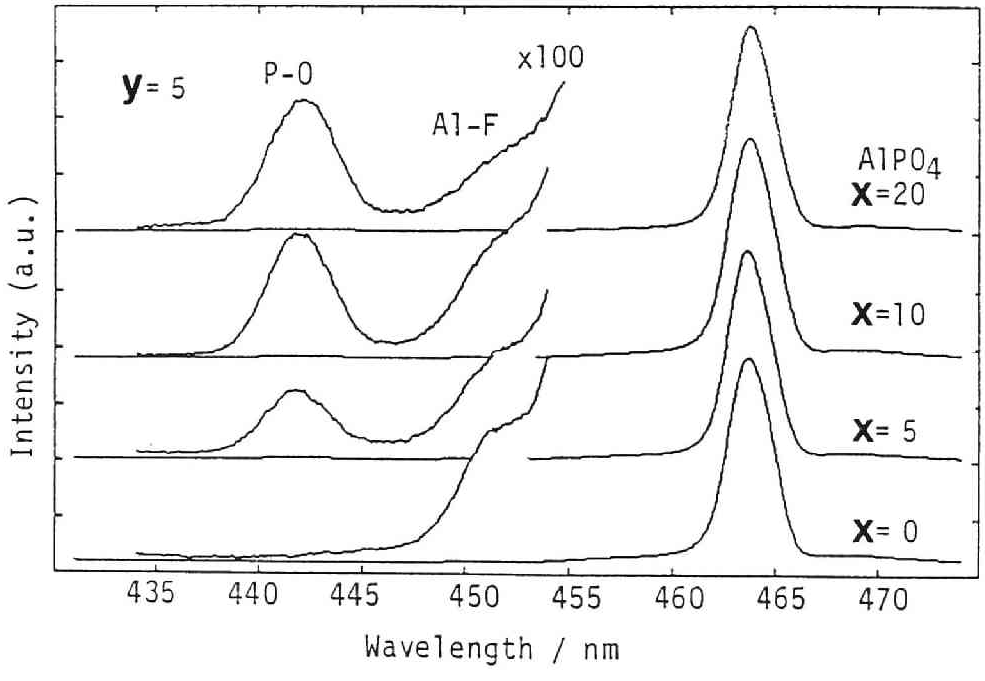

Fig.8. Excitation spectra of Eu^{3+} ions in $(50-x-y)AlF_3 \cdot xAlPO_4 \cdot yEuF_3 \cdot 30CaF_2 \cdot 20BaF_2$ glasses of y=5. Phonon sideband can be observed in the higher energy side of $^5D_2 \leftarrow {}^7F_0$ transition.

IV. DISCUSSION

A. Local structure of Eu^{3+} ions in fluoride glasses

As shown in Fig.4, the *IS* of Eu^{3+} in the present fluoroaluminate glasses is lower than that of EuF_3. Since the *IS* of a Mössbauer nucleus of an absorber with respect to a source can be expressed by the following equation[41],

$$IS = C\{|\Psi a(0)|^2 - |\Psi s(0)|^2\}. \qquad (1)$$

The lower IS can be attributed to a lower electron density at the ^{151}Eu nucleus, $|\Psi_a(0)|^2$, owing to a smaller covalency of Eu-F bond. This result suggests that the local basicity of Eu^{3+} ions in glasses[42] is lower than that in the single europium(III) fluoride. Since the IS can be a measure of the covalency, bond length, or coordination number[10], the negative IS value for these fluoride glasses (Fig.4) suggest that the Eu-F bond length is longer in these glasses than that of EuF_3(III) crystal (CN=9) due to higher coordination states of Eu^{3+}. This is probably caused by the fact that the second nearest neighbor of Eu^{3+}, which forms the chemical bond with the nearest F^- ions, is an acidic cation: i.e., Al^{3+} rather than Ca^{2+} and Ba^{2+}. The phonon sideband spectra of y=0 samples showed that the phonon energy was about $600cm^{-1}$. The Raman studies on the AlF_3-CaF_2-BaF_2 glasses[43,44] revealed that the band observed around $560\sim600cm^{-1}$ is due to the stretching vibration of AlF_6 group. Thus, it may be clear that the F^- ions of the Al-F bonds with the highest frequency are coordinated to the Eu^{3+}, and contribute to its nonradiative decay in these aluminum-based fluoride glasses.

B. Local structure in fluorophosphate glasses

As is shown in Fig.2, the *IS* of Eu^{3+} increased with increasing $AlPO_4$ content. The slope of increase in IS against x is remarkable compared with IS of Eu^{3+} in a phosphate glass ($70P_2O_5 \cdot 30Na_2O \cdot 1Eu_2O_3$)[45]. If IS of 0.23 mm/sec is a typical value for phosphate glasses and the slope of the change in IS versus $AlPO_4$ content is constant, the IS of the fluorophosphate glass at x=45mol% will become almost the same as that of the phosphate glass. It indicates that oxide ions preferentially coordinate to the rare earth ion, although a large amount of fluoride ions still exist at this composition. In the phonon sideband spectra, the additional band appeared around $1060cm^{-1}$ by incorporating $AlPO_4$. This band has already been assigned to the $P\text{-}O^-$ stretching mode of phosphate end member in the Raman spectroscopy[46,47]. The electron-phonon coupling strength of this vibrational mode increases with $AlPO_4$ content and is saturated at higher amount as is shown in Fig.9. Therefore, it is probable that the oxide anions in the $P\text{-}O^-$ bonds preferentially coordinate to the Eu^{3+} in these fluorophosphate glasses.

The increase of fluorescence intensity ratio of $(^5D_0 \rightarrow {}^7F_2)/(^5D_0 \rightarrow {}^7F_1)$ can be explained as follows. It is known that the $^5D_0 \rightarrow {}^7F_2$ transition is electric-dipole allowed and its transition probability depends on the Judd-Ofelt Ω_2 parameter, which reflects most largely the asymmetry of ligand field[3]. On the other hand, the $^5D_0 \rightarrow {}^7F_1$ transition is magnetic-dipole allowed and thus its probability is independent of electric field gradient. Therefore, the above intensity ratio is considered to be a measure of ligand field symmetry[48]. Because the strength of

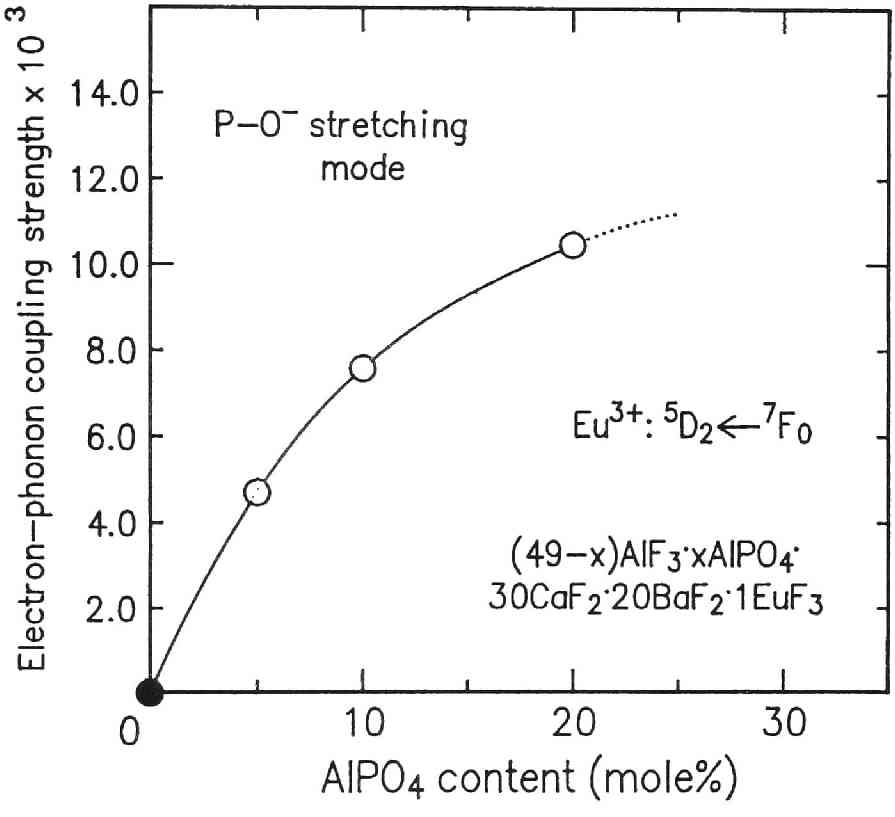

Fig.9. Compositional dependence of the electron-phonon coupling strength of P-O^- stretching mode in the phonon sideband spectra of Eu^{3+} ions for $(49-x)AlF_3 \cdot xAlPO_4 \cdot 1EuF_3 \cdot 30CaF_2 \cdot 20BaF_2$ glasses.

ligand field can be increased by divalent oxide anions rather than monovalent fluoride anions, the coordination of oxide anions to rare earth ion should effectively increase the ligand field strength and the mixed anion coordination also increases the electric field gradient. The gradual increase in the FWHM of ^{151}Eu-Mössbauer peak shown in Fig.3 can be ascribed to the increased quadrupole splitting of eight transition components [10,49], since the quadrupole splitting of the Mössbauer transition is proportional to the electric field gradient at nucleus [10].

C. Nonradiative decay due to ion-phonon interaction

The rate of relaxation of an excited state is governed by the combination of probabilities for radiative (A) and nonradiative (W) processes. The lifetime τ of an excited state is given by

$$\tau^{-1} = \Sigma A + \Sigma W \qquad (2)$$

where the summation of A is for radiative transitions terminating on all lower final states and that of W includes those by ion-phonon and ion-ion interactions. Among nonradiative processes, the relaxation by multiphonon emission due to the ion-phonon interaction is significant. For x=1 series where the cross relaxation due to the ion-ion interaction is negligible because of the low europium concentration, the emission lines from higher ^5D_J levels become smaller with increasing $AlPO_4$ content, compared to those from $^5D_0$ level. This phenomenon can be ascribed to the different energy gap to the next lower level ΔE and to an increased electron-phonon coupling strength of the $P\text{-}O^-$ stretching

mode with the highest phonon energy. According to Miyakawa and Dexter [2], the rate of multiphonon decay can be expressed by the following equations,

$$W_p(T) = W_0(0)\cdot\exp(-\alpha\Delta E), \quad (3)$$

$$\alpha = (\hbar\omega)^{-1}[\ln\{p/g(n+1)\}-1], \quad (4)$$

$$p = \Delta E/\hbar\omega, \quad (5)$$

where $\hbar\omega$ is the phonon energy, p corresponds to the number of phonons consumed during multiphonon relaxation, and g is the electron-phonon coupling strength. $W_0(0)$ is the transition probability extrapolated to zero energy gap, which is independent of the electronic nature of rare-earth ions, and n is the Planck distribution function on the population of phonon as a function of $h\omega$ and temperature, being expressed by $n = \{\exp(\hbar\omega/kT)-1\}^{-1}$ [50]. The radiative quantum efficiency η is defined by,

$$\eta \quad \Sigma A / (\Sigma A + \Sigma W) = \tau \Sigma A \quad (6)$$

Since the ΔE of $^5D_0$ is much larger than those of other ^5D_J ($J \geq 1$) states, the nonradiative decay process by multiphonon relaxation can be extremely small and thus the radiative decay becomes a determinative factor on the relaxation process. On the other hand, the radiative quantum efficiency from higher ^5D_J levels is greatly influenced by the nonradiative decay rate due to their smaller energy gap[31]. For the fluorophosphate glasses, the contribution of Al-F stretching mode on W_p can be negligibly small, since the phonon energy of $P\text{-}O^-$ stretching mode is much higher, which leads to conservation of ΔE in much lower order process. Assuming the constant phonon energy ($\hbar\omega$ = 1060 cm^{-1}) against $AlPO_4$ addition, which is a good approximation as is seen from Figs.7 and 8, one can calculate $W_p(T)$ for a given

energy gap as a function of the electron-phonon coupling strength according to eqs.(3)-(5). The results of calculation for $^5D_1$ (ΔE=1750 cm^{-1}), $^5D_2$(ΔE=2500 cm^{-1}) and $^5D_3$(ΔE=2800 cm^{-1}) levels at 300 K are shown in Fig.10. The range of abscissa corresponds to the values obtained from the results of the phonon sideband spectra in Figs.7, 8 and 9. Apparently, W_p(300 K) is a monotonously increasing function of g ; it increases rapidly at

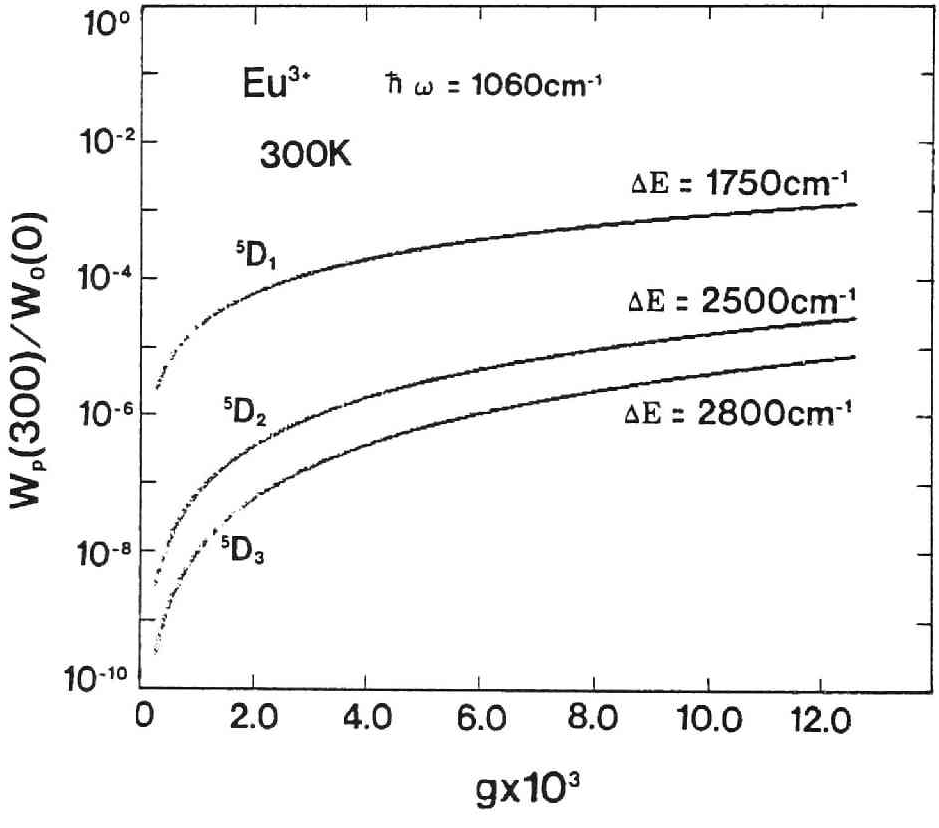

Fig.10. Variation of the nonradiative decay rate of Eu^{3+} excited states as a function of the electron-phonon coupling strength of P-O^- stretching mode(1060cm^{-1}) at 300 K.

lower g (i.e., at lower phosphate content) and increases gradually with increasing g. As g increased rapidly at lower phosphate content as is seen in Fig.9, addition of small amount of phosphate to a fluoride glass seems to effectively reduce the radiative quantum efficiency of excited states with a small ΔE.

D. Nonradiative decay due to ion-ion interaction

In the glasses with the same x (0 or 5), the intensity ratio of emission lines from higher ^5D_J (J=1,2,3) levels to those from $^5D_0$ level was always smaller for the y=5 series (Fig.6) than that for the y=1 series (Fig.5). The smaller ratio can be ascribed to the increased ion-ion interaction between Eu^{3+} ions, which causes direct energy transfer from the excited donors to neighboring acceptors, leading to the cross relaxation[23]. The critical rare earth concentration for ion-ion interaction depends on the kind of coordination anions and on the structure of connecting polyhedra. In the case of the present coordination states of Eu^{3+} (CN>9) as discussed in section A, the 5 mol% EuF_3 seems not to be a sufficient concentration for an EuF_nO_m polyhedron to share the corner or edge with another Eu-polyhedron when they were homogeneously dispersed in random structures. From the compositional variation of IS with different EuF_3 concentrations of the fluoride glasses (Fig.4), however, the local basicity of Eu^{3+} in the y=1 glass is lower than that in the glasses with y>3mol%. Since the anions coordinating to Eu^{3+} are all F^- ions in fluoride glasses, the change of IS or local basicity in Fig.4 is ascribed to the change in averaged electronegativity of the second nearest neighbor cations. Accordingly, the averaged basicity in the y=1

glass can be lower (Al^{3+} rich) than that for glasses with y>3, where the presence of more basic Eu^{3+} ions at the second neighbors of Eu^{3+} caused its increased local basicity. Consequently, the ion-ion interaction effectively occurs around this composition. The possible cross relaxation mechanisms for the ^5D_J quenching of Eu^{3+} can be $(^5D_J \rightarrow {}^5D_{J'}) \Longrightarrow (^7F_J{}^* \leftarrow {}^7F_0)$, where $4 > J > J' \geq 0$ and $6 \geq J^* > 1$. Therefore, the cross relaxation between Eu^{3+} ions results in the reduction of the quantum efficiency of higher ^5D_J levels.

V. CONCLUSIONS

Fluorophosphate glasses were prepared in the system of AlF_3-$AlPO_4$-EuF_3-MF_2(M=Ca,Ba) and the compositional dependences of Eu^{3+}-fluorescence properties were investigated. It was found that with an increase of $AlPO_4$ content, the fluorescence intensities from Eu^{3+}:^5D_J(J=1,2,3) levels were decreased and the intensity ratio of $(^5D_0 \rightarrow {}^7F_2)/(^5D_0 \rightarrow {}^7F_1)$ was increased. The local structure and multiphonon relaxation mechanisms were investigated by measuring the ^{151}Eu Mössbauer effect and phonon sideband spectra associated with the $^5D_2 \leftarrow {}^7F_0$ transition. It was concluded that the $P\text{-}O^-$ stretching mode with the highest phonon energy contributes to the rapid multiphonon relaxation of ^5D_J states and that the covalency and asymmetry of Eu^{3+}-ligand field were increased by the addition of $AlPO_4$ to the present glasses. The ion-ion interaction became predominant for 5mol% EuF_3 rather than for 1mol% doped glasses.

REFERENCES

[1] C.B. Layne, W.H. Lowdermilk and M.J. Weber, *Phys. Rev. B* **16**(1), (1977) 10-20.

[2] T. Miyakawa and D.L. Dexter, *Phys. Rev. B* 1, (1970) 2961-69.

[3] M.J. Weber, in "*Optical Properties of Ions in Crystals*", (ed. H.M. Crosswhite and H.W. Moos, Intersci. Pub. NY, 1966) pp.467-484.

[4] S. Tanabe and K. Hirao, *Bull. Ceram. Soc. Jpn.* **26**(2), (1991) 144-48.

[5] J.R. Morgan, E.P. Chock, W.D. Hopewell, M.A. El-Sayd and R. Orbach, *J. Phys. Chem.* **85**, (1981) 747-751.

[6] G. Boulton, M. Bouderbala and J. Seriot, *J. Less-Common Metals* **112**, (1985) 41-66.

[7] T.F. Belliveau and D.J. Simkin, *J. Non-Cryst. Solids* **110**, (1989) 127-141.

[8] H. Toratani, T. Izumitani and H. Kuroda, *J. Non-Cryst. Solids* **52**, (1982) 303-13.

[9] S. Tanabe, K. Hirao and N. Soga, Proc. Annual meeting of Ceramic Society of Japan, in May (1989) p.337.

[10] S. Tanabe, K. Hirao and N. Soga, *J. Non-Cryst. Solids* **113**, (1989) 178-184.

[11] J. Krogh-Moe, *Phys. Chem. Glasses* **3**, (1962) 101-110.

[12] A.H. Silver and P.J. Bray, *J. Chem. Phys.* **29**, (1958) 984-990.

[13] P.J. Bray and J.G. O'Keefe, *Phys. Chem. Glasses* **4**, (1963) 37-46.

[14] W.L. Konijnendijk and J.M. Stevels, *J. Non-Cryst. Solids* **18**, (1975) 307

[15] H. Kuroda, S. Shionoya and T. Kushida, *J. Phys. Soc. Jpn.* **33**, (1972) 125-141.

[16] E.I. Kamitsos, M.A. Karakassides and G.D. Chryssikos, *J. Phys. Chem.* **91**, (1987) 1073-79.

[17] J.E. Shelby, *J. Am. Ceram. Soc.* **66**, (1983) 225-27.

[18] D.L. Griscom, in *"Borate Glasses"*, (ed. L.D. Pye, V.D. Frechette and N.J. Kreidl, Plenum, NY, 1978) p.11.

[19] M.J. Weber, *Phys. Rev. B* **4**(9), (1971) 2932-39.

[20] H.Y-P. Hong and K. Dwight, *Mater. Res. Bull.* **9** (12), (1974) 1661-65.

[21] F. Kellendonk and G. Blasse, *J. Chem. Phys.* **75**(2), (1981) 561-571.

[22] J.P. van der Ziel, L. Kopft and L.G. Van Uitert, *Phys. Rev. B* **6**(2), (1972) 615-623.

[23] F.W. Tian, C. Fouassier and P. Hagenmuller, *J. Phys. Chem. Solids* **48**(3), (1987) 245-48.

[24] J. Mascetti, C. Fouassier and P. Hagenmuller, *J. Solid State Chem.***50**,

(1983) 204-212.

[25] C. Fouassier, B. Saubat and P. Hagenmuller, *J. Luminesc.* **23**, (1981) 405-412.

[26] D.L. Graf and W.F. Bradley, *Acta Crystallogr.* **15**, (1962) 238-242.

[27] G. Huber, in *"Current Topics in Material Science, vol.4"*, (ed. E. Kaldis, North-Holland Publishing Company, Amsterdam, 1980) pp.1-45.

[28] S. Ohishi, C. Nishikawa and I. Tate, *Chem. Express* **2**(10), (1987) 647-650.

[29] W.C. Nieuwpoort, G. Blasse and A. Bril, in *"Optical Properties of Ions in Crystals"*, (ed. H.M. Crosswhite and H.W. Moos, Interscience, NY, 1967) pp.161-168.

[30] T. Hanada and N. Soga, *J. Am. Ceram. Soc.* **70**, (1987) C-362-66.

[31] S. Tanabe, S. Todoroki, K. Hirao and N. Soga, *J. Non-Cryst. Solids* **122**, (1990) 59-65.

[32] J.P. van der Ziel, L.G. Van Uitert, W.H. Grodkiewicz and R.M. Mikulyak, *J. Appl. Phys.* **60**(12) (1986) 4262-67.

[33] S.A. Pollack D.B. Chang and N.L. Moise, *J.Appl.Phys.* **60**(12), (1986) 4077-86.

[34] D.C. Yeh, W.A. Sibley, M. Suscavage and M.G. Drexhage, *J. Appl. Phys.* **62**(1), (1987) 266-275.

[35] C.B. Layne and M.J.Weber, *Phys. Rev. B* **16**(7), (1977) 3259-61.

[36] M.J. Weber, C.Layne, R.Saroyan and D.Milam, *Opt. Commun.* **18**, (1976) 171-177.

[37] J.J. Videau, J. Portier and B. Piriou, *Rev. Chim. Min.* **16**, (1979) 393-398.

[38] I. Yasui, H. Hagiwara and Y. Arai, *Ext. Abst. 5th Int. Symp. Halide Glasses*, (1988) 497-502.

[39] O. Berkooz, *J. Phys. Chem. Solids* **30**, (1969) 1763-67.

[40] E.V. Sayre and S. Feed, *J. Chem. Phys.* **24**, (1956) 1213-19.

[41] G. Gerth, P. Kienle and K. Luchner, *Phys. Lett.* **27A**(8), (1968) 557-58.

[42] S. Tanabe, N. Soga, K. Hirao and T. Hanada, *J. Am. Ceram. Soc.* **73**(6), (1990) 1733-36.

[43] Y. Kawamoto and A. Kono, *J. Non-Cryst. Solids* **85**, (1986) 335-345.

[44] H. Inoue, T. Nanba, H. Hagiwara, T. Kanazawa and I. Yasui, *Ext. Abst. 5th Int. Symp. Halide Glasses*, (1988) 463-68.

[45] S.Tanabe and S.Todoroki, *unpublished data of ^{151}Eu Mössbauer spectroscopy.*

[46] J-J. Videau, J. Portier and B. Piriou, *J. Non-Cryst. Solids* **48**, (1982) 385-392.

[47] M. Scagliotti, M. Villa and G. Chiodelli, *J. Non-Cryst. Solids* **93**, (1987) 350-355.

[48] P.K. Gallagher, C.R. Kurkjian and P.M. Bridenbaugh, *Phys. Chem. Glasses* **6**(3) (1965) 95-103.

[49] M.P. Barton and N.N. Greenwood, in *"Mössbauer Effect Data Index"*, (ed. J.D. Stevens and V.E. Stevens, (Plenum, NY, 1973) p.395.

[50] C. Kittel, *"Introduction to Solid State Physics,"* (6th ed., John Wiley & Sons, Inc., NY, 1986) p.101.

Chapter 4.

INFRARED TO VISIBLE UPCONVERSION OF RARE EARTH IONS IN GLASSES WITH III-V SEMICONDUCTOR LASER

4.1. Research for Short Wavelength Laser and Frequency Upconversion Fluorescence of Rare Earth Ions

I. INTRODUCTION

Recently, the development of III-V group diode laser emitting a high-power infrared radiation, stimulated a great demand for the frequency converting device. This is because a short wavelength laser offers unique opportunities in enhancement of optical data density as well as speed of laser printing. To achieve a compact blue laser, the limit of the band gap of III-V semiconductor of direct transition, will be a problem, with the wavelength longer than 0.7μm, red in color to near-infrared. To obtain green or blue emissions with shorter wavelength, it is necessary to develop the II-VI group or IV-IV group semiconductor lasers with wider band gap, such as ZnSe or SiC. Although the current effort worldwide is concentrated on II-VI heterostructures, there have been several problems; the suppression of the activity of *p*-type carriers, and the difficulty in formation of the complete *pn*-junction[1]. Accordingly, it needs a long time to realize the CW-action of II-VI or IV-IV diode with a sufficient power at room temperature. On the other hand, high-power

diode lasers with the longer wavelength than 0.78μm came to be available by the recent development of III-V semiconductors[2-4]. One method to obtain laser radiations with shorter wavelength is the second harmonic generation (*SHG*) by the single crystalline nonlinear optical (*NLO*) device with a high second order susceptibility. By this method, the conversion efficiency becomes low with an inefficient coherence characteristics of laser diode (*LD*), therefore, it is necessary to form a large device structure to confine the pumping light in *NLO* crystals with a large $\chi^{(2)}$. The second method is to pump the Nd^{3+}:YAG or Nd^{3+}:YVO_4 single crystals with *LD*s and generate 2ω of 1.06 or 0.94μm radiation with *NLO* single crystals such as KTP. Since the conversion efficiency of *LD*-pumped solid-state rare earth crystals are high (~50%) and the coherence of their laser radiation is sufficiently good, the conversion efficiency depends on that of the *NLO* crystals. In this case, rare earth doped laser can be considered as a filter to gain the coherence characteristics of *LD*. While it must be necessary by these two methods to obtain phase matching of ω and 2ω in an anisotropic *NLO* single crystal, there is no need by upconversion, the third method. The frequency upconversion by rare earth doped crystals and glasses has attracted a great interest, since the 4f energy levels of rare earth ions in solids are utilized to convert infrared pumping light into visible or ultraviolet light by multistep excitation. The concept of upconversion phenomena of Er^{3+} and Ho^{3+} ions were proposed as a way of infrared quantum counter (IRQC) by Bloembergen[5] and the green emission was first observed in an Yb-Er doped germanate glass with infrared pumping by Auzel[6]. With the development of

higher power III-V LDs, laser oscillations in green and blue regions have been reported in Er^{3+}:$LiYF_4$[7], Tm^{3+}:$LiYF_4$[8] and Nd^{3+}:LaF_3[9] crystals at lower temperature than 77K. In contrast to crystals, the research field of upconversion in glass has become wider with the discovery of heavy metal fluoride glass (HMFG) by Poulain[10]. This is because the nonradiative loss due

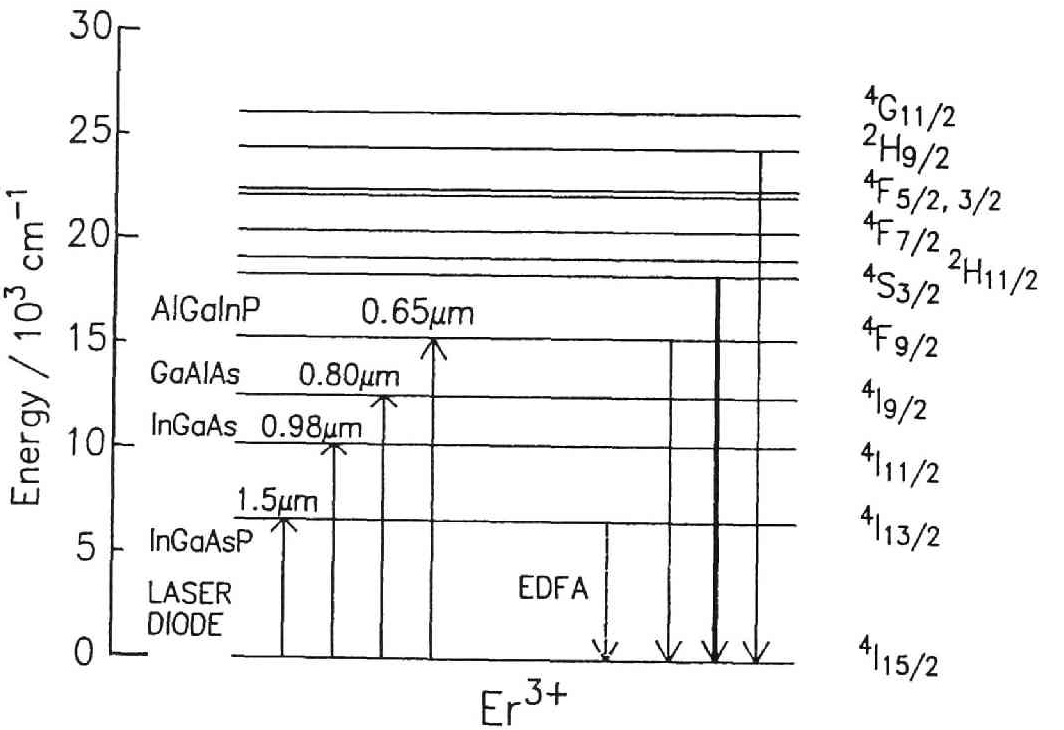

Fig.1: Energy level of Er^{3+} ion and the kind of III-V laser diode with corresponding wavelength.

to multiphonon relaxation can be suppressed in these glass systems due to their lower phonon energies than those of conventional oxide glasses. Moreover, the laser action should be possible at room temperature by taking a fiber form to confine the pumping light from *LD* efficiently to maintain a high intensity over a long interaction length. However, to realize the upconversion lasing in glass at room temperature, it is necessary to improve the excitation and emission efficiency of rare earth ions doped in glasses. Because the optical properties of rare earth ions are influenced by the ligand field, the electron-phonon interaction, and the vibrational properties of hosts, it should be necessary for material design to clarify the relationship between the glass composition and the above structural properties as well as to predict the fluorescence properties based on the radiative and nonradiative theories of rare earth ions[11].

II. UPCONVERSION PROCESS OF RARE EARTH IN SOLIDS

The normal(one-step) fluorescence is the process to emit a light with longer wavelength by exciting with a shorter wavelength such as UV light from a halogen lamp. In an upconversion process, an ion is first promoted to a long-lived intermediate excited state by near-infrared absorption, and is then raised to a still higher state followed by the emission of UV or visible light. Especially, laser actions have been recently reported in Ho^{3+}[12], Pr^{3+}[13], or Er^{3+}[14] doped fluoride glass fibers at room temperature and Tm^{3+}[15] at 77K. Figure 1 shows the energy level diagram of Er^{3+} ion, in which the electronic levels for

absorption exist at 1.5μm, 0.98μm, 0.80μm, and 0.65μm. These wavelengths of absorption bands correspond to those of (In,Ga)(As,P), (In,Ga)As, (Ga,Al)As, and (In,Ga,Al)P laser diodes, respectively, all of which has become available for many purposes such as optical communication, optical data storage and so on. Thus it is easy to pump Er^{3+} ion with *LD*s available in practical points of view. Green upconversion emissions have been

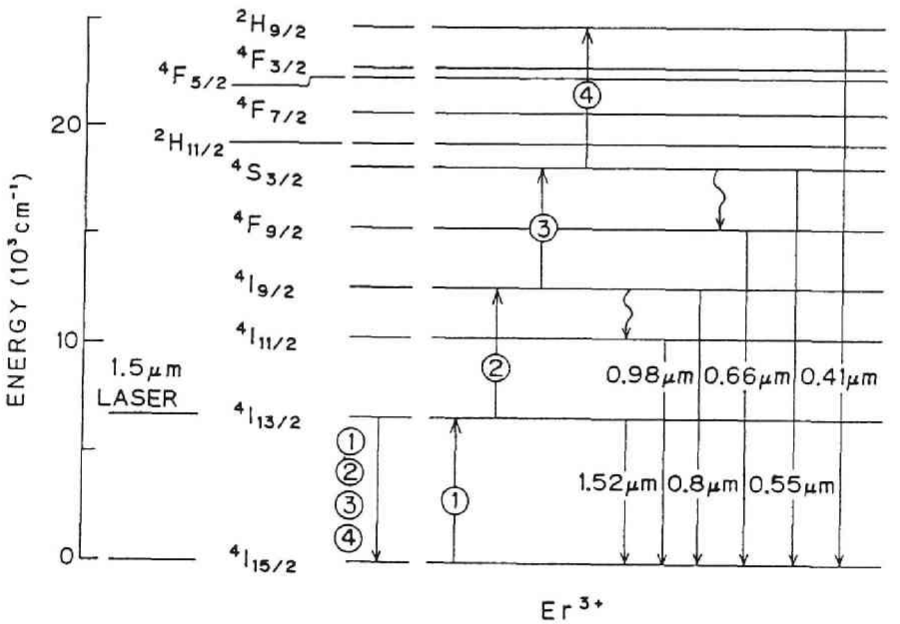

Fig.2: A possible multistep excitation mechanism of Er^{3+} ion by 1.5μm laser.

observed due to the $^4S_{3/2} \rightarrow {}^4I_{15/2}$ transition in most fluoride glasses. Represented in Fig.2 is a multistep excited state absorption mechanism by 1.5μm radiation, whereas the sensitization by the energy transfer from adjacent ions can also be a

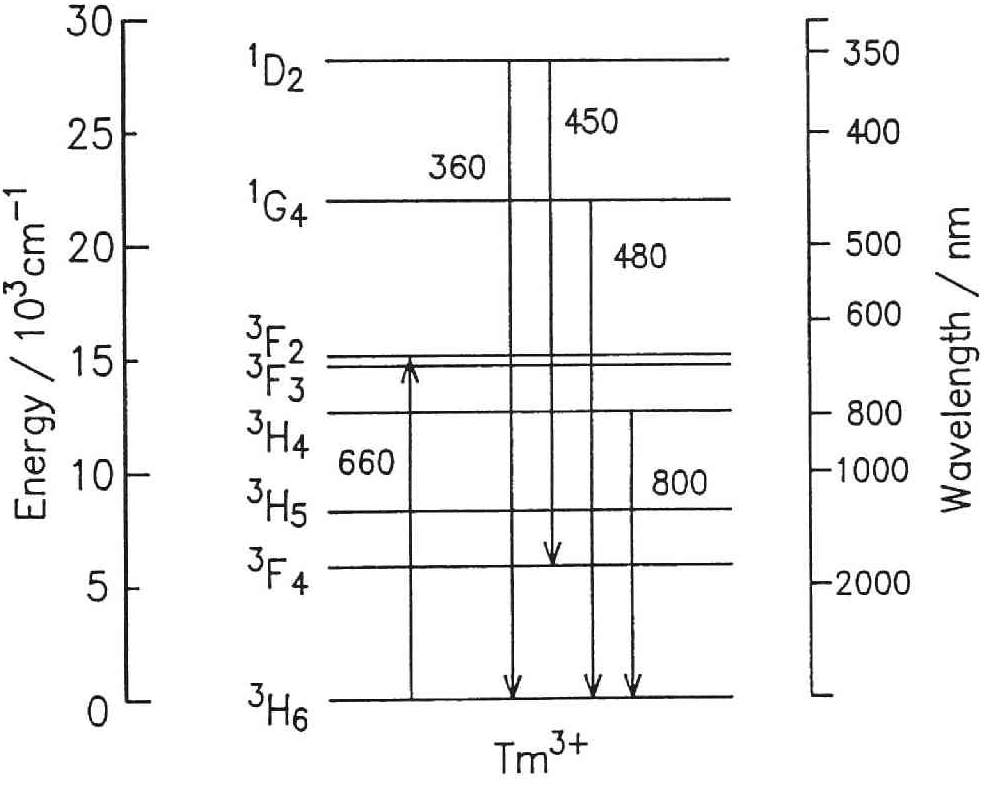

Fig.3: Energy level of Tm^{3+} ion.

possible mechanism. The controlling mechanism depends on various conditions such as the rare earth concentration, phonon energy of host, excitation wavelength and so on.

In the case of Tm^{3+} ion, upconversions are reported by two ways. The first is to pump at 1.06μm from Nd:YAG[16] and the second is to co-pump at 0.647 and 0.678μm from Kr^{+} laser[17]. Figure 3 shows the energy level diagram of Tm^{3+} ion, in which two stable (long-lived) levels to emit blue fluorescence exist ($^1D_2$ and $^1G_4$). This is the reason why Tm^{3+} ion attract much attention in spite of the difficulty in pumping compared with Er^{3+}.

4.2. MULTIPHONON RELAXATION AND UPCONVERSION INTENSITY OF Er^{3+} IN FLUOROPHOSPHATE GLASSES

I. INTRODUCTION

The conversion of infrared light to visible light, "frequency upconversion" phenomena of rare earth ions in solids is attracting much research interest. The device applications are potential short-wavelength upconversion lasers[16-19] pumped with the infrared radiation from III-V laser diodes (*LD*). The glasses are particularly attractive hosts because they can be fabricated as optical fibers to confine the pumping light from the *LD* efficiently to maintain a high intensity over a long interaction length, and also because different kinds of ions can be incorporated in various proportions. However, the optical properties of fluorescent ions are largely influenced by their ligand field and the vibrational properties of the host. Thus, it is important to investigate the coordination states and multiphonon relaxation mechanisms of the rare earth ions in multicomponent glasses in order to design optical devices. One of the advantages of fluoride hosts is their lower phonon energy compared with those of the oxide hosts, which contribute to a reduction in the nonradiative loss due to multiphonon relaxation[20,21]. In this study, fluoride and fluorophosphate glass systems, which have been used as Nd^{3+}-laser hosts, were chosen as hosts of Er^{3+} ions and the upconvesion properties were studied by exciting with a (Ga,Al)As laser diode emitting 0.80-μm infrared radiation. It is well known that the rate of the multiphonon relaxation is dominated by

lattice phonons. Therefore, the phonon sideband[22,23] was measured for Eu^{3+}-doped glasses in order to get information about the phonon mode coupled to the rare earth ions. Moreover, the ^{151}Eu Mössbauer effect[24] was measured to determine the local structure of rare earth ions in the glass. The compositions of the glasses investigated are those of AlF_3-based fluoride and fluorophosphates. The AlF_3 system was chosen since it is chemically stable and can incorporate a substantial amount of phosphate and rare earth ions in vitreous states.

II. EXPERIMENTAL

Glasses with compositions $(45-x)AlF_3 \cdot xAlPO_4 \cdot 5ErF_3 \cdot 30CaF_2$ $20BaF_2$(x=0,5,10,20) were prepared by the same method described in Chapter 4. The glass obtained was annealed, cut, and polished with diamond paste into 3x3x1 mm^3 size.

The fluorescence and excitation spectra were measured with a *Hitachi-850* Fluorescence Spectrophotometer. A xenon lamp and a GaAs/(Ga,Al)As laser diode (*SONY SLD301-XT*, λ = 802 nm, P<100 mW) were used as the excitation source of normal and upconversion fluorescence, respectively.

The ^{151}Eu Mössbauer effect measurement was also carried out by the same method as in Chapter 2.

III. EXPERIMENTAL RESULTS

A. Upconversion intensity of Er^{3+} in fluoride and fluorophosphate glasses

Figure 1 shows the compositional variation of upconversion

fluorescence spectra for $(45-x)AlF_3 \cdot xAlPO_4 \cdot 5ErF_3 \cdot 30CaF_2$ $20BaF_2$ glasses(x=0, 5, 10, 20). A homogeneous glass was not obtained for the composition of $x \geq 25$. It is clear that the fluorescence intensity of glasses decreased drastically with increasing $AlPO_4$ content. At 20mole% $AlPO_4$, the green emission was hardly

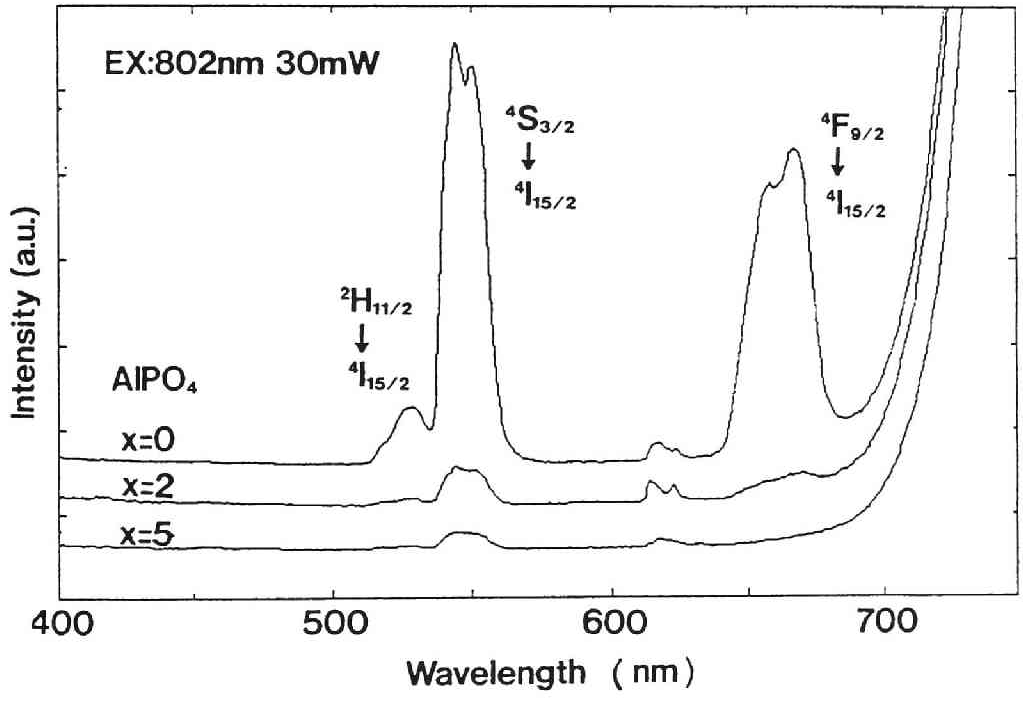

FIG.1: Compositional variation of upconversion fluorescence spectra in the fluorophosphate glasses $(45-x)AlF_3 \cdot xAlPO_4$ $5ErF_3 \cdot 30CaF_2 \cdot 20BaF_2$.

observable with the human eye at 30 mW excitation. The 410-nm emission peak due to the $^2H_{9/2} \rightarrow {}^4I_{15/2}$ transition, which appeared by excitation of the $^4G_{11/2} \leftarrow {}^4I_{15/2}$ transition at 378-nm, was barely observed for all the samples with the present laser apparatus, indicating that an excitation process more than two steps may be necessary to reach the $^2H_{9/2}$ level.

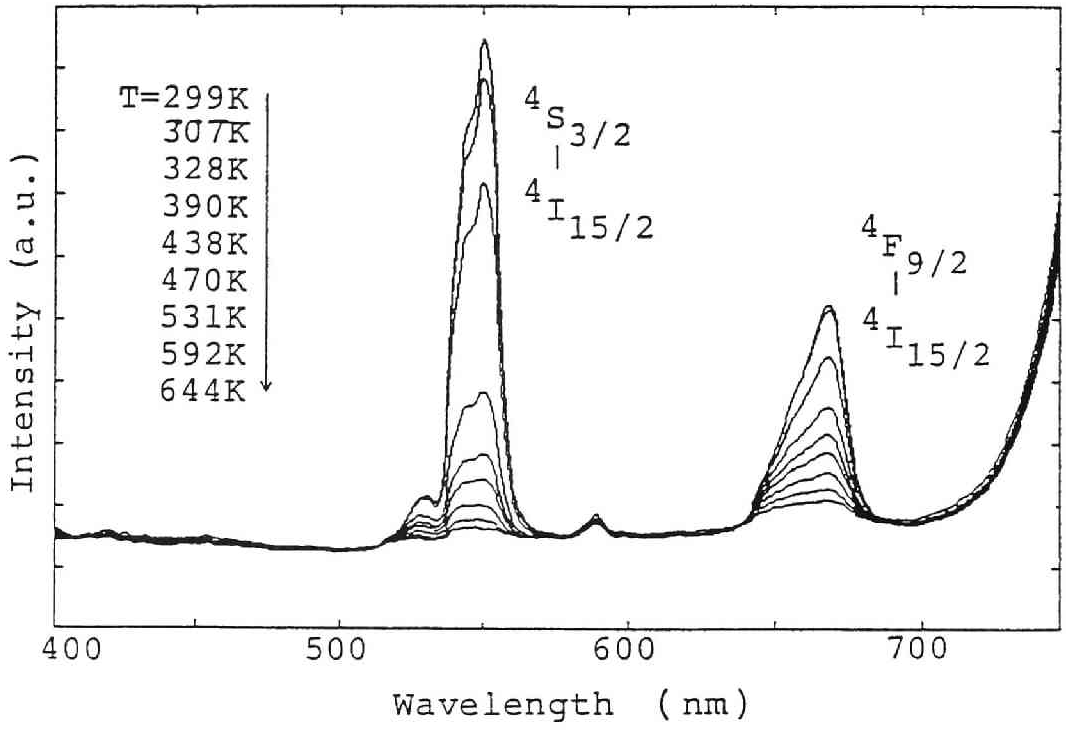

FIG.2: Temperature variation of upconversion fluorescence spectra in fluoride glass (x=0).

B. Temperature dependence of Er^{3+} upconversion intensity

The temperature variation of the upconversion fluorescences of $45AlF_3 \cdot 5ErF_3 \cdot 30CaF_2$ $20BaF_2$ glass (x=0) is shown in Fig.2. The fluorescence intensity decreases with increasing temperature in the range from room temperature, 299 to 644K. In Fig. 3 the integrated area of $^4S_{3/2}+^2H_{9/2} \rightarrow {}^4I_{15/2}$ green fluorescence around 550nm is plotted as a function of temperature for both (a) fluoride glass (with x=0) and (b) fluorophosphate glass (with x=5). It was found that the intensity decreased by less than 1/10 from room temperature to 350 °C for the fluoride glass, while it decreased by about 1/2 for the fluorophosphate glass.

C. Phonon sideband spectra of Eu^{3+}

The phonon sideband spectra associated with $Eu^{3+}: {}^5D_2 \leftarrow {}^7F_0$ transition are shown for $(45-x)AlF_3 \cdot xAlPO_4 \cdot 5EuF_3 \cdot 30CaF_2 \cdot 20BaF_2$ glasses (x=0,5,10,20) in Fig.4. The intense band due to the pure electronic transition is placed around 464nm, while the phonon sideband coupled to the rare earth ions is observed in the higher energy range. The band around 442 nm appears above x=5 and its intensity increases with increasing x. The intensity of the shoulder around 451 nm decreases with increasing x. The phonon energy, $\hbar\omega$ of two bands are found to be about 1060 and 600 cm^{-1}.

D. ^{151}Eu Mössbauer spectroscopy

All the europium ions in these glasses existed in the trivalent state as Eu^{3+}. In Fig. 5 the compositional dependence of the isomer shift IS is plotted as a function of the $AlPO_4$ con-

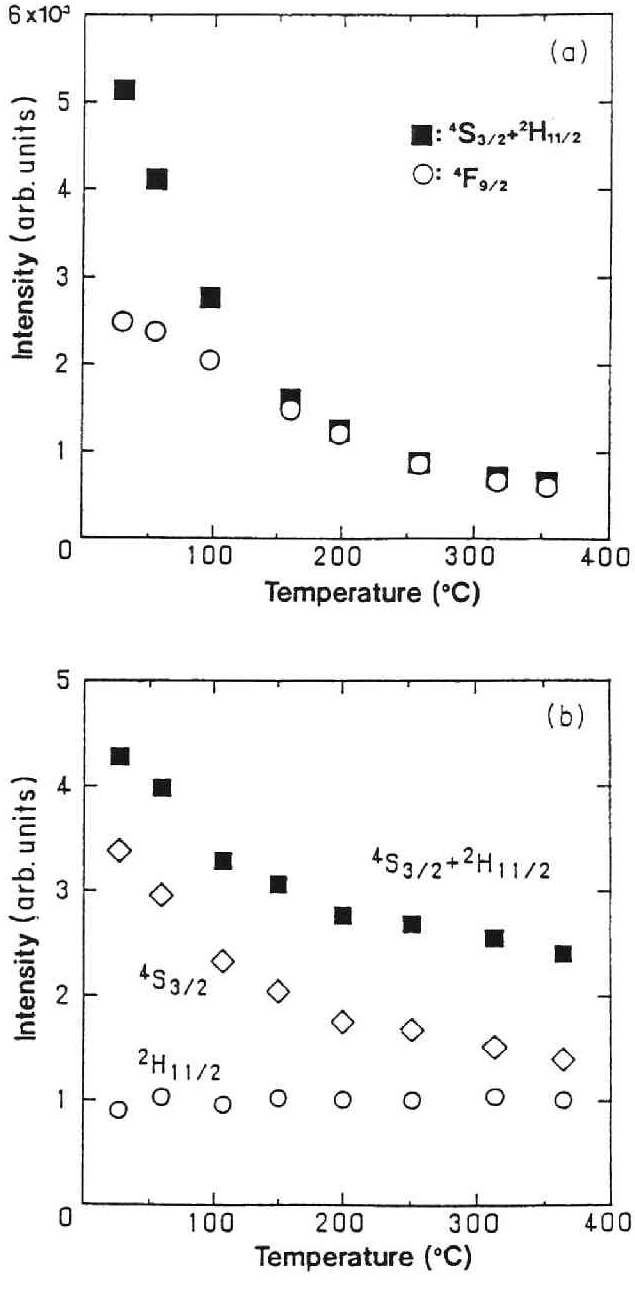

FIG.3: Temperature dependence of upconversion intensity of (a) the fluoride glass (x=0) and (b) the fluorophosphate glass(x=5).

tent. The IS of the fluoride glass (x=0) was lower than that of EuF_3 (0 mm/sec), while that of fluorophosphate glasses increases with increasing $AlPO_4$ content, and becomes positive above 10 mol% $AlPO_4$.

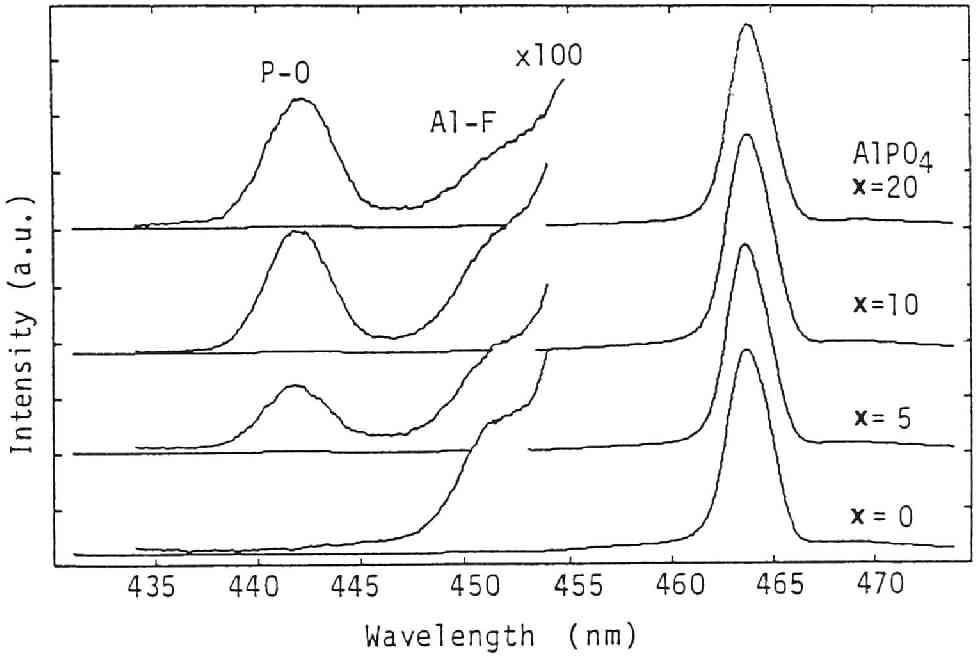

FIG.4: Phonon sideband spectra of fluorophosphate glasses having different $AlPO_4$ content.

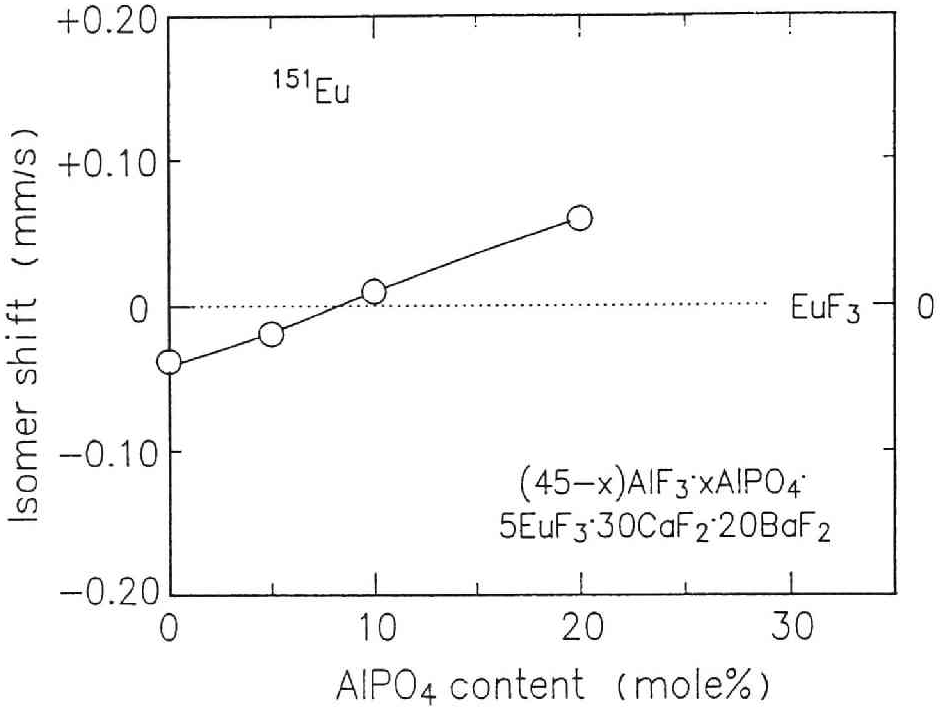

FIG.5: Compositional dependence of the isomer shift of $^{151}Eu^{3+}$ in fluorophosphate glasses

IV. DISCUSSION

A. Local structure and multiphonon relaxation mechanisms of rare earth in fluoride and fluorophosphate glasses

From the Mössbauer results, all the europium ions in the present glasses were found to exist in the trivalent state as Eu^{3+}. Since the mass and ionic radius of the Eu^{3+} ion are similar to those of Er^{3+}, their chemical environment should be simi-

lar. The isomer shift IS of a Mössbauer nucleus of an absorber with respect to a source can be expressed as[26,27],

$$IS=C\{|\Psi a(0)|^2- |\Psi s(0)|^2\}, \qquad (1)$$

where C is a constant related to the radius ratio of excited to ground states and is positive for ^{151}Eu nuclei[24]. Thus, the lower IS can be attributed to a lower electron density at ^{151}Eu nucleus, $|\Psi(0)|^2$[24]. As the electronegativity of F (x_F=3.98) is larger than that of O (x_O=3.44)[28] the covalency of the Eu-O bond is larger than that of the Eu-F bond. Therefore, the increasing tendency of the IS of Eu^{3+} ion in the fluorophosphate glass shown in Fig.6 indicates the increased s-electron density of Eu^{3+}, i.e., covalency of Eu ligand by the oxygen coordination. Since the IS of Eu^{3+} in a phosphate glass ($70P_2O_5 \cdot 30Na_2O \cdot 1Eu_2O_3$), where no F^- ions exist, is 0.23 mm/sec, the increasing slope of IS against x in Fig.6 indicates a preferential coordination of divalent O^{2-} to a rare earth ion rather than monovalent F^- ions in a mixed anion host. From the peak assignment of the phonon sideband spectra in Fig.4, it is clear that the band around 1060 cm^{-1} is due to the $P-O^-$ stretching vibrations of the phosphate end member[29,30], and the band around 600 cm^{-1} to the Al-F stretching mode[31]. Therefore, in fluoride glasses the Al-F bond is coordinated to the Eu^{3+} ion, while in fluorophosphate glasses the oxygen ions of $P-O^-$ bonds are coordinated to the rare earth ion. In addition, as plotted in Fig.6, the electron-phonon coupling strength g of the $P-O^-$ stretching mode, which is given as the intensity ratio of the phonon sideband to that of the pure electronic line[16,22], increases with increasing x and almost saturates around x=30. Accordingly, phonons due

to the $P-O^-$ bond with the highest frequency are considered to contribute to the multiphonon relaxation of rare earth ions.

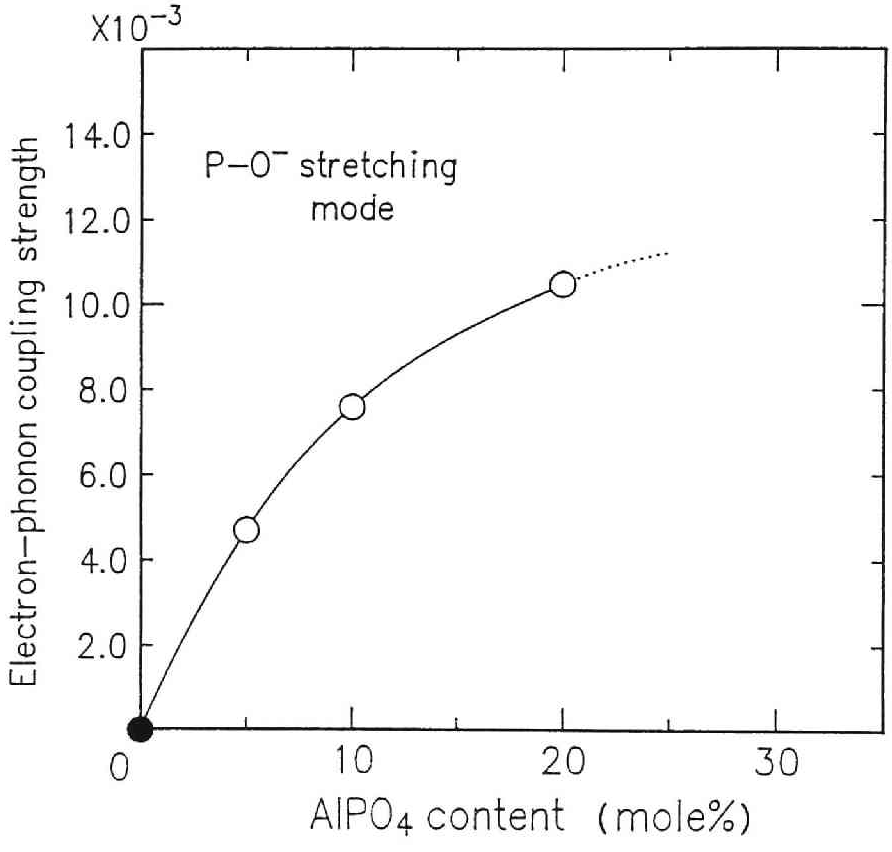

FIG.6: Compositional dependence of the electron-phonon coupling strength of the P-O stretching mode.

B. Upconversion of Er^{3+} in glass

The energy-level diagram and a possible upconversion mechanism of Er^{3+} by 0.80-μm excitation are shown in Fig. 7. The

efficiency of upconversion fluorescence depends upon the probability of multistep excitation by the excited state absorption or the energy transfer between adjacent excited ions, as well as the quantum efficiency of the emitting level. By either process, the probability becomes proportional to the lifetime of the intermediate excited states. The lifetime of an excited state, τ, is dominated by the radiative and nonradiative decay rates and given by

$$1/\tau = W_{RD} + W_p + \ldots , \qquad (2)$$

where W_{RD} is the radiative decay rate and W_p is the nonradiative decay rate due to the multiphonon relaxation. To minimize the nonradiative loss, it is advantageous to suppress W_p, which is given at T=0 K by[32]

$$W_p(0)=W_0(0)\cdot\exp[-\alpha\Delta E/\hbar\omega] \qquad (3)$$

$$\alpha = \ln(p/g)-1 \qquad (4)$$

$$p \simeq \Delta E/\hbar\omega \qquad (5)$$

where ΔE is the energy gap to the next lower level, g is the electron-phonon coupling strength, p is the number of phonons consumed during multiphonon relaxation and $W_0(0)$ is the decay rate at $\Delta E=0$ and T=0. Accordingly, W_p increases with increasing $\hbar\omega$ and g. The presence of high energy stretching vibrations of network polyhedra[20] in most oxide glasses lowers the efficiency of upconversion. However, in some heavy metal oxide glasses, the cutoff frequency is still low and comparable to those of fluoride glasses[33] which results in the observation of the upconversion fluorescence in oxide glasses such as tellurite and gallate systems[34]. In fluorophosphate glasses, the cutoff frequency was 1060 cm^{-1}, which is higher than those of germanate and tellu-

rite glasses. Furthermore, as shown in Fig.8, the rapid increase of the electron-phonon coupling strength g with phosphate addition also contributes to W_p.

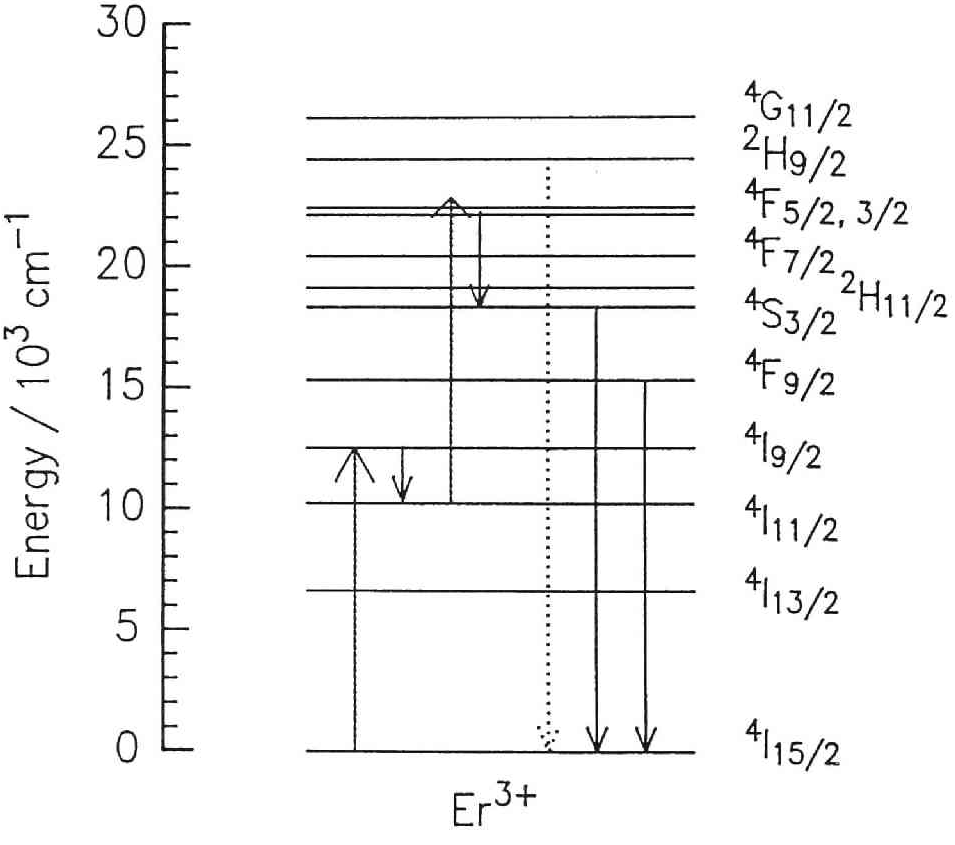

FIG.7: Energy level diagram and a possible mechanism of two-step excitation for the Er^{3+} ion under 800-nm excitation.

Therefore, the compositional dependence of fluorescence intensity in Fig.1 can be attributed to the coupling of the high-energy phonon to rare earth ions in fluorophosphate glasses, since the multiphonon decay rate increases with increasing $\hbar\omega$ and g, as expected from eqs.(3)-(5).

C. Temperature dependence of upconversion fluorescence

The rate of multiphonon relaxation at a temperature T is influenced by the population of the phonon mode, which is given by the Planck distribution function[35], n(T), where $n(T) = [\exp(\hbar\omega/kT)-1]^{-1}$. In the relaxation process of creating p Stokes-phonons, the probability becomes proportional to $[n(T)+1]^p$. The multiphonon relaxation rate is then given by[16,20,36],

$$W_p(T)=W_p(0)\cdot[n(T)+1]^p$$
$$=W_p(0)\cdot[1-\exp(-\hbar\omega/kT)]^{-p} \qquad (6)$$

where $W_p(0)$ is the multiphonon decay rate at 0 K given by eq.(3). For the host of larger $\hbar\omega$, the temperature dependence become small, whereas $W_p(0)$ is large. Assuming that W_p is large enough compared with W_{RD}, which holds for the levels with low quantum efficiency such as Er^{3+}:$^4I_{9/2}$ and Er^{3+}:$^4I_{11/2}$, one can calculate the relative lifetime of the intermediate excited state of the Er^{3+} ion by Eqs.(2), (3) and (6). Since the probability of upconversion excitation is expected to be proportional to the lifetime of the intermediate excited state, it is interesting to investigate the temperature dependence of the intermediate levels of the Er^{3+} ion. In the case of 800-nm excitation of Er^{3+} in

this study, the absorption occurs from the ground $^4I_{15/2}$ to the excited $^4I_{9/2}$ level. The energy gap of $^4I_{9/2}$ to the next $^4I_{11/2}$ level is about 2000 cm^{-1}, while that from $^4I_{11/2}$ to $^4I_{13/2}$ is about 3300 cm^{-1}. The estimated phonon energy dependence of the relative lifetime of $^4I_{9/2}$ and $^4I_{11/2}$ are shown as a function of temperature in Fig.8 (a) and (b), respectively. Clearly, the temperature dependence of the fluoride host ($\hbar\omega$ = 600 cm^{-1}) is larger than that of the fluorophosphate glass ($\hbar\omega$ = 1100 cm^{-1}). The phonon energy of 800 cm^{-1} corresponds to that of tellurite glasses[34], in which the lifetime is long compared with that of the fluorophosphate glass. Here, the ratio of the lifetime between different $\hbar\omega$ is also a function of the energy gap. The ratio of the lifetime of the fluoride to that of the fluorophosphate is larger for the energy gap of 3300 cm^{-1} ($^4I_{11/2}$) than for 2000 cm^{-1} ($^4I_{9/2}$). The relative ratio of the upconversion intensity of two glasses shown in Figs.3(a) and 3(b) is plotted in Fig.9 in addition to that of $40AlF_3 \cdot 10ErF_3 \cdot 30CaF_2 \cdot 20BaF_2$ glass. This tendency is similar to that shown in Fig.8(b) rather than that in Fig. 8(a). Accordingly, the level crucial to the efficiency of upconversion process can be $^4I_{11/2}$ rather than $^4I_{9/2}$. This interpretation is supported by the fact that the emission due to the $^2H_{9/2} \rightarrow {}^4I_{15/2}$ transition is not efficiently observed in the upconversion spectra under 802-nm excitation, which indicates that the second step excitation does not start from $^4I_{9/2}$ level and thus a three step excitation is needed to reach the $^2H_{9/2}$ level. Therefore, we conclude that the $^4I_{9/2}$ level decays to $^4I_{11/2}$ level by a rapid multiphonon relaxation and excitation process starting from this level.

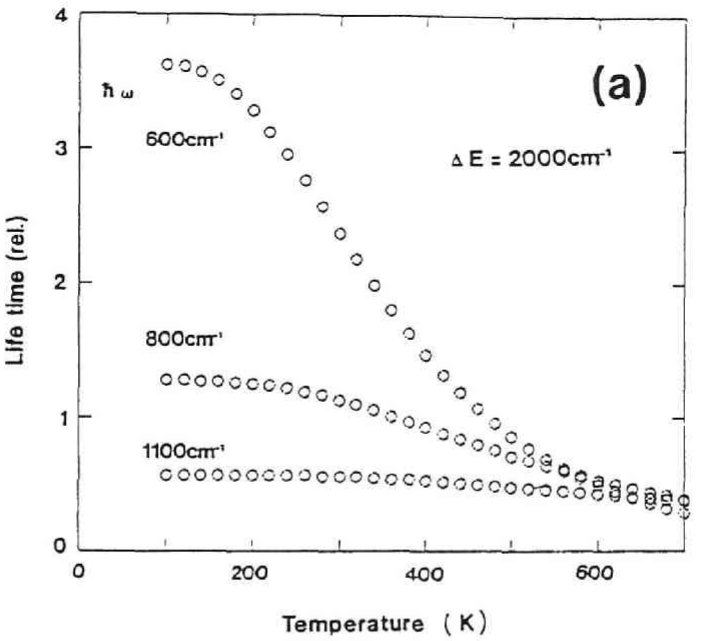

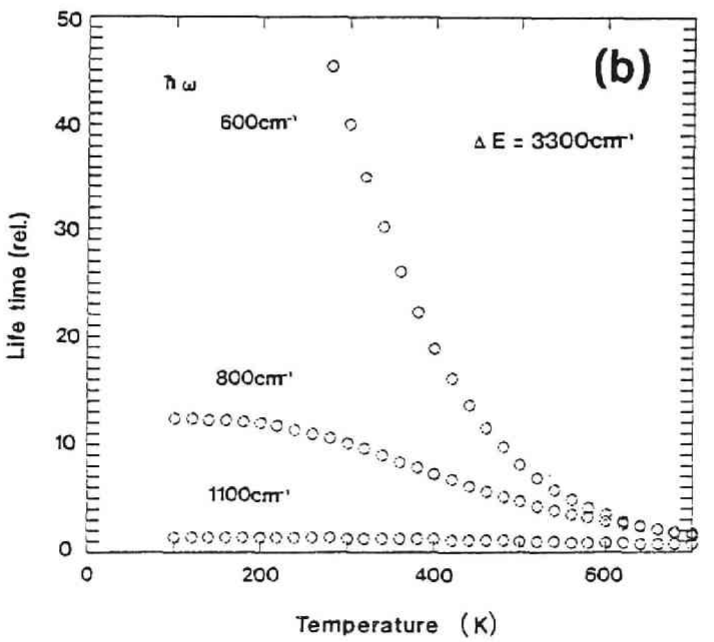

FIG.8: Temperature dependence of the calculated lifetime of Er^{3+}: (a) $^4I_{9/2}$ and (b) $^4I_{11/2}$ level for various $\hbar\omega$.

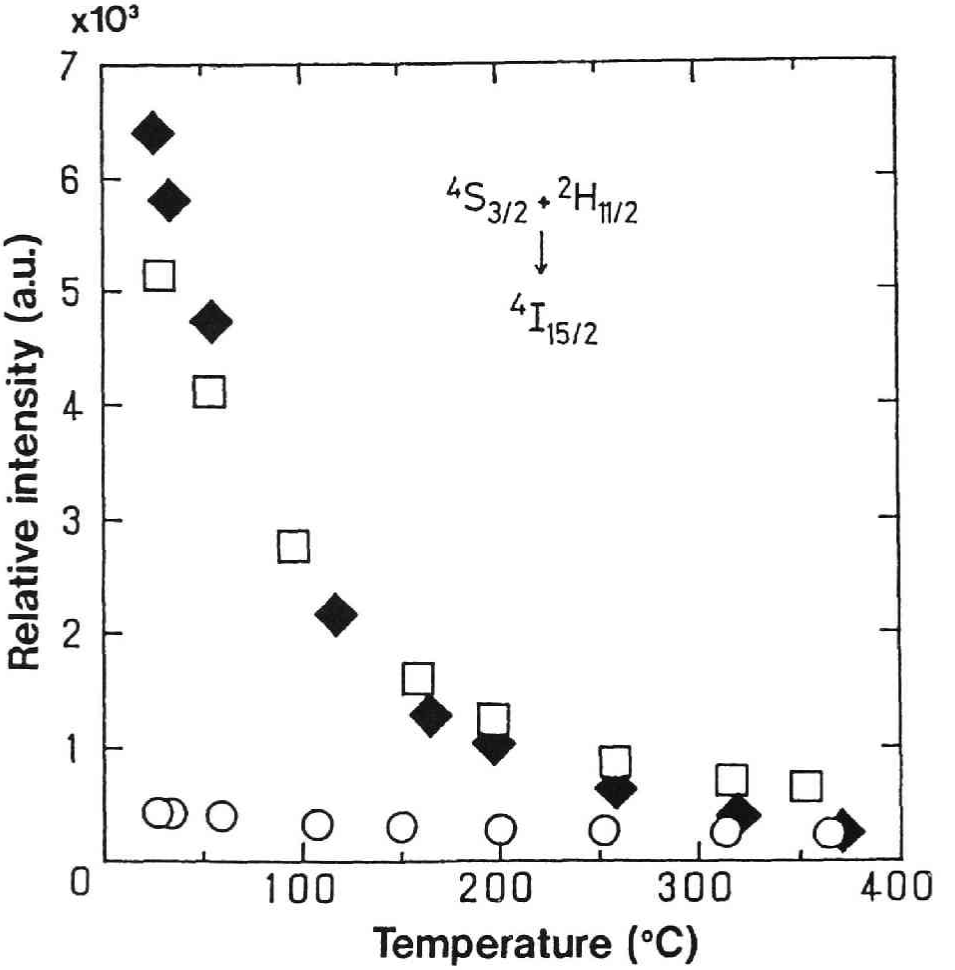

FIG.9: Temperature dependence of the intensity of upconversion fluorescence for □:y=0 and ○:y=5 glass. That of the $40AlF_3 \cdot 10ErF_3 \cdot 30CaF_2 \cdot 20BaF_2$ glass is also shown by ◆ for comparison.

V. CONCLUSIONS

The upconversion properties of Er^{3+} ions were studied for the fluorophosphate glasses $(45-x)AlF_3 \cdot xAlPO_4 \cdot 5ErF_3 \cdot 30CaF_2 \cdot 20BaF_2$, with use of the infrared radiation from a (Ga,Al)As laser diode (λ=802 nm) as an excitation source. Green upconversion fluorescence due to the $^4S_{3/2} \rightarrow {}^4I_{15/2}$ transition could be observed for the fluoride glass, while the fluorescence intensity for fluorophosphate glasses decreased drastically with increasing $AlPO_4$ content. It was found from the phonon sideband spectra of Eu^{3+} that the phonon with $\hbar\omega$ = 1060 cm^{-1}, corresponding to $P\text{-}O^-$ stretching vibration, became coupled to the multiphonon relaxation of rare earth ions and its electron-phonon coupling strength increased drastically with increasing phosphate content. The temperature dependence of upconversion intensity was large for the fluoride system, while it was small for the fluorophosphate system. These tendencies could be well explained by considering the multiphonon decay rate of the Er^{3+} intermediate level and its temperature dependence, which are functions of the phonon energy of the host and the energy gap to the next-lower level of Er^{3+}. These differences in local structure and multiphonon mechanisms were confirmed by the ^{151}Eu Mössbauer spectroscopic measurement. It is concluded that the the efficiency of the upconversion process is dominated by the lifetime of the intermediate level, which is influenced by the phonon mode locally coupled to the rare earth ion in the glass.

4.3. UPCONVERSION FLUORESCENCES OF Er^{3+} IN HEAVY METAL OXIDE GLASSES

I. INTRODUCTION

It is well known that some rare earth ions when incorporated into a suitable host structure, can upconvert infrared radiation to visible emission. This upconversion fluorescence receives much interest, since this has the possibility to bring about the new laser system. The Er^{3+} ion is the most popular one among them and the upconversion fluorescence has been observed in some fluoride crystals and glasses[36-38], in which the maximum phonon energy is small enough to reduce nonradiative loss due to multi-phonon relaxation[21]. However, in oxide glasses, there are few reports on upconversion phenomenon because of the large nonradiative losses. This absence can be ascribed to the fact that there exist the stretching vibrations of the glass network former polyhedron in oxide glasses[39] and hence these high energy phonons increase the nonradiative loss since they can conserve the energy gap in the lowest-order process. For this reason, it can be considered that the upconversion is difficult in silicate and borate glasses. Indeed, Si-O(~1100 cm^{-1}) and B-O(~1400 cm^{-1}) bonds are coupled with the doped rare earth ions as shown by the phonon sideband measurement of Eu^{3+}-doped silicate[22] and borate[23] glasses. In order to improve the chemical durability and stability of the material, particularly, the stability at high temperature, oxide system can be better as a host glass

rather than halide systems such as fluoride, chloride and bromide glasses. Therefore, in the oxide glass systems without the so-called network-former (*NWF*) compounds, it may be possible to realize the upconversion fluorescence, since they have a structure with the lower cutoff phonon energy. In this section, oxide glasses such as tellurite[40,41] and gallate[33,42-44] were chosen as host glasses of Er^{3+} ion and visible fluorescence spectra were obtained by exciting with the 800 nm radiation from diode laser.

II. EXPERIMENTAL

Glasses were prepared by using reagent grade PbO, Bi_2O_3, Ga_2O_3, $SrCO_3$, TeO_2, GeO_2 and Na_2CO_3 as starting materials. The glass compositions investigated here are listed in Table 1. The germanate glass system was chosen because the phonon energy is the lowest among the conventional *NWF* compounds. The powder of batch composition was melted in a platinum crucible for 30 min. at suitable temperature, which is also listed for each sample in Table 1. The melt was poured on a stainless steel and pressed with a plate. The fluorescence spectra were measured with *Hitachi-850* Fluorescence Spectrophotometer. As ultraviolet and infrared excitation sources, a Xe-lamp and (Ga,Al)As diode laser (λ = 798.3 nm, *Matsushita Electric Corp.*) were used, respectively.

Table 1: Compositions of Glasses

Composition	Melting Temperature (°C)
$70GeO_2 \cdot 30Na_2O \cdot 1Er_2O_3$	1300
$70TeO_2 \cdot 30Na_2O \cdot 1Er_2O_3$	800
$66.7SrO \cdot 33.3Ga_2O_3 \cdot 1Er_2O_3$	1500
$62PbO \cdot 20Bi_2O_3 \cdot 17Ga_2O_3 \cdot 1Er_2O_3$	1100

III. RESULTS AND DISCUSSION

Upconversion fluorescence was observed successfully in the gallate, tellurite and lead bismuth based oxide glasses. In the germanate glass system, no upconversion fluorescence was observed with the present exciting condition (maximum power = 55mW). The normal and upconversion fluorescence spectra of $70TeO_2 \cdot 30Na_2O \cdot 1Er_2O_3$, $66.7SrO \cdot 33.3Ga_2O_3 \cdot 1Er_2O_3$ and $62PbO \cdot 20Bi_2O_3$ $17Ga_2O_3$ $1Er_2O_3$ glass are shown in Fig.1, 2 and 3, respectively. As it was difficult to compare the absolute intensity each other, the ordinate is shown in the arbitrary unit. The most intense peak around 550 nm is due to $^4S_{3/2} \rightarrow {}^4I_{15/2}$ transition, which revealed green for human eyes. The light path through the glass specimens excited by the laser appeared green, although the pump laser source was in the infrared region. The power dependence of the fluorescence spectra for the Sr-Ga-O glass is shown in Fig.4. The fluorescence intensity is varied with the power of pumping laser source. The dependence of the fluorescence intensity on the power was almost quadratic rather than linear. It indicates that the two step excitation either by two photon absorption or

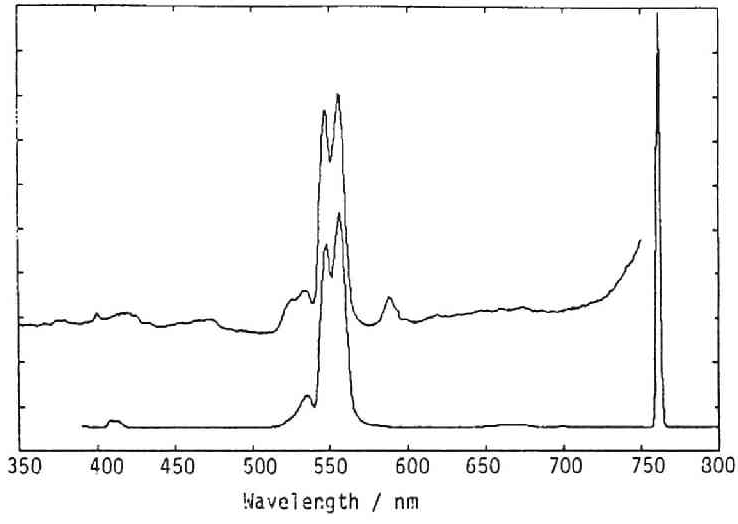

Fig.1: Normal and upconversion-pumped fluorescence of $70TeO_2 \cdot 30Na_2O \cdot 1Er_2O_3$ glass. The upper line shows the IR-excited upconversion-pumped fluorescence and the bottom line shows the UV-excited normal fluorescence.

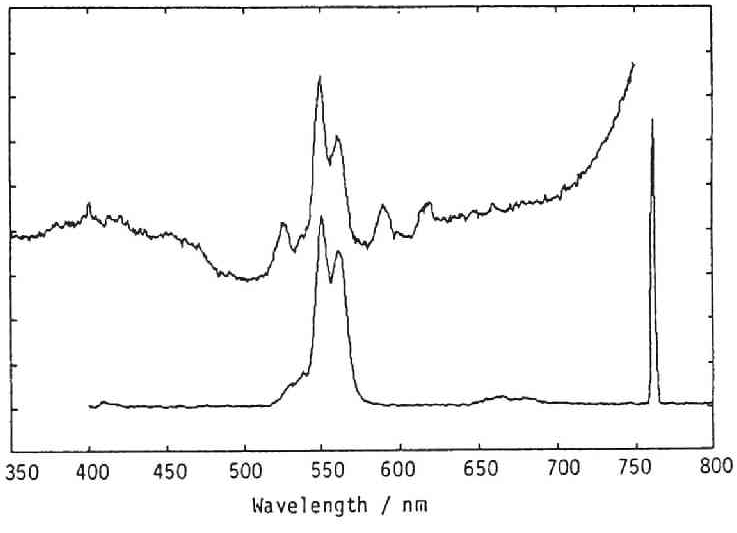

Fig.2: Normal and upconversion-pumped fluorescence of $66.7SrO \cdot 33.3Ga_2O_3 \cdot 1Er_2O_3$ glass. The upper line shows the upconversion-pumped fluorescence.

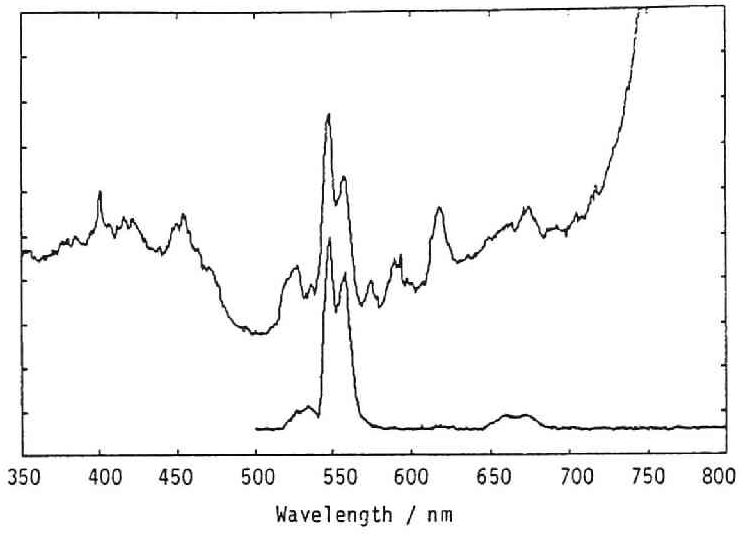

Fig.3: Normal and upconversion-pumped fluorescence of $62PbO \cdot 20Bi_2O_3 \cdot 17Ga_2O_3 \cdot 1Er_2O_3$ glass. The upper line shows the upconversion-pumped fluorescence.

by energy transfer between two excited Er^{3+} ions, certainly occurs even in this oxide glass host. Thus, this is the first case of the efficient upconversion fluorescence in the oxide glass. In this material, it is expected that this process occurs even at higher temperature than room temperature, since the temperature dependence of nonradiative decay rate is considered to be small according to the next equation[16,20],

$$W_p(T)=W_p(0)\cdot[n(T)+1]^p$$
$$=W_p(0)\cdot[\exp(\hbar\omega/kT)/\{\exp(\hbar\omega/kT)-1\}]^p$$

where $W_p(T)$ and $W_p(0)$ are the nonradiative decay rate at temperature T and 0 K, respectively, p is the phonon number consumed during multiphonon relaxation. Thus, for the host of higher

phonon energy $\hbar\omega$, $\hbar\omega/kT$ becomes large and the number of phonon, p becomes small, leading to small temperature dependence of nonradiative loss due to multiphonon decay. As the $W_p(0)$ is a decreasing function of p, it is probable that the $W_p(T)$ is larger

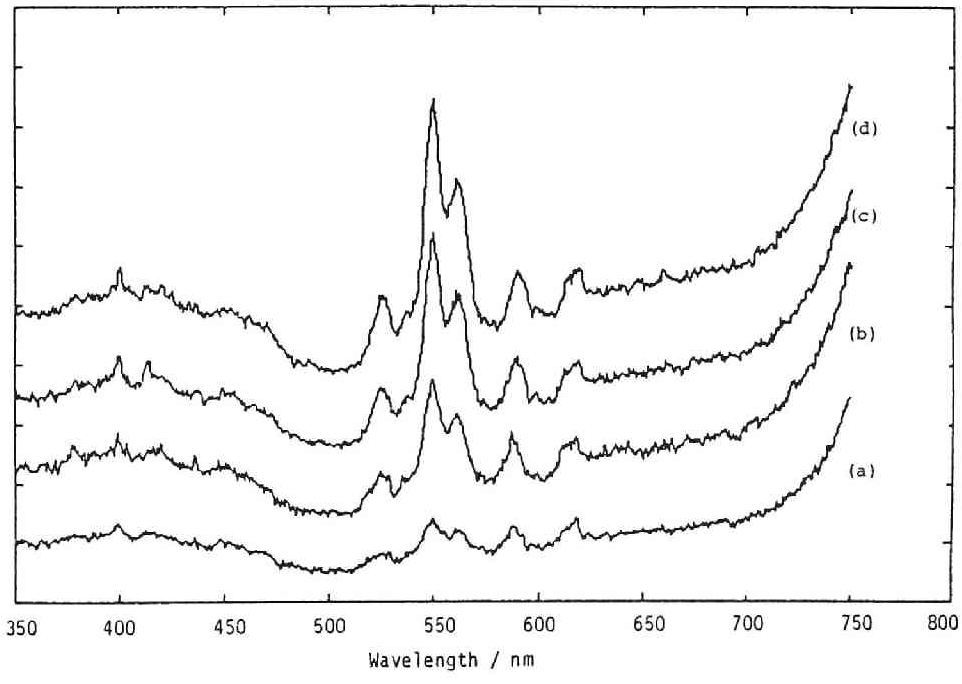

Fig.4: Excitation power dependence of upconversion-pumped fluorescence of $66.7SrO \cdot 33.3Ga_2O_3 \cdot 1Er_2O_3$ glass: the excitation powers are (a)20mW, (b)35mW, (c)50mW and (d)55mW.

than those of halide glasses at relatively lower temperature. In spite of this estimation, the upconversion occurred efficiently still at room temperature. Thus the small temperature dependence can increase the upper temperature limit of observable upconversion emission.

IV. CONCLUSIONS

Upconversion fluorescence can be observed at room temperature in Er^{3+}-doped oxide glasses with no sensitizing ions such as Yb^{3+} in the systems of TeO_2- and Ga_2O_3-based ones. A diode laser operating at 798 nm corresponding to the $Er^{3+}:{}^4I_{9/2}\leftarrow{}^4I_{15/2}$ absorption was used as the pumping source for excitation and the green emission around 550 nm due to the ${}^4S_{3/2}\rightarrow{}^4I_{15/2}$ could be observed. The two step process for upconversion was suggested by the quadratic changes of fluorescence intensity against the pumping power. The possibility was shown that these oxide glasses can become one candidate for a high temperature upconversion device.

REFERENCES

[1] N. Soga and S. Tanabe, *Chemistry* **45**(11), (1990) 804-05.

[2] M. Ikeda, A. Toda, K. Nakano, Y. Mori and N. Watanabe, *Appl. Phys. Lett.* **50**, (1987) 1033-35.

[3] S. Kawata, K. Kobayashi, H. Fujii, I. Hino, A. Gomyo, H. Hotta and T. Suzuki, *Electron. Lett.* **24**, (1988) 1489-91.

[4] T. Tanaka, H. Yanagisawa, H. Kakibayashi, S. Minagawa and T. Kajimura, *Appl. Phys. Lett.* **59**, (1991) 1943-46.

[5] N. Bloembergen, *Phys. Rev.* **2**, (1959) 84-85.

[6] F. Auzel, *C. R. Acad. Sci.* **262**, (1966) 1016-19.

[7] F. Tong, W.P. Risk, R.M. Macfarlane and W. Lenth, *Electron. Lett.* **25**, (1989) 1389-91.

[8] R.M. Macfarlane, R. Wannemacher, T. Herbert and W. Lenth, *CLEO* (1991) CWF1.

[9] R.M. Macfarlane, T. Tong, A.J. Silversmith and W. Lenth, *Appl. Phys. Lett.* **52**, (1988) 1300-02.

[10] M. Poulain, M. Poulain, and J. Lucas, *Mater. Res. Bull.* **10**, (1975) 243.

[11] S. Tanabe, K. Hirao and H. Toratani, *Solid State Physics* **27**(3), (1992) 186-196.

[12] J.Y. Allain, M. Monerie and H. Poignant, *Electron. Lett.* **26**, (1990) 261-263.

[13] R.G. Smart, D.C. Hanna, A.C. Tropper, S.T. Davey, S.F. Carter and D. Szebesta, *Electron. Lett.* **27**, (1991) 1307-09.

[14] T.J. Whitley, C.A. Millan, R. Wyatt, M.C. Brierley and D. Szebesta, *Electron. Lett.* **27**, (1991) 1785-87.

[15] J.Y. Allain, M. Monerie and H. Poignant, *Electron. Lett.* **26**, (1990) 166-68.

[16] H. Kuroda, S. Shionoya and T. Kushida, *J. Phys. Soc. Japan* **33**(1), (1972) 125-141.

[17] S.A. Pollack, D.B. Chang and N.L. Moise, *J. Appl. Phys.* **60**(12), (1986) 4077-86.

[18] J.P. van der Ziel, L.G. Van Uitert, W.H. Grodkiewicz and R.M.Mikulyak,

*J. Appl. Phys.*60(1), (1986) 4262-67.

[19] D.C. Yeh, W.A. Sibley, M. Suscavage and M.G. Drexhage, *J.Appl.Phys.* 62(1), (1987) 266-275.

[20] C.B. Layne, W.H. Lowdermilk and M.J. Weber, *Phys. Rev. B* **16**(1), (1977) 10-20.

[21] C.B. Layne and M.J. Weber, *Phys. Rev. B* 16(7), (1977) 3259-61.

[22] H. Toratani, T. Izumitani and H. Kuroda, *J. Non-Cryst. Solids* **52**, (1982) 303-313.

[23] S. Tanabe, S. Todoroki, K. Hirao and N. Soga, *J. Non-Cryst. Solids* **122**, (1990) 59-65.

[24] S. Tanabe, K. Hirao and N. Soga, *J. Non-Cryst. Solids* **113**, (1989) 178-184.

[25] O. Berkooz, *J. Phys. Chem. Solids* **30**, (1969) 1763-67.

[26] P. Brix, S. Hüfner, P. Kienle and D. Quitmann, *Phys. Lett.* **13**(2), (1964) 140-42.

[27] G. Gerth, P. Kienle and K. Luchner, *Phys. Lett.* **27A**(8), (1968) 557-58.

[28] A.L. Allred, *J. Inorg. Nucl. Chem.* **17**, (1961) 215.

[29] J-J. Videau, J. Portier and B. Piriou, *J. Non-Cryst. Solids* **48**, (1982) 385-392.

[30] M. Villa, G. Chiodelli and M. Scagliotti, *Solid State Ionics* **18&19**, (1986) 382-87.

[31] Y. Kawamoto and A. Kono, *J. Non-Cryst. Solids* **85**, (1986) 335-345.

[32] T. Miyakawa and D.L. Dexter, *Phys. Rev. B* 1(7), (1970) 2961-69.

[33] W.H. Dumbaugh, *Phys. Chem. Glasses* **27**(3), (1986) 119-123.

[34] S. Tanabe, K. Hirao and N. Soga, *J. Non-Cryst. Solids* **122**, (1990) 79-82.

[35] C. Kittel, *Introduction to Solid State Physics*, (6 ed., John Wiley & Sons, Inc., New York, (1986) p.101.

[36] M.D. Shinn, W.A. Sibley, M.G. Drexhage and R.N. Brown, *Phys. Rev. B* **27**(11), (1983) 6635-648.

[37] K. Okada, K. Miura, I. Masuda and T. Yamashita, *Ext. Abst. 5th Int. Symp. Halide Glasses* (1988) pp.146-151.

[38] W.A. Sibley and D.C. Yeh, *ibid.*, (1988) pp.564-69.

[39] K. Hirao and N. Soga, *J. Ceram. Soc. Jpn.* **97**, (1989) 359-364.

[40] J.E. Stanworth, *Nature* **4301**, (1952) 581-82.

[41] T. Yoko, K. Kamiya, K. Tanaka, H. Yamada and S. Sakka, *J. Ceram. Soc. Jpn.* **97**, (1989) 289-294.

[42] L.L. Lyudina, T.A. Sidorov, T.G. Sheinina, L.V. Milova, E.M. Galaktionova and E.I. Levedeva, *Neorg. Mat.* **11**, (1975) 573.

[43] T. Kokubo, Y. Inaka and S. Sakka, *J. Non-Cryst. Solids* **80**, (1986) 518-526.

[44] K. Fukumi and S. Sakka, *Phys. Chem. Glasses* **29**, (1988) 1-8.

Chapter 5.

UPCONVERSION MECHANISMS OF RARE EARTH DOPED GLASSES BY TUNABLE LASER SPECTROSCOPY

Since the upconversion is a phenomenon of emitting a photon with higher energy than that of an exciting photon, more than two photons must contribute to the excitation. The multistep excitation with high efficiency occurs either by the energy transfer *(Addition de Photon par Transfert d'Energie, APTE)* between adjacent two ions or the *excited state absorption (ESA)* in a single ion. These two pathways are represented in Fig.6.1. Now it is obvious that the main mechanisms for upconversion depends on the kind and concentration of rare earth ions, the composition of host, and excitation wavelengths. However, the knowledge is not yet available on the relationship between the mechanisms and these factors. In order to design an efficient upconversion laser glass, it is necessary to clarify whether *APTE* or *ESA* is the controlling mechanism for the upconversion of a glass. I could reach the next conclusion; one method to distinguish *ESA* and *APTE* mechanisms is to see how the upconversion efficiency varies with the wavelength of the pump light.* In the case of *APTE* mechanism, the incident light is absorbed only in the transition from the ground state, so the wavelength dependence of efficiency should depend only on the ground state absorption. For *ESA* mechanism, on the other hand, the efficiency depends also on the excited state absorption cross section of the transition

---

* S. Tanabe, *Text of the 23rd Summer Seminar for Young Glass Scientists*, (Ceram. Soc. Jpn., 1991) 65-75.

from a certain intermediate level. In general, the *ESA* cross section will not vary with wavelength in the same way as the ground state absorption. Therefore, a tunable source such as a dye laser can be used to verify the upconversion mechanism by

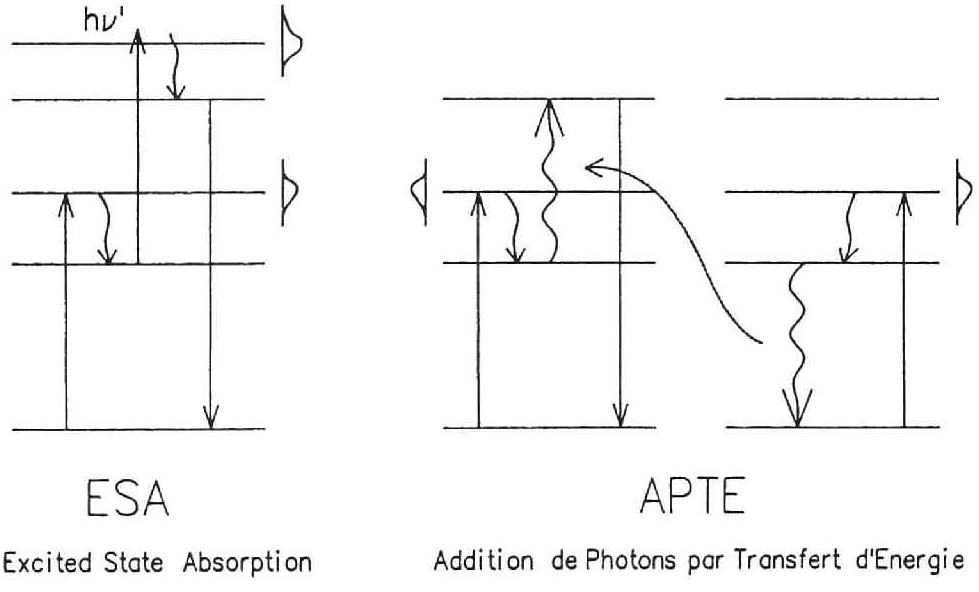

Fig.1: Upconversion mechanisms; (a) Excited state absorption and (b)Addition of photons by transfer of energy.

tuning across the Er^{3+} absorption profile. In section 5.1, a tunable DCM-dye laser excited by an Ar^{+} laser was used as a pumping source in the wavelength range corresponding to $^4F_{9/2} \leftarrow {}^4I_{15/2}$ absorption around 0.65μm.**

In addition to green emission of Er^{3+}, a blue laser is also an attractive material because there is a need for higher density in the optical data storage as well as for multicolorization of visible lasers. While, it has been difficult to obtain blue emission by Er^{3+} and Ho^{3+} ions, the Tm^{3+} ion has stable excited levels emitting blue fluorescence; $^1D_2$ and $^1G_4$. In section 6.2, a fluoroaluminate glass was chosen as a host of Tm^{3+} ion and upconversion characteristics were investigated by a single wavelength pumping around 0.65μm. To design an efficient UV or blue laser, it is also important to clarify the mechanisms in the Tm^{3+} doped glass. Therefore, the excitation spectra was monitored by tuning across the Tm^{3+}:$^3F_{2,3} \leftarrow {}^3H_6$ absorption profile with DCM-dye laser source and the excitation processes leading to UV and blue upconversions were discussed.

** S. Tanabe, S. Yoshii, K. Hirao and N. Soga, *"Science and Technology of New Glasses"*, (ed. S. Sakka and N. Soga, Ceram. Soc. Jpn., 1991) 193-98.

5.1. ANALYSIS OF Er^{3+} UPCONVERSION MECHANISMS IN FLUORIDE GLASS BY DCM-DYE LASER

I. INTRODUCTION

Infrared-excited visible luminescence of rare earth ions doped in crystals and glasses has been attracting a great interest[1-3]. In particular Er^{3+} fluorescence upconversion is widely investigated since the high power III-V group laser diode (*LD*) with the infrared wavelength of 1.48μm[1], 0.98μm[2] and 0.80μm[3] can be used as exciting sources. These wavelengths correspond to the absorption from the ground state $^4I_{15/2}$ to the first($^4I_{13/2}$), second ($^4I_{11/2}$) and third($^4I_{9/2}$) excited states of Er^{3+} ion, respectively. To excite Er^{3+} into the fourth excited level ($^4F_{9/2}$), the pump source of ~0.65μm is necessary. However, the *LD* of this wavelength range is not usually available partly because of the difficulty in the present fabrication technology for high power (Al,Ga,In)P diode lasers of wider band gap with quantum well structures. Therefore, there is not yet a report on 0.65μm-pumped Er^{3+} green upconversion until now. In the case of 0.98μm or 0.80μm pumping, the green emission from $^4S_{3/2}$ level obeyed quadratic law[2,3], indicating two-step excitation either by the energy transfer *(Addition de Photons par Transfert d'Energie, APTE)* between adjacent two ions or the *excited state absorption (ESA)* in a single ion. For the design of an efficient upconversion laser glass, it is necessary to clarify whether *APTE* or *ESA* is a controlling mechanism.

In the *APTE* process, the incident light is absorbed only in the transition from the ground state, so the wavelength dependence of efficiency depends only on the $^4F_{9/2} \leftarrow {}^4I_{15/2}$ transition. For *ESA* mechanisms, however, the efficiency depends also on the excited state absorption cross section of the transition from a certain intermediate level, such as $^4I_{13/2}$ or $^4I_{11/2}$. Since the *ESA* cross sections from these Er^{3+} levels do not vary with wavelength in the same way as the ground state absorption, a tunable dye laser was used to verify the upconversion mechanism by tuning across the Er^{3+} absorption profile. In this study, a DCM-dye laser excited by an Ar^+ laser was used as a pumping source in the wavelength range corresponding to $^4F_{9/2} \leftarrow {}^4I_{15/2}$ absorption around $0.65\mu m$.

II. EXPERIMENTAL

A. *Sample Preparation*

A fluoride glass with the composition of $40AlF_3 \cdot 22CaF_2$ $22BaF_2$ $15YF_3$ $1ErF_3$ was prepared by a conventional melting method. The glass obtained was annealed at 435°C for 15min. and polished into $10x10x4mm^3$ after being cut by diamond saws.

B. *Spectroscopic Measurement*

To get the phonon sideband spectra of rare earth ions[4], the Eu^{3+}-doped glass with the same composition instead of Er^{3+} was also prepared. Fluorescence and excitation spectra were measured with a *Hitachi-850* Fluorescence Spectrophotometer. As upconversion pump sources, an (Al,Ga)As laser diode (*SONY SLD-302XT*, 802nm) and a dye-laser (*Spectra Physics Model 375* Dye Laser)

excited by an Ar^+ laser (*Coherent innova 70*) were used. DCM dye was used to obtain tunable range from 620 to 700 nm. Shematic figure of the measurement is shown in Fig.1. Absorption spectra was measured with a *Shimadzu UV-2200* Recording Spectrophotometer. Refractive index was measured with an Abbe's refractometer.

C. *Judd-Ofelt Analysis*

From the measured oscillator strength of various observed transitions and n_D, a least square fitting approach was used on Judd-Ofelt treatment as follows.

The line strength for the electric dipole transition between an initial J manifold $|(S,L)J\rangle$ and a final J manifold $|(S',L')J'\rangle$ is obtained by[5]

$$S[(S,L)J;(S',L')J'] = \sum_{t=2,4,6} \Omega_t |\langle (S,L)J||U^{(t)}||(S',L')J'\rangle|^2, \quad (1)$$

where three terms $\langle||U^{(t)}||\rangle$ are the reduced matrix elements of the unit tensor operators calculated in the intermediate-coupling approximation, and the coefficient Ω_2, Ω_4 and Ω_6 are the intensity parameters.

The line strengths for electric dipole transitions are related to the integrated absorbance and are given by[5]

$$\int_{band} k(\lambda)d\lambda = \frac{8\pi^3 e^3 \bar{\lambda}\, \rho_N}{3ch(2J+1)n^2}\, \chi S_{JJ'}, \quad (2)$$

where $k(\lambda)$ is the absorption coefficient, $\bar{\lambda}$ is the mean wavelength of the absorption band, ρ_N is the concentration of the rare earth ion, and the χ terms correct the effective field at a well localized center in a medium of isotropic refractive index n and are given by $\chi = n(n^2+2)^2/9$ for electric dipole transitions.

Since the reduced matrix elements, $\langle||U^{(t)}||\rangle$ are constant characteristic to each transition as shown in Table 1, three Ω_t parameters can be obtained experimentally from the line strengths of more than three bands. In this study, six bands indicated in Table 1 were used, although the $^2K_{15/2} \leftarrow {}^4I_{15/2}$ transition include a magnetic dipole contribution a little(< 1%).

Table I. Reduced Matrix Elements of $U^{(t)}$ for Er^{3+} ion used for the fitting of Ω and calculation of A. Typical mean wavelengths $\bar{\lambda}$ are included. Two transitions indicated by * include a magnetic dipole contribution[6].

[SL]J	[S'L']J'	$[U^{(2)}]^2$	$[U^{(4)}]^2$	$[U^{(6)}]^2$	$\bar{\lambda}$ (μm)	Band
$^4I_{13/2}$	$^4I_{15/2}$*	0.0188	0.1176	1.4617	1.50	
$^4I_{11/2}$	$^4I_{15/2}$	0.0259	0.0001	0.3994	0.98	
$^4I_{9/2}$	$^4I_{15/2}$	0.0	0.1452	0.0064	0.80	
$^4F_{9/2}$	$^4I_{15/2}$	0.0	0.5655	0.4651	0.65	-- 1
	$^4I_{13/2}$	0.0096	0.1576	0.0870		
	$^4I_{11/2}$	0.0671	0.0088	1.2611		
	$^4I_{9/2}$	0.096	0.0061	0.012		
$^4S_{3/2}$	$^4I_{15/2}$	0.0	0.0	0.2285	0.54	┐
	$^4I_{13/2}$	0.0	0.0	0.3481		
	$^4I_{11/2}$	0.0	0.037	0.0789		2
	$^4I_{9/2}$	0.0	0.0729	0.2560		
$^2H_{11/2}$	$^4I_{15/2}$	0.7056	0.4109	0.0870	0.52	┘
$^4F_{7/2}$	$^4I_{15/2}$	0.0	0.1467	0.6273	0.48	— 3
$^4F_{5/2}$	$^4I_{15/2}$	0.0	0.0	0.2237	0.45	┐ 4
$^4F_{3/2}$		0.0	0.0	0.1204	0.44	┘
$^2H_{9/2}$	$^4I_{15/2}$	0.0	0.078	0.17	0.41	— 5
$^2G_{11/2}$	$^4I_{15/2}$	0.9178	0.5271	0.1197	0.38	┐
$^2G_{9/2}$		0.0	0.2416	0.1235	0.37	┤ 6
$^2K_{15/2}$	*	0.0219	0.0041	0.0758	0.37	┤
$^2G_{7/2}$		0.0	0.0174	0.1163	0.36	┘

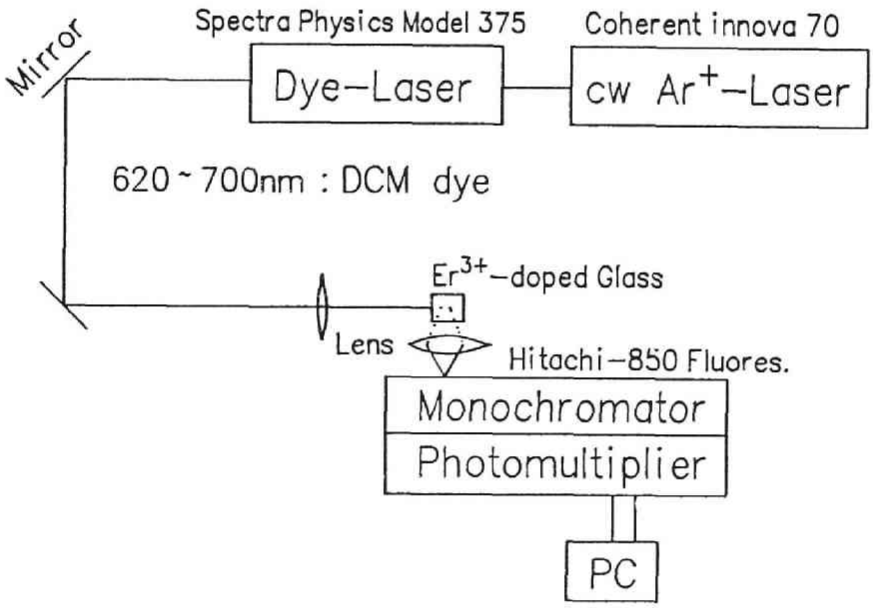

Fig.1: Schematic figure of the fluorescence measurement by DCM dye laser excitation.

III. RESULTS AND DISCUSSION

The absorption spectrum of the glass is shown in Fig.2. Also shown is the excitation spectrum of $^4S_{3/2} \rightarrow {}^4I_{15/2}$ emission at 550nm. The differences in relative excitation efficiencies of corresponding levels from the relative absorption intensities can be ascribed to the presence of the radiative decay process above $^4S_{3/2}$ level, such as that from $^2H_{9/2}$.

From the measured oscillator strengths of six bands and n_D=1.432, a least square fitting approach was used on Judd-Ofelt treatment. The obtained intensity parameters were Ω_2 = 2.35 x 10^{-20} cm^2, Ω_4 = 1.71x10^{-20} cm^2 and Ω_6 = 1.26x$10^{-20}$$cm^2$. The calculated oscillator strengths showed good agreement with the measured oscillator strengths, which are shown in Table 2. The rms deviation of them was 0.054x10^{-20} cm^2 (1.8%).

Table 2: Mean wavelength, observed and calculated line strengths of six bands from Judd-Ofelt analysis.

Band	λ (nm)	S($10^{-20}cm^2$)	S_c($10^{-20}cm^2$)
*	800	——	0.256
1	651.8	1.585	1.55
2	520.6	2.829	2.76
3	486.5	1.036	1.04
4	448.5	0.434	0.434
5	405.9	0.306	0.348
6	376.6	4.072	4.11

Ω_2=2.36x$10^{-20}cm^2$
Ω_4=1.71x$10^{-20}cm^2$
Ω_6=1.26x$10^{-20}cm^2$ rms = 0.054x$10^{-20}cm^2$ (1.8%)

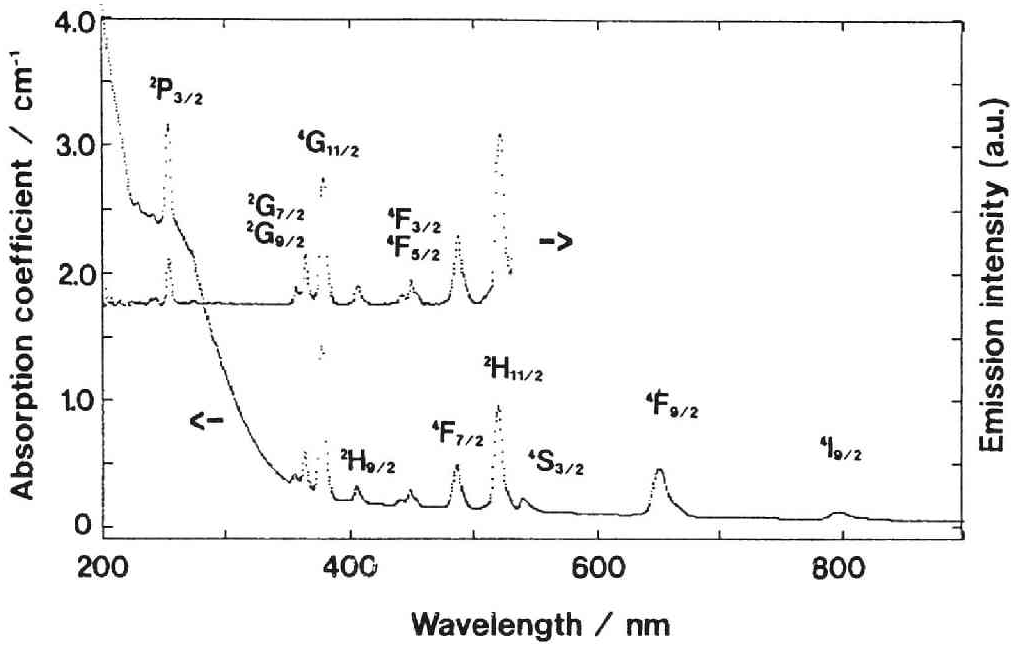

Fig.2: Absorption spectrum of Er^{3+} and excitation spectrum of Er^{3+}:$^4S_{3/2} \rightarrow {}^4I_{15/2}$ emission in the glass.

It is clear that the absorption cross section or line strength S_c of $^4I_{9/2}$ (* 800nm), which corresponds to the energy of (Al,Ga)As diode laser, is much smaller (1/6) than that of $^4F_{9/2}$(band 1). Therefore, the *GSA* transition probability is much higher by 0.65μm excitation, which should result in the efficient pumping compared with the 0.80μm excitation. The fluorescence spectrum by 0.65μm excitation is shown in Fig.3(a) with the fluorescence spectrum by 379nm excitation of $^4G_{11/2} \leftarrow {}^4I_{15/2}$(b), which has the largest absorption cross section in the UV range. The smaller intensity of 550nm emission than that of 660 nm in (a) is due to the existence of the second step excitation proc-

ess. The spectra variations with the power of 0.65μm radiation are shown in Fig.4. The intensities of emissions from $^4F_{9/2}$ and $^4I_{9/2}$ levels increased almost linearly with the excitation power, while that from $^4S_{3/2}$ level increased nonlinearly. A small peak at 840nm is ascribed to $^4S_{3/2}\rightarrow{}^4I_{13/2}$ emission[2], which also shows nonlinear dependence.

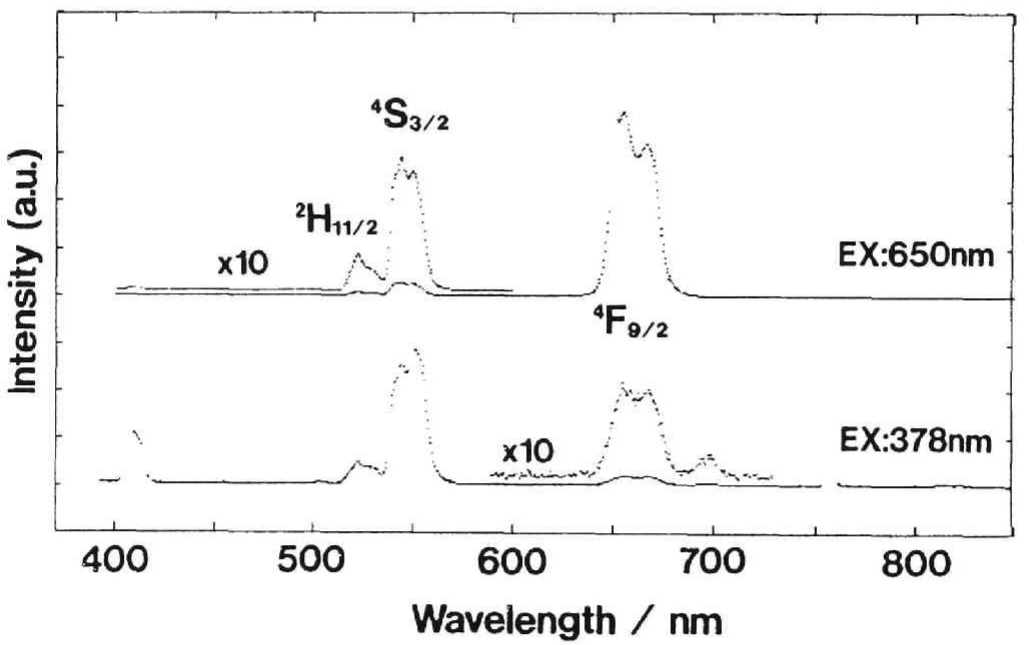

Fig.3: Fluorescence spectra of the glass; (a)DCM-laser excitation (650nm, 150mW), (b)UV-excitation(379nm).

The radiative transition probabilities, radiative lifetime, and branching ratios from $^4S_{3/2}$ and $^4F_{9/2}$ levels are calculated with the obtained Ω_t parameters and listed in Table 3.

From the calculated radiative lifetime and measured lifetime τ_f, the quantum efficiencies of these two levels were calculated by the relation $\eta = \tau_f/\tau_R$, to find $\eta(^4S_{3/2})=0.323$ and $\eta(^4F_{9/2})=0.041$. Therefore, the decay process of Er^{3+} ions in this glass is mainly composed of nonradiative ones by multiphonon relaxation and energy transfer.

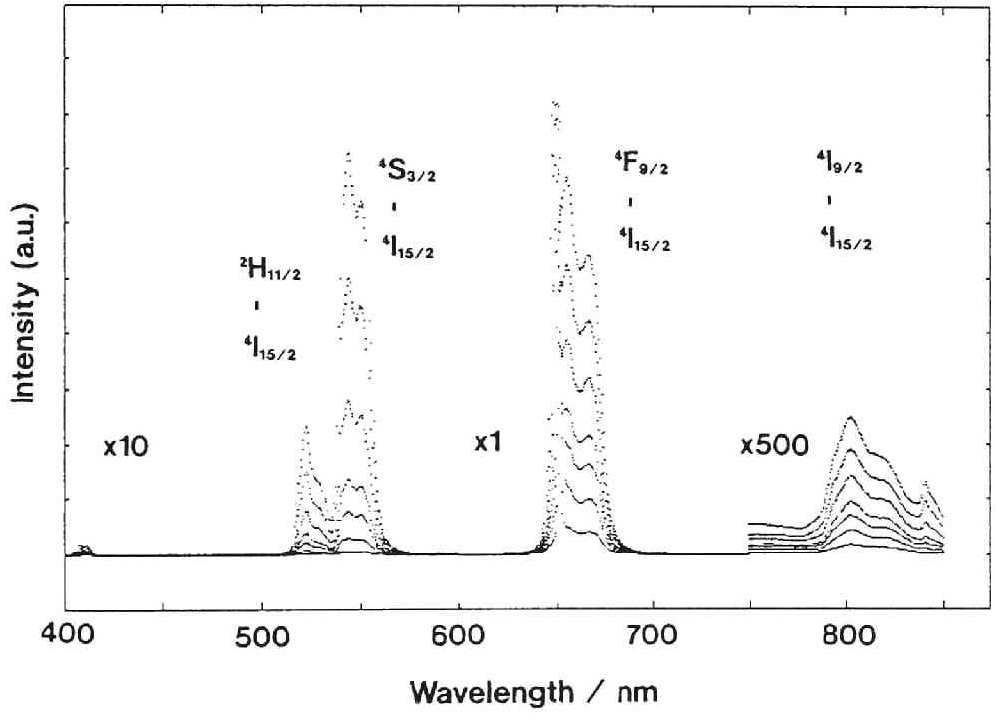

Fig.4: Variation of fluorescence spectra with pumping(650nm) power. The powers are 300, 200, 150, 100, 70 , 40, 20 mW from upside to downside. The wavelength range of 400-600nm is multiplied by 10 times and that of 750-850nm is by 500 times.

Table 3: Calculated radiative transition probabilities A, radiative lifetime τ_R and branching ratios β of Er^{3+} ions in the glass. Wavelengths are determined from emission spectra when possible from Fig.4.

Transition	λ (μm)	A(sec^{-1})	τ_R(μsec)	β	η
$^4S_{3/2} \rightarrow {}^4I_{15/2}$	0.55	864.7	752	0.65	0.343
$\rightarrow {}^4I_{13/2}$	0.84	369.8		0.27	
$\rightarrow {}^4I_{11/2}$	1.20	47.0		0.04	
$\rightarrow {}^4I_{9/2}$	1.66	48.9		0.04	
$^4F_{9/2} \rightarrow {}^4I_{15/2}$	0.66	1079.8	845	0.91	0.041
$\rightarrow {}^4I_{13/2}$	1.15	52.8		0.04	
$\rightarrow {}^4I_{11/2}$	1.93	49.0		0.04	
$\rightarrow {}^4I_{9/2}$	3.47	1.2		0.00	

The power dependences of the intensity of main emissions are plotted in Fig.5. Although there seems to be the effect of saturation at higher power than 100mW, the upconversion emission almost obeys the quadratic law, indicating two-step excitation.

The variations of fluorescence spectra with the excitation wavelength are shown in Fig.6. The excitation power was fixed at 100 mW. It can be seen that the shapes of the fluorescence peaks do not change with the pumping wavelength except their intensities. This result means that only the excitation efficiency varies but the kind of the excited site do not change by different energy pumping. Therefore, for rare earth ions with multiplet J-states, the effect of fluorescence line narrowing (*FLN*) can be hardly observed, while this is not the case for Eu^{3+} ion, the simple energy level ($^5D_0 \leftarrow {}^7F_0$) of which is capable of *FLN* studies[7]. In recent *FLN* studies of Er^{3+} in silicate, fluoride and fluorophosphate glasses[8], no variations in the fluorescence

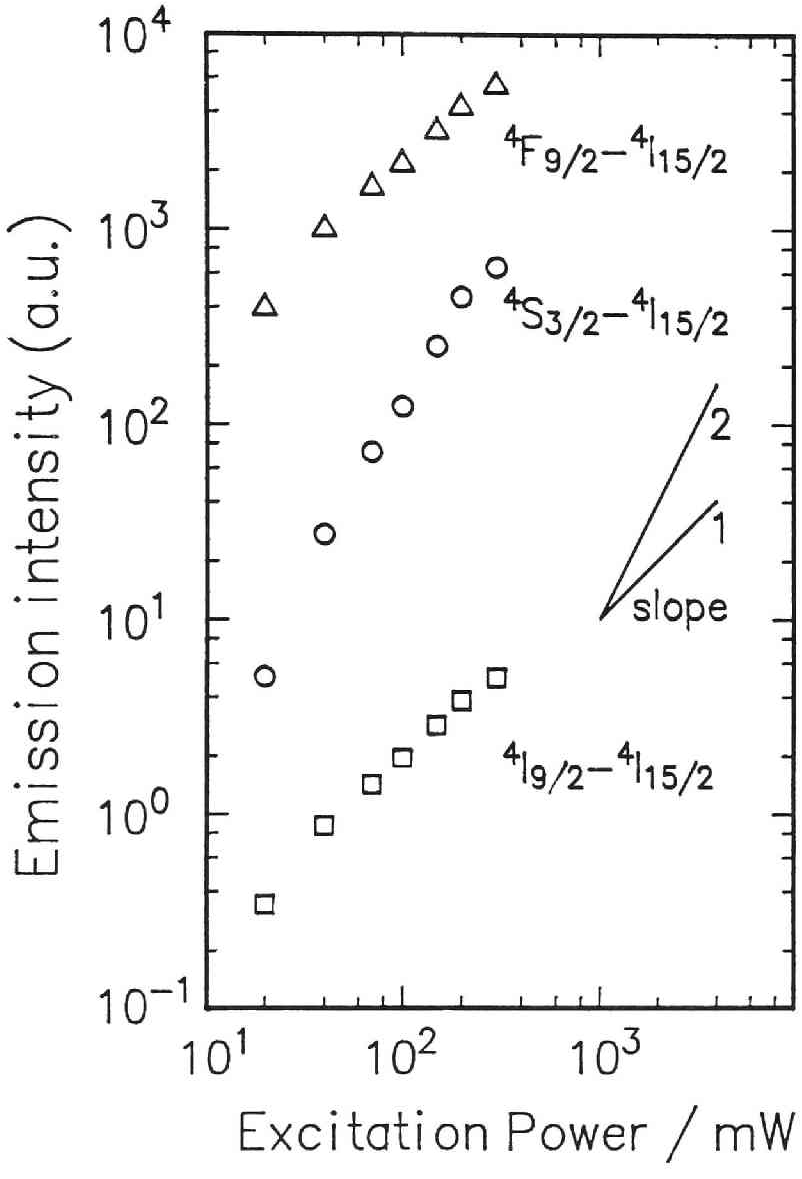

Fig.5: The log-log plot of emission intensities against the pumping power.

spectra with excitation wavelength nor any deviations from a simple exponential fluorescence decay were detected at room temperature. Because of a combination of homogeneous broadening and site-to-site variations in the energy levels comparable to the Stark splittings, the fluorescence can be treated as homogeneous.

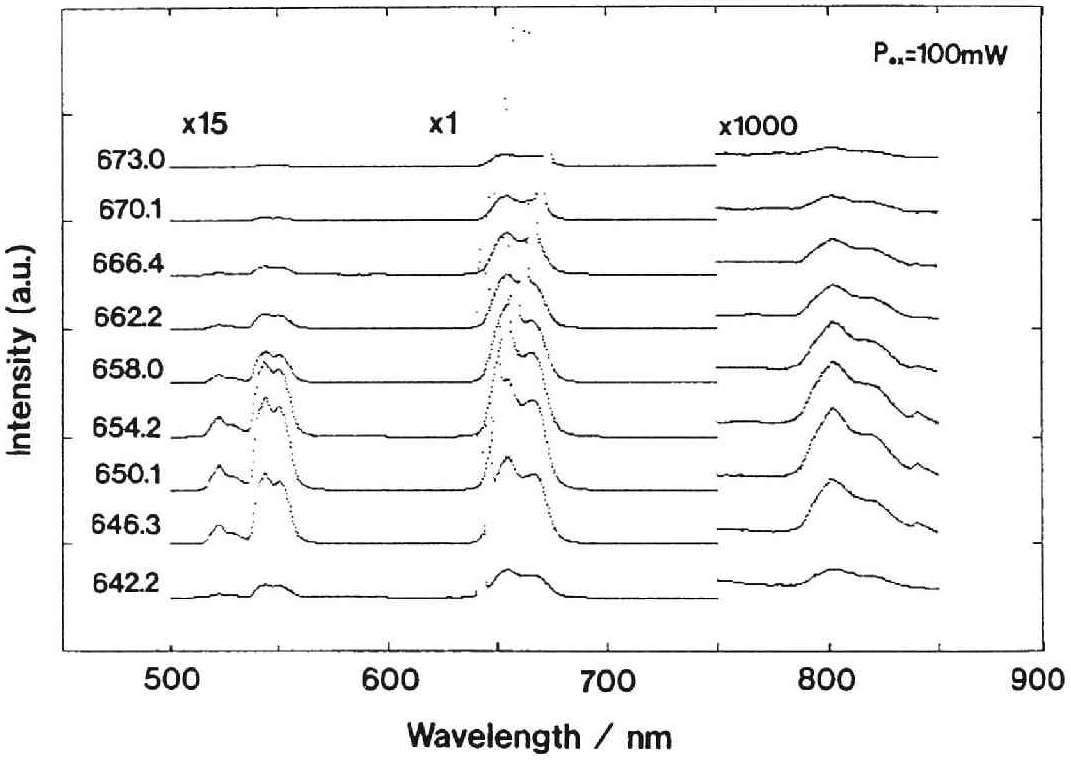

Fig.6: Variations of fluorescence spectra with pumping(100mW) wavelength. The wavelength is shown at the right side of each spectrum in nanometer. The range of 500-600 nm is multiplied by 15 times and that of 750-850nm is by 1000 times.

The excitation spectra of upconversion emission and one-step emission are shown in Fig.7. It can be seen that the positions of two peaks are almost superposed. The excitation profile of one-step emission almost corresponds to the *GSA* profile shown in

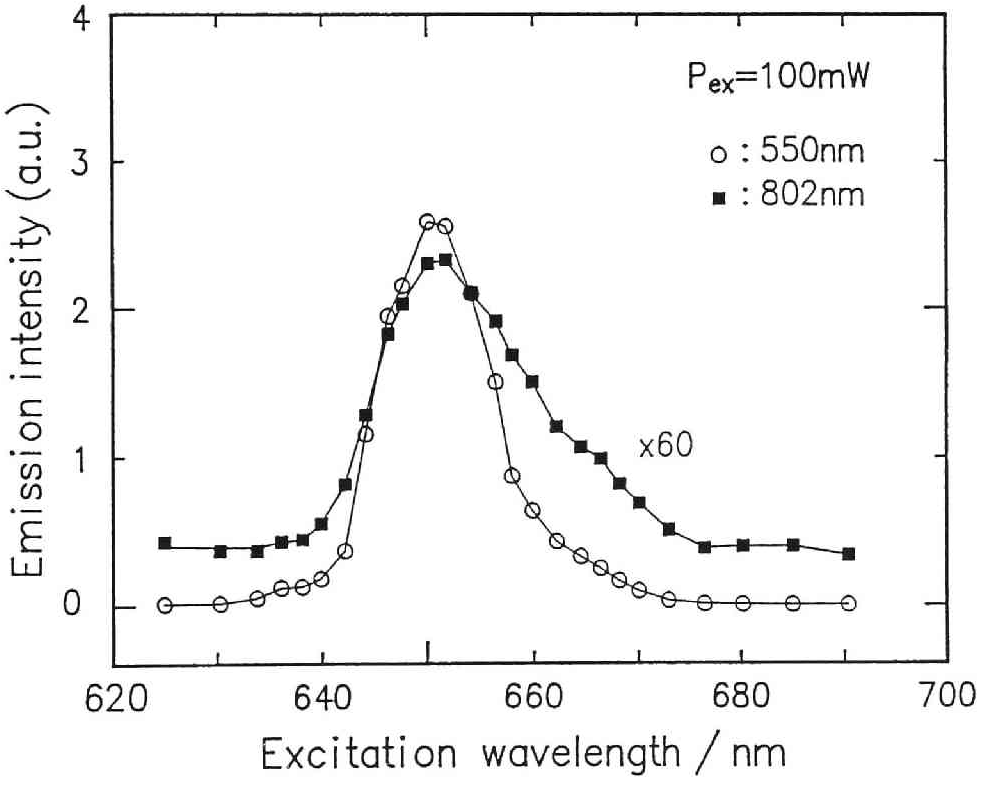

Fig.7: Excitation spectra of $^4S_{3/2} \rightarrow {}^4I_{15/2}$ emission (550nm) and $^4I_{9/2} \rightarrow {}^4I_{15/2}$ emission (802nm).

Fig.8. This result indicates that the emission from $^4I_{9/2}$ level occurs after nonradiative decay from $^4F_{9/2}$ level. Since the $^2H_{9/2} \rightarrow {}^4I_{15/2}$ emission at 410nm was not clearly observed by two step excitation, the possible intermediate level for an *ESA* mechanism is uniquely $^4I_{13/2}$. In this case, the $^4F_{5/2} \leftarrow {}^4I_{13/2}$ can be the

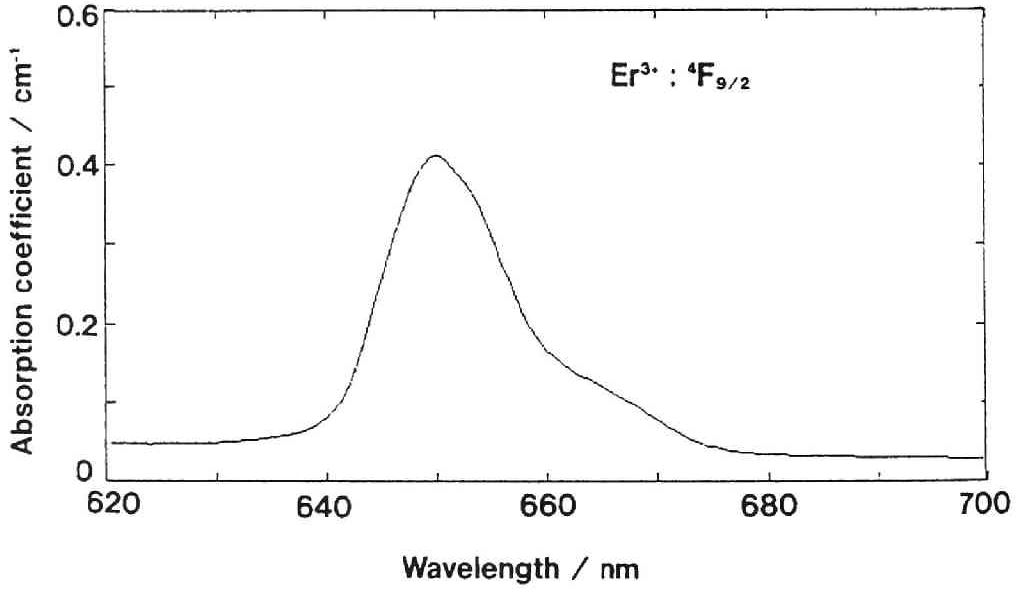

Fig.8: Absorption spectrum of Er^{3+}:$^4F_{9/2} \leftarrow {}^4I_{15/2}$ transition in the glass.

possible *ESA* transition, the peak of which should be at 645nm. However, the upconversion excitation peak is placed at 650nm. Thus, an *APTE* process should be the main mechanism of upconversion in this glass. For the *APTE* between two ions, the upconversion profile becomes the square of the *GSA* profile. Another

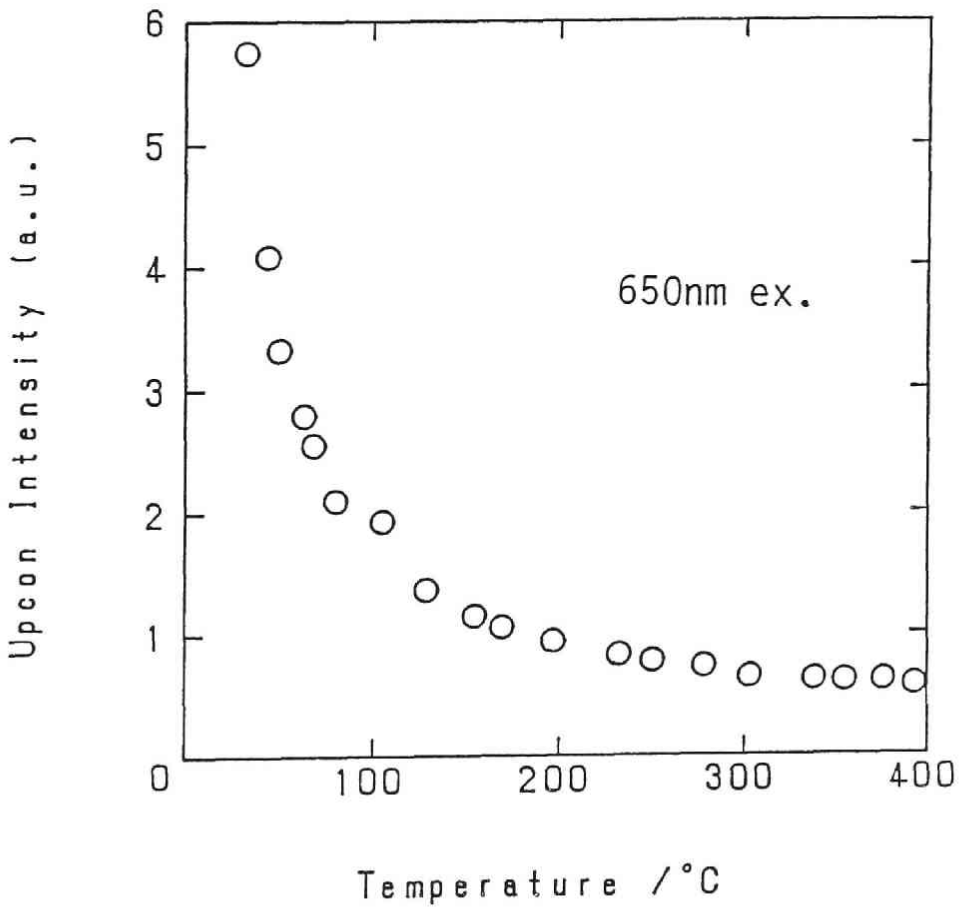

Fig.9: Temperature dependence of the upconversion intensity by 650nm excitation.

concern is between which level the *APTE* occurs. The temperature dependence of upconversion efficiency was plotted in Fig.9. The efficiency should vary with the lifetime of the intermediate level and emitting level. The temperature dependence of the lifetime of an excited state, τ_f is largely influenced by the

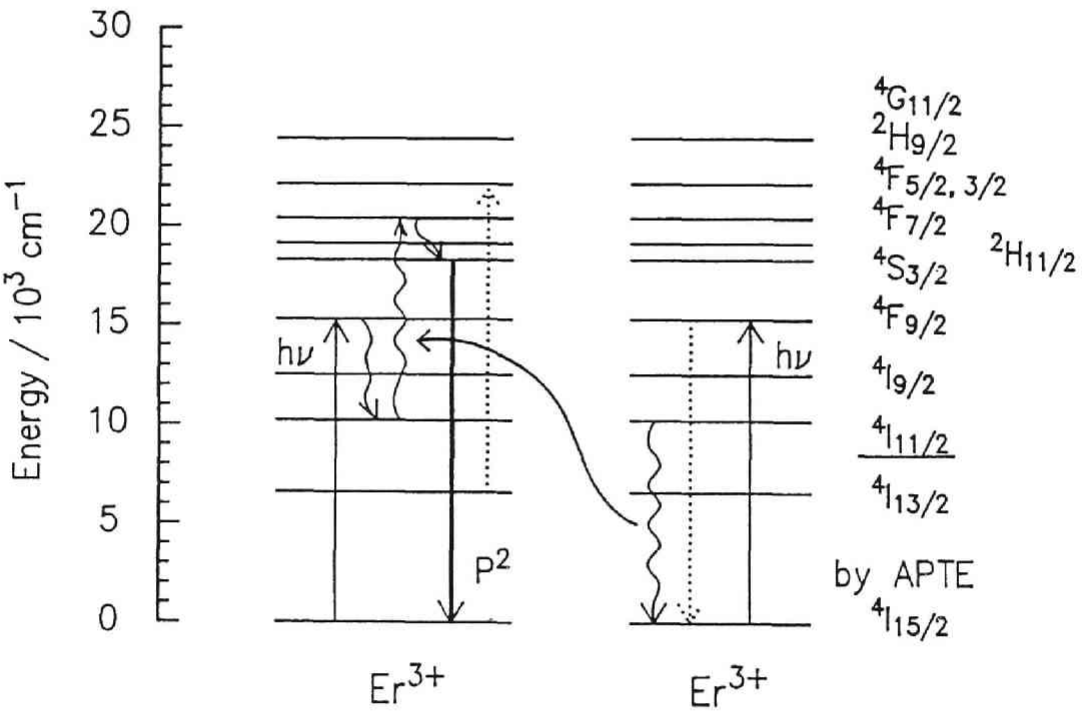

Fig.10: Controlling mechanisms of Er^{3+} upconversion in the present glass.

multiphonon decay rate, W_P, since the radiative decay rate, W_R ($-\Sigma A$) does not vary with temperature. Since it was shown that $\eta \ll 1$, which holds for the level with a small energy gap, $\tau(T)$ is dominated by the nonradiative process and given by the next equation,

$$\tau_f(T) \simeq W_P(T)^{-1} = C\{1-\exp(-\hbar\omega/kT)\}^{P},$$

where $\hbar\omega$ is the phonon energy, p is the number of phonons consumed during multiphonon decay and C is a constant related to $W_P(0)$. From the phonon sideband spectrum, the phonon energy in this glass was found to be $600cm^{-1}$, which corresponds to that of the Al-F stretching vibration from Raman spectra[9]. By the above equation and the measured temperature dependence, it is possible to estimate the number of phonons, p and the energy gap $p\hbar\omega=\Delta E$, which resulted in $3500cm^{-1}$. This energy gap almost corresponds to that of $^4I_{11/2}$. Therefore, as shown in Fig.10, the *APTE* between $^4I_{11/2}$ excited Er^{3+} ions is considered to be the main process leading to the present upconversion in this glass.

IV. CONCLUSIONS

The upconversion characteristics of Er^{3+}-doped fluoroaluminate glass were investigated by DCM-dye laser in the excitation wavelength range of 0.62~0.69μm. The power dependence of 0.55μm emission due to $^4S_{3/2}\rightarrow{}^4I_{15/2}$ obeyed quadratic law, indicating two-step process. The excitation spectra of upconversion and infrared emissions were compared and both of them had a similar profile to that of $^4F_{9/2}\leftarrow{}^4I_{15/2}$ absorption. It was found that the excited state absorption from any ^4I_J level (J=9/2, 11/2, 13/2)

was not the main mechanism. From the temperature dependence of efficiency, the energy transfer between $^4I_{11/2}$ excited Er^{3+} ions was found to be the controlling process to upconversion of this glass.

The 0.65μm excitation is promising for Er^{3+}-upconversion because of the larger absorption cross section of *GSA* than 0.80μm. The practical use will be possible by the development of AlGaInP laser diode[10] with the corresponding wavelength.

5.2. UV AND BLUE UPCONVERSIONS AND THEIR MECHANISMS IN Tm^{3+} DOPED FLUORIDE GLASS

I. INTRODUCTION

A blue laser is an attractive material because there is a need for higher density in the optical data storage as well as for multicolorization of visible lasers. Frequency upconversion of rare earth doped glasses have the possibility of infrared-pumped visible laser with III-V semiconductor laser. For example, Er^{3+} ions can efficiently convert infrared radiations of popular laser diodes (λ=1.5, 0.98, 0.80μm) into green emission around 0.55μm[1,2,11]. However, it has been difficult to obtain blue emission by Er^{3+} and Ho^{3+}[12]. On the other hand, Tm^{3+} ion has stable excited levels emitting blue fluorescence ($^1D_2$, $^1G_4$). Fluoride glasses can be considered as a candidate for Tm^{3+} blue upconversion laser, since the nonradiative loss due to multiphonon relaxation is suppressed by their lower phonon energy[13]. Recently, a blue upconversion lasing was obtained in a fluorozirconate glass fiber by co-pumping at 676.4 and 647.1nm using a krypton ion laser[14]. Although, these pumping wavelengths are not infrared region but visible red, the pumping laser source around 0.65μm has come to be available by the development of AlGaInP semiconductor lasers with quantum well structures[10,15]. In this section, fluoroaluminate glass was chosen as a host of Tm^{3+} ion and upconversion characteristics were investigated by a single wavelength pumping around 0.65μm. To design an efficient upconvertor, it is also important to clarify the mechanisms in

the glass. Therefore, the excitation spectra was monitored[16] by tuning across the Tm^{3+}: $^3F_{2,3} \leftarrow {}^3H_6$ absorption profile with DCM dye laser source and the excitation process leading to upconversion was discussed.

II. EXPERIMENT

Glass in the composition $40.5AlF_3 \cdot 21.8CaF_2 \cdot 21.8BaF_2$ $14.9YF_3$ $1TmF_3$ was prepared by using reagent grade AlF_3, CaF_2, BaF_2, YF_3, and TmF_3. A small amount of $NH_4F \cdot HF$ was also added to complete the fluorination. The powders of batch composition were well mixed in an alumina mortar and melted in a platinum crucible at 1000 °C for 15 min. The melt was poured on a stainless steel and pressed with a stainless plate. The glass obtained was annealed at 435 °C for 15 min. and cut into 4x4x1mm shape and polished with diamond paste. The density was measured by Archimedes' method to calculate the number of Tm^{3+} ions per unit volume, ρ_N, with the molar weight. The refractive index, n_D was measured with Abbe's refractometer. Absorption spectrum was measured with a *Shimadzu UV-3101PC* Recording Spectrophotometer in the wavelength range of 200 ~ 2000 nm. From the integrated absorbance, three intensity parameters Ω_t (t=2,4,6) were determined, which identify the ligand field and dominate the transition probabilities in the glass. Since the line strength, S for electric-dipole transitions between an initial |aJ> and final |bJ'> manifold is given by[17,18],

$$S[aJ;bJ'] = \sum_{t=2,4,6} \Omega_t \langle aJ||U^{(t)}||bJ'\rangle^2 \qquad (1)$$

where $\langle aJ||U^{(t)}||bJ'\rangle^2$'s denote the reduced matrix elements of

unit tensor operators for the corresponding transition, a least square fitting approach was done by using ρ_N, n_D and the integrated absorbance of 5 bands listed in Table 1.

Table 1: $\langle SLJ||U^{(t)}||S'L'J'\rangle$ for f^{12}

SLJ	S'L'J'	$\langle U^{(2)}\rangle^2$	$\langle U^{(4)}\rangle^2$	$\langle U^{(6)}\rangle^2$	λ (μm)	
$^3H_6$	$^3F_4$	0.5589	0.7462	0.2574	1.7	-1
	$^3H_5$ *	0.1074	0.2313	0.6382	1.2	
	$^3H_4$	0.2187	0.0944	0.5758	0.79	-2
	$^3F_3$	0.0	0.3163	0.8409	0.68	]3
	$^3F_2$	0.0	0.0000	0.2591	0.65	
	$^1G_4$	0.0452	0.0694	0.0122	0.47	-4
	$^1D_2$	0.0	0.3133	0.0934	0.36	-5

* including magnetic dipole contribution.

Fluorescence spectra were recorded with a *Hitachi-850* Fluorescence Spectrophotometer. As an excitation source, a dye laser apparatus (*Spectra Physics Model 375 Dye Laser*) excited by an Ar^+ laser (*Coherent innova 70*) was used with the propylene carbonate solution of DCM-dye (Dicyanomethylene-2-methyl-6-*p*-dimethylaminostyryl-4*H*-pyran), having the emission wavelength range of 630 ~ 700 nm, which correspond to the Tm^{3+}: $^3F_{2,3} \leftarrow {}^3H_6$ ground state absorption. The excitation wavelength was tuned with a tuning wedge and the power was controlled by the power of Ar^+ laser and determined by a power meter (*Coherent 210 Power Meter*). The maximum power of 0.65μm radiation obtained was

360mW.

III. RESULTS

The absorption spectrum of the fluoroaluminate glass is shown in Fig.1. Each assignment in Fig.1 corresponds to the upper level of the transition from the ground $^3H_6$ state. With

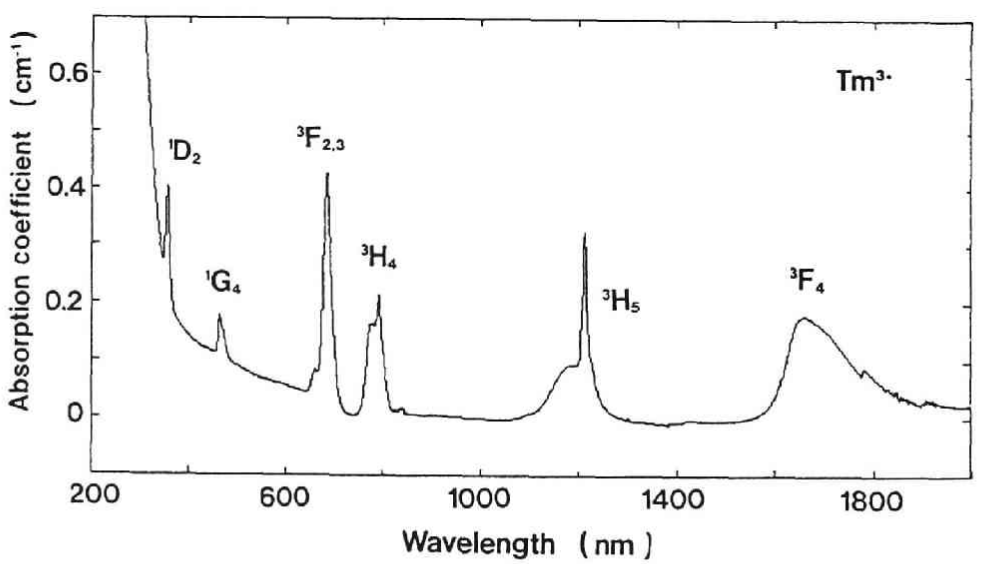

FIG.1. Absorption spectrum of glass.

the obtained line strength of 5 bands listed in Table 1, a least square fitting approach was done by using $\rho_N = 1.698 \times 10^{20}$ cm^{-3} and $n_D = 1.432$. The obtained parameters were $\Omega_2 = 1.75 \times 10^{-20}$ cm^2, $\Omega_4 = 1.33 \times 10^{-20} cm^2$ and $\Omega_6 = 1.27 \times 10^{-20} cm^2$. The %rms deviation was only 0.20 %, indicating a good fit.

Table 2: Measured and calculated line strengths for 5 bands of Tm^{3+} in the glass.

Band	λ (nm)	$S(10^{-20} cm^2)$	$S_c(10^{-20} cm^2)$
1	1696	2.288	2.295
2	785.6	1.236	1.238
3	684.6	1.816	1.813
4	467.1	0.281	0.187
5	356.4	0.521	0.534

$\Omega_2 = 1.75 \times 10^{-20} cm^2$

$\Omega_4 = 1.33 \times 10^{-20} cm^2$

$\Omega_6 = 1.27 \times 10^{-20} cm^2$ %rms = 0.20 %

An efficient upconversion could be obtained around 0.655μm excitation. The fluorescence spectrum with 0.655μm excitation is shown in Fig.2 for some various pumping powers. The largest peak overscaled is due to the Rayleigh scattering of the incident light. There can be seen upconversion fluorescences peaked at 363, 451, 476nm and one-step fluorescence at 793nm. The blue emissions at 451nm and 476nm could be clearly detected by human eyes with the pumping power less than 100mW. The power dependence of emission intensity on the incident pumping power is

plotted in Fig.3. Apparently, the 793nm emission shows linear dependence against pumping power and other emissions nonlinear dependences.

The variation of fluorescence spectra with the excitation wavelength is shown in Fig.4. The excitation power was fixed at

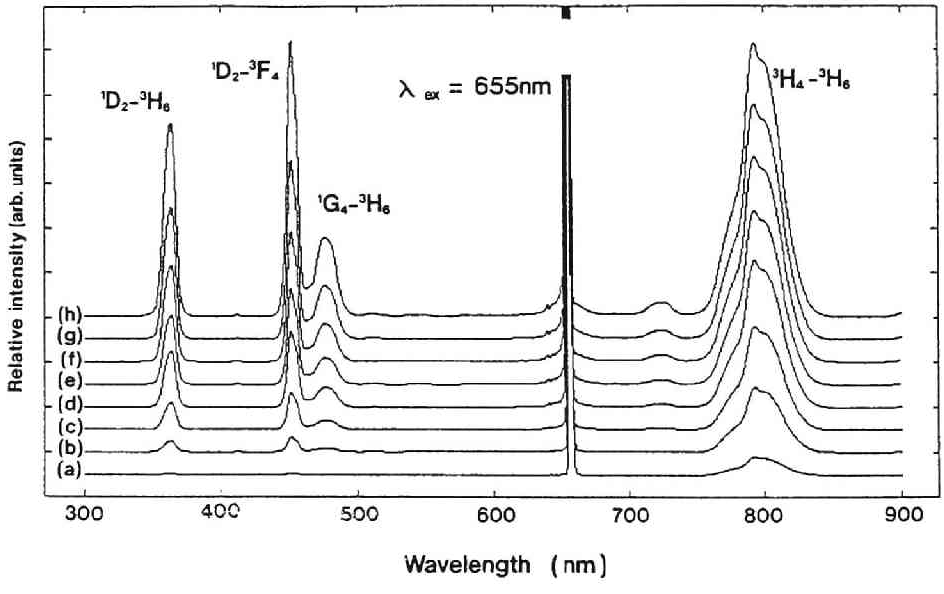

FIG.2. Emission spectra of glass pumped by 0.655μm with the power of (a)20mW, (b)60mW, (c)100mW, (d)150mW, (e)200mW, (f)250mW, (g)300mW and (h)360mW.

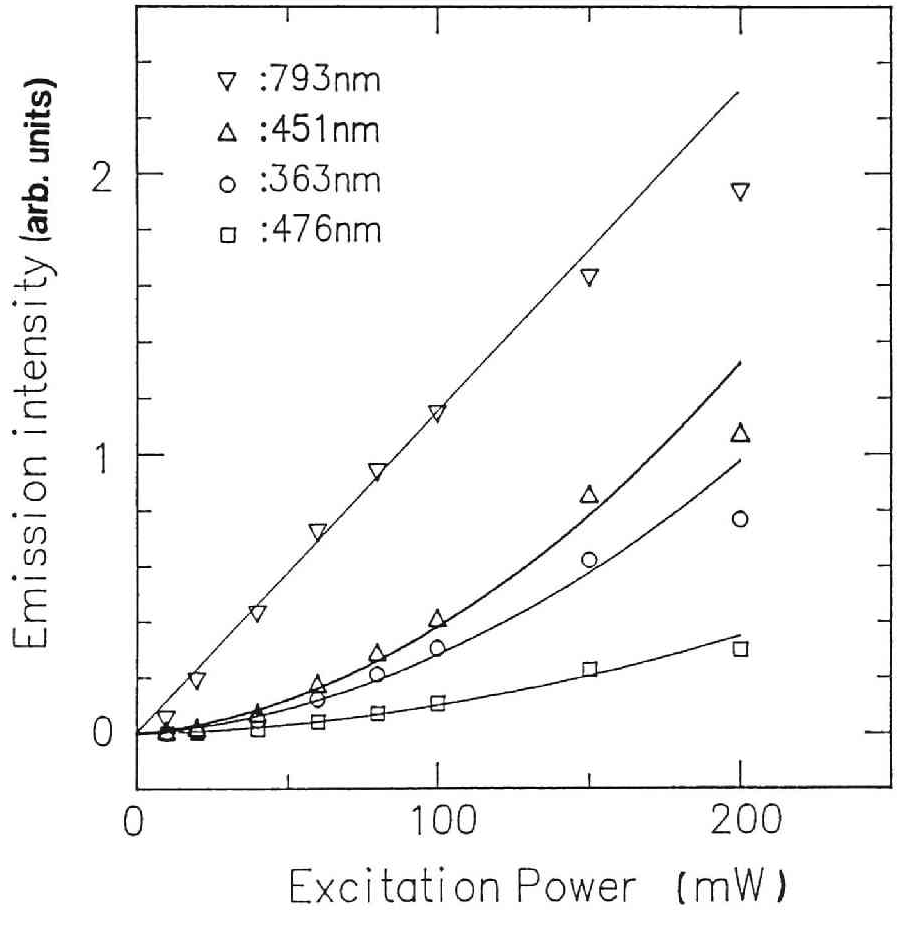

FIG.3. Dependence of the emission intensity on the 0.655μm pumping power.

100mW. Figure 4 shows that the intensities of the upconversion fluorescence at UV and blue region increased up to around 650nm excitation and decreased with an increase of the excitation wavelength. On the other hand, the intensity of the one-step fluorescence around 790nm range increased with an increase of the excitation wavelength and showed a maximum around 682nm excitation.

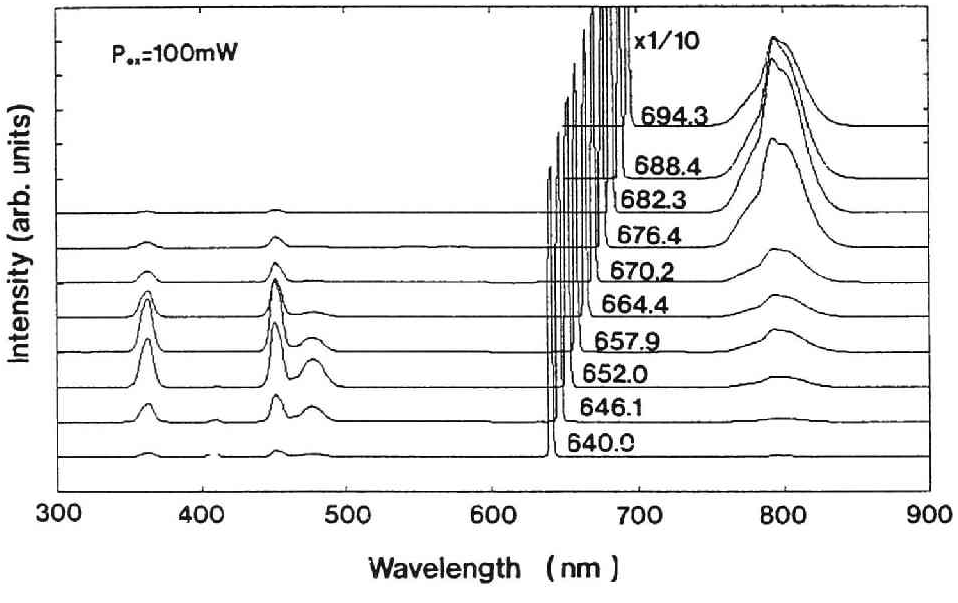

FIG.4. Variation of fluorescence spectra with pumping wavelength. The pumping wavelength is shown in *nm* scale and the power is fixed at 100mW.

IV. DISCUSSION

A. Fluorescence spectra of Tm^{3+} in glass

In the fluorescence spectra of Tm^{3+}-doped silica fiber reported by Hanna et al.[20], the emission around 460~470nm was observed, but the emission peak from $^1D_2$ level and that from $^1G_4$ level were not separated well. It is presumably due to the large Stark splitting and inhomogeneous broadening as well as energy shifts of the levels in the oxide host. On the other hand in the fluoride host in this study, the emissions at 451nm due to $^1D_2 \rightarrow {}^3F_4$ transition and 476nm due to $^1G_4 \rightarrow {}^3H_6$ is clearly separated. In addition to the blue emissions, the 360nm emission in the UV range is clearly observed, which is due to $^1D_2 \rightarrow {}^3H_6$. The relative intensity of this UV emission was larger compared with the spectrum of the doped silica glass[20], in which the peak around 370nm is only weakly detected. This is ascribed to the different branching ratio, β from $^1D_2$ level, owing to the different ratio of spontaneous emission probabilities, A. The β from $|aJ\rangle$ state can be defined by,

$$\beta[aJ;bJ'] = \frac{A[aJ;bJ']}{\sum_{bJ'} A[aJ;bJ']} \qquad (2)$$

where the denominator is the summation to all lower terminal states $|bJ'\rangle$'s. Thus the factors dominating the branching ratio from $^1D_2$ to the lower states are the relative values of A, which are the functions of reduced matrix elements of each transition and also a set of Ω_t-intensity parameters of a given ligand field. Here, the spontaneous emission probability A for electric-dipole transitions is obtained by the following equation

[17,18],

$$A[aJ;bJ'] = \frac{64\pi^2 e^2}{3h(2J+1)} \frac{1}{\lambda^3} \frac{n(n^2+2)^2}{9} S[aJ;bJ'] \qquad (3)$$

where S[aJ;bJ'] is defined by eq.(1) in the previous section A.

Table 3 shows the sets of $\langle||U^{(t)}||\rangle^2$'s for all the possible radiative transitions from $^1D_2$ level[19]. As seen from Table 3, the $\langle||U^{(2)}||\rangle^2$ for $^1D_2 \rightarrow {}^3H_6$ transition is 0, while that for $^1D_2 \rightarrow {}^3F_4$ transition is non-zero and large. Since the values of $\langle||U^{(t)}||\rangle^2$ for the transitions to other terminal states than $^3F_4$ and $^3H_6$ are negligibly small, the branching ratio of 0.36μm emission, $\beta[^1D_2;{}^3H_6]$ is dominated by the value of Ω_2 and Ω_4.

Table 3: Reduced matrix elements $\langle(SL)J||U^{(t)}||(S'L')J'\rangle^2$ of radiative transitions from $^1D_2$ level of Tm^{3+}[19]. Typical wavelengths are included.

(SL)J	(S'L')J'	$[U^{(2)}]^2$	$[U^{(4)}]^2$	$[U^{(6)}]^2$	λ (μm)
$^1D_2$	$^3H_6$	0	0.3133	0.0934	0.36
	$^3F_4$	0.5792	0.0968	0.0194	0.45
	$^3H_5$	0	0.0017	0.0164	0.50
	$^3H_4$	0.1147	0.0138	0.2307	0.65
	$^3F_3$	0.1637	0.0714	0.0	0.76
	$^3F_2$	0.0639	0.3093	0.0	0.80
	$^1G_4$	0.1926	0.1666	0.0006	1.8

From the eqs.(2), (3) and Table 3, the branching ratios of 360nm and 450nm emissions in the present glass were calculated with the Ω_t values to find 0.40 and 0.45, respectively (Table 4). This

result is in accordance with the observed fluorescence spectra in Fig.3. Since the $\langle||U^{(2)}||\rangle^2$ of the $^1D_2 \rightarrow {}^3F_4$ transition is large, the β of the blue emission would be largely enhanced by the increased value of Ω_2, which reflects the asymmetry of ligand field[22]. As is often observed for most glass systems, Ω_2 of rare earth ions in oxide glasses are larger than those in fluoride glasses[23]. This is ascribed to the larger electric field gradient by divalent oxide ions than that by monovalent fluoride ions and also due to the effect of covalency of the chemical bond between rare earth and ligand anion. On the other hand, $\Omega_{4,6}$ are not so largely varied with the host composition [22]. Therefore, the β of the transitions with a large $\langle||U^{(4)}||\rangle^2$ is relatively enhanced in fluoride hosts where Ω_2 is small. That is the reason for the increased β of $^1D_2 \rightarrow {}^3H_6$ transition up to β=40% in the fluoride host with a smaller Ω_2 value in the present glass.

Table 4: Spontaneous emission probability A and branching ratio β of radiative transitions from the $^1D_2$ level of Tm^{3+} in the glass.

(SL)J	(S'L')J'	A(sec^{-1})	β
$^1D_2$	$^3H_6$	4586	0.40
	$^3F_4$	5119	0.45
	$^3H_5$	74	0.01
	$^3H_4$	745	0.07
	$^3F_3$	347	0.03
	$^3F_2$	408	0.04
	$^1G_4$	38	0.00

B. Pumping power dependence of fluorescence intensity

As seen in Fig.2, the intensity of upconversion emission increased drastically with increasing excitation power, while the intensity at 793nm increased linearly. At higher pumping powers, the intensity of upconversion fluorescence is comparable to that of one-step fluorescence. The nonlinear power dependence of emission intensities in UV and blue region on the incident pumping power in Fig.3 indicates the multi-step excitation. The log-log plot is shown in Fig.5. Each slope corresponds to the number of steps needed to the excitation, although there seems to be the effect of saturation at higher pumping power. This saturation is probably due to the depopulation of the ground level. Therefore, both the UV and blue emissions occur by a two step process with 0.65μm excitation in this fluoride glass.

C. Wavelength dependence of fluorescence intensity

As seen in Fig.4, the suitable pumping wavelengths for upconversion fluorescences were different from that for the one-step fluorescence. The laser excitation spectra for each emission are plotted in Fig.6. It can be seen that the excitation efficiency of the 793nm-fluorescence shows a maximum around 683nm, while those of three upconversion fluorescences shift to higher energy side. The former profile is almost the same as that of the ground state absorption ($^3F_{2,3} \leftarrow {}^3H_6$) spectrum, which is shown in Fig.7. This is due to the fact that the emission from $^3H_4$ level occurs after the multiphonon relaxation from $^3F_{2,3}$ level. On the other hand, the three upconversion profiles

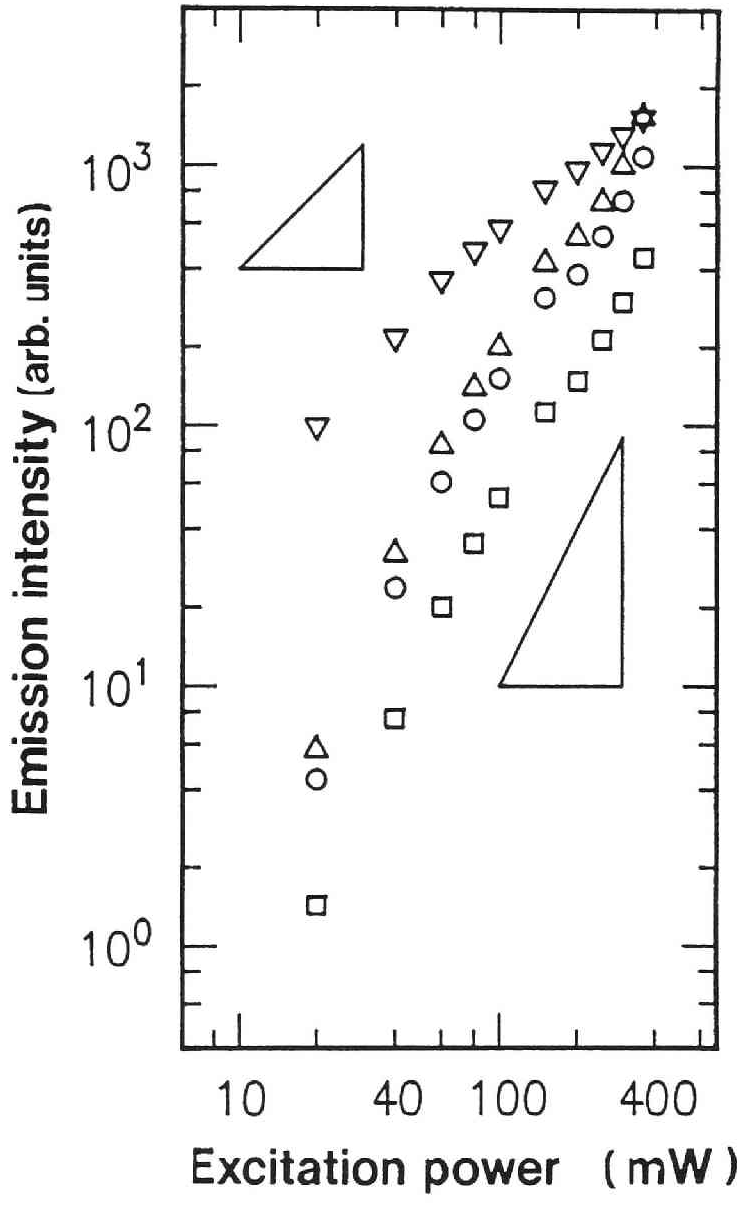

FIG.5. The log-log plot of the emission intensity and pumping power.
▽:793nm, △:451nm, ◯:363nm, and □:476nm.
The triangles indicate the slope of 2 and 1.

are different from the *GSA* profile. These results can be ascribed to the presence of *ESA* mechanisms and not *APTE* for the upconversion emissions. It is obvious that the Tm^{3+} is first promoted to $^3F_{2,3}$ level and then is raised from a certain lower intermediate level to a still higher state by the second step

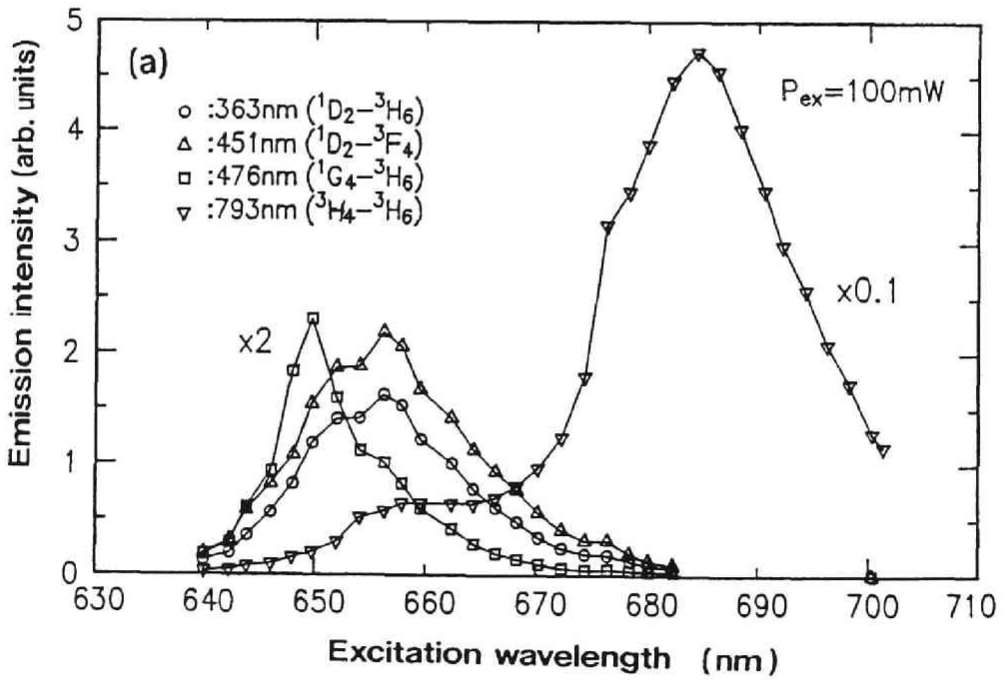

FIG.6. Emission intensities as a function of excitation wavelength.

excitation. To reach the UV-emitting $^1D_2$ level by the second incident photon, $^3H_4$ level, which is ~1800cm^{-1} below $^3F_3$, is considered to be the intermediate level from which *ESA* occurs. The efficient wavelength for $^1D_2 \leftarrow {}^3H_4$ absorption was estimated from the absorption spectrum and found to be about 650nm. It is

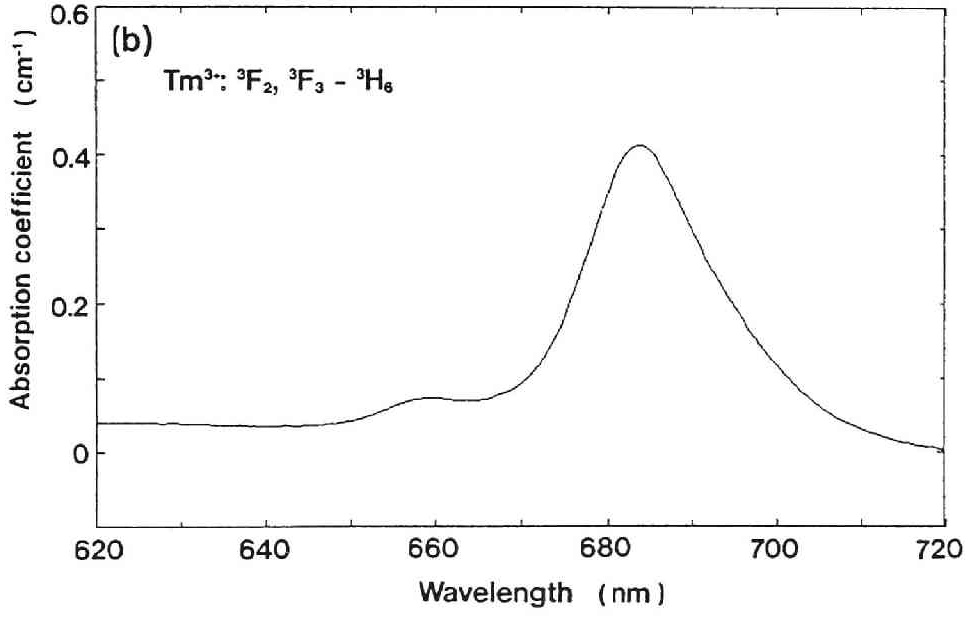

FIG.7. Absorption spectrum of Tm^{3+}:$^4F_{2,3} \leftarrow {}^3H_6$ transition in the glass.

reasonable that the excitation profiles of 360nm and 450nm are equivalent except their intensity ratio determined only by the β from $^1D_2$. Because of the absence of higher final levels with a suitable energy for *ESA* by two-step process, the main mechanism leading to the upconversion of $^1D_2 \rightarrow {}^3H_6$, $^3F_4$ can be concluded to be the *ESA* from the $^3H_4$ to $^1D_2$ level. The energy gap of $^3H_4$ to the next lower level is large enough to keep a long lifetime in this fluoride host with the phonon energy of 600cm^{-1}[24], which is ascribed to Al-F stretching vibration in the glass. The wavelength of 655nm at maximum in Fig.6 is placed between that of *ESA* and *GSA* of Tm^{3+}. A small shift of the peak to lower energy side than that of *ESA* can be due to the contribution of *GSA* efficiency, which shows a maximum at 682nm in Figs.6 and 7. In this glass, the upconversion is attained by a single wavelength pumping, owing to the overlapping of these two absorption energy range around 655nm.

Fig.8 shows the upconversion fluorescences with various pumping wavelengths. Apparently, the emission intensity from $^1G_4$ varies differently. This is not the effect of the fluorescence line narrowing for different sites in amorphous states, which could be observed for transitions involving the level with a singlet J-state (J=0, 1/2) such as Eu^{3+}:$^5D_0$[25] or at most, a doublet J-state (J=3/2) such as Nd^{3+}:$^4F_{3/2}$ at low temperatures [26], by using lasers with a much narrower spectral width (~0.3 cm^{-1}). Thus, in the case of $^1G_4 \rightarrow {}^3H_6$ fluorescence at 476nm, other mechanism can contribute than that of $^1D_2$ emissions because the excitation profile observed also in Fig.6 is different. The first possibility is the $^3F_4$ level, which is populated after the

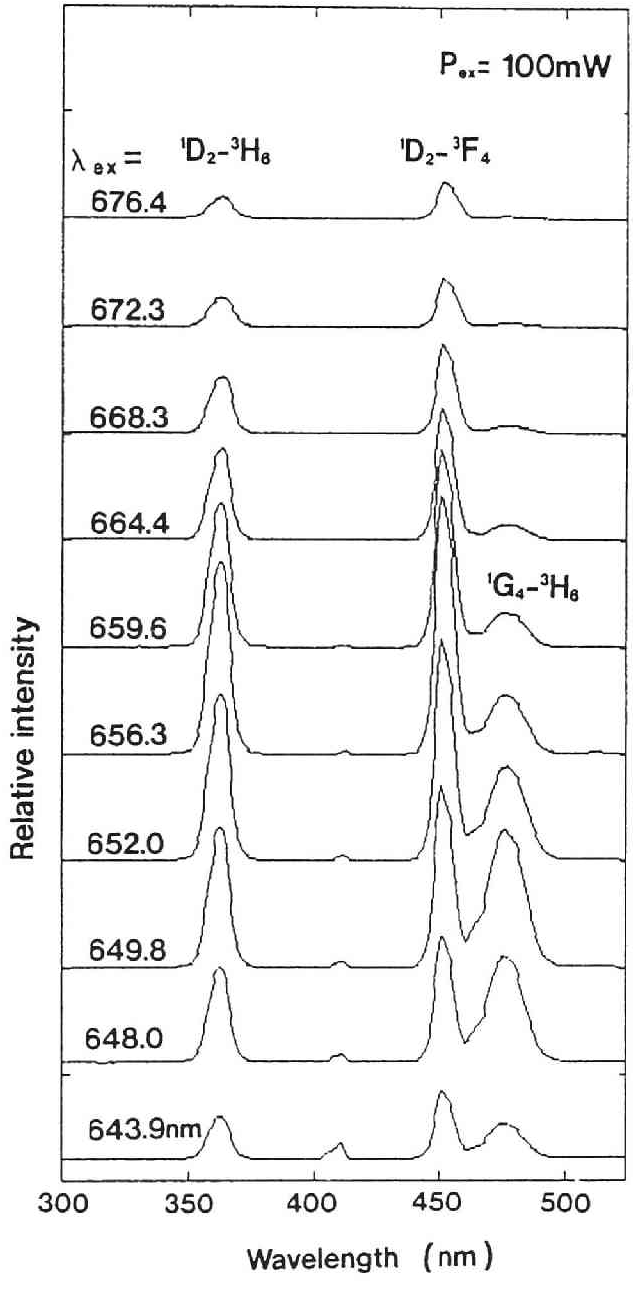

FIG.8. Variation of upconversion spectra with different pumping wavelengths, λ_{ex}. The λex is shown in each spectrum.

multiphonon decay from $^3H_4$ and pumped with the second incident photon with about 645nm to $^1G_4$ level. A larger energy difference of $^1G_4 \leftarrow {}^3F_4$ *ESA* transition from *GSA* can be the reason for the shift of the excitation profile of $^1G_4$ emission to a higher energy side than that of $^1D_2$. The second possible mechanism is the same *ESA* as $^1D_2$ followed by the multiphonon decay between $^1D_2 \rightsquigarrow {}^1G_4$. This process seems plausible to explain a small

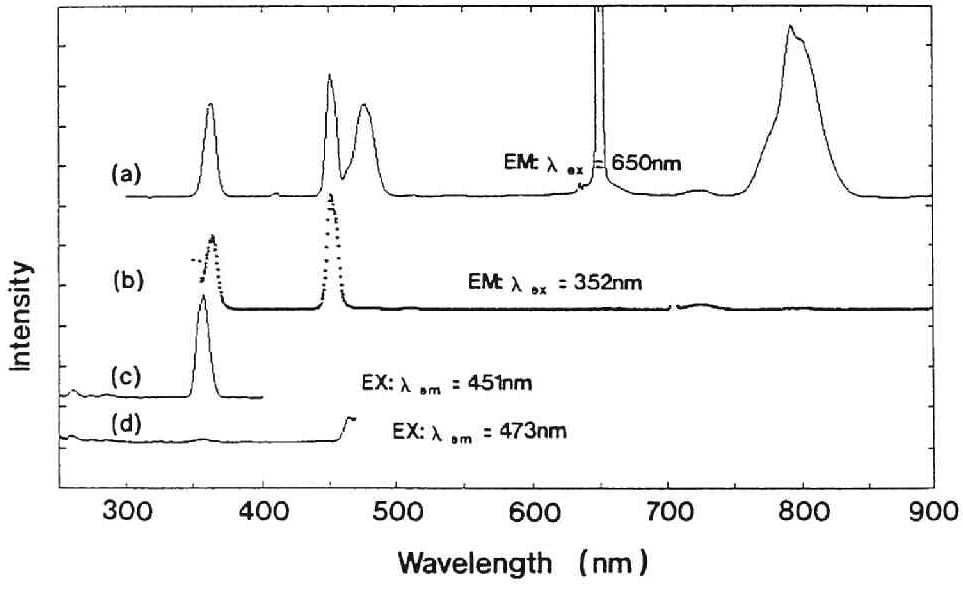

FIG.9. Emission and excitation spectra of blue emissions: (a)Emission spectrum by 650nm excitation, (b)Emission spectrum by 352nm excitation, (c)Excitation spectrum of 451nm emission, and (d)Excitation spectrum of 473nm emission.

overlapping of both profiles around 655nm in Fig.6. In order to confirm the possibility of the multiphonon decay, the fluorescence and excitation spectra were measured. Shown in Fig. 9 (a) and (b) are the fluorescence spectra by the laser (λ = 650 nm) and Xe-lamp(λ=352nm) excitations, respectively. The peak around 476nm is clearly observed in (a), whereas it is scarcely seen in (b), and moreover, the emission from $^3H_4$ around 790nm is quite weak. Both results indicate that the multiphonon decay rate from $^1D_2$ to the next lower level is too small to populate $^1G_4$ and still lower levels such as $^3H_4$. This is supported by the excitation results in Fig.9(c) and (d), that UV-excitation around 350nm is responsible for the 451nm emission but not for the 473nm emission. Accordingly, the contribution of the second mechanism is negligibly small and the *ESA* from $^3F_4$ is responsible for the upconversion from $^1G_4$ level.

D. Contribution of nonradiative decay process to upconversion mechanisms

In the former section C, the multiphonon relaxation(*MPR*) rate at $^1D_2 \rightsquigarrow {}^1G_4$ was found to be negligibly slow in this fluoride host. However, it would be impossible to observe $^1G_4$ upconversion by the proposed mechanism, if the nonradiative decay did not occur from $^3F_{2,3}$ and $^3H_4$ levels to $^3F_4$ level. To check both mechanisms, the *MPR* rate, $W_p(T)$ was calculated for the levels of Tm^{3+} ion by the following equations[27],

$$W_p(T)=W_0(0)\cdot\exp[-\alpha\Delta E/\hbar\omega] \quad (4)$$

$$\alpha = \ln\{p/g[n(T)+1]\}-1 \quad (5)$$

$$p \simeq \Delta E/\hbar\omega \quad (6)$$

where ΔE is the energy gap to the next lower level, g is the electron-phonon coupling strength, p is the phonon number consumed during *MPR* and $W_0(0)$ is the decay rate at $\Delta E=0$ and T=0. The temperature dependence of W_p arises from its dependence upon the Planck distribution function, n(T)[28] on the occupation number of the phonon mode;

$$n(T)=[\exp(\hbar\omega/kT)-1]^{-1}. \qquad (7)$$

In the calculation, only integer values for the number of phonons p and a temperature-independent constant value of g were used. In Fig.10, the ΔE dependences of $W_p(300K)$ are plotted for various phonon energies. Apparently, W_p decreases with increasing ΔE and decreasing $\hbar\omega$. Since g depends on the structure or lattice nature of host and not on the electronic nature of each wave function[29], it is possible to compare the relative W_p for excited states of Tm^{3+} with various ΔE in this glass. It can be seen that the W_p for $^1D_2$, $^1G_4$ and $^3F_4$ levels are much lower in a few orders of magnitude, for which much longer lifetimes are expected than those for $^3F_3$ and $^3H_5$ levels, where the electrons are to decay rapidly to $^3H_4$ and $^3F_4$ levels, respectively. This tendency is more pronounced for the lower phonon energy, i.e. also in the the present fluoride glass ($\hbar\omega=600cm^{-1}$). Accordingly, the nonradiative lifetime of $^1D_2$, $^1G_4$ and $^3F_4$ can be increased effectively with decreasing phonon energy of the host. The latter two levels play a dominating role as an emitting or intermediate state on the upconversion efficiency of the $^1G_4 \rightarrow {}^3H_6$ emission. On the upconversion efficiency from the $^1D_2$ level, the lifetime of the $^3H_4$ level also becomes a dominating factor as an intermediate state. The W_p of $^3H_4$ level is slower than that

of $^3F_3$, however, it is still faster than that of $^3F_4$. As a consequence, the next relation is expected for the nonradiative lifetime, $^3F_3 < {}^3H_5 << {}^3H_4 << {}^3F_4 < {}^1G_4 \simeq {}^1D_2$. Thus the lifetime of $^3F_4$ can be between them. From the discussion in section C and the calculated W_p, the quantum efficiency of $^1D_2$ level is considered to be almost unity, whereas those of $^3F_3$ and $^3H_5$ are almost zero.

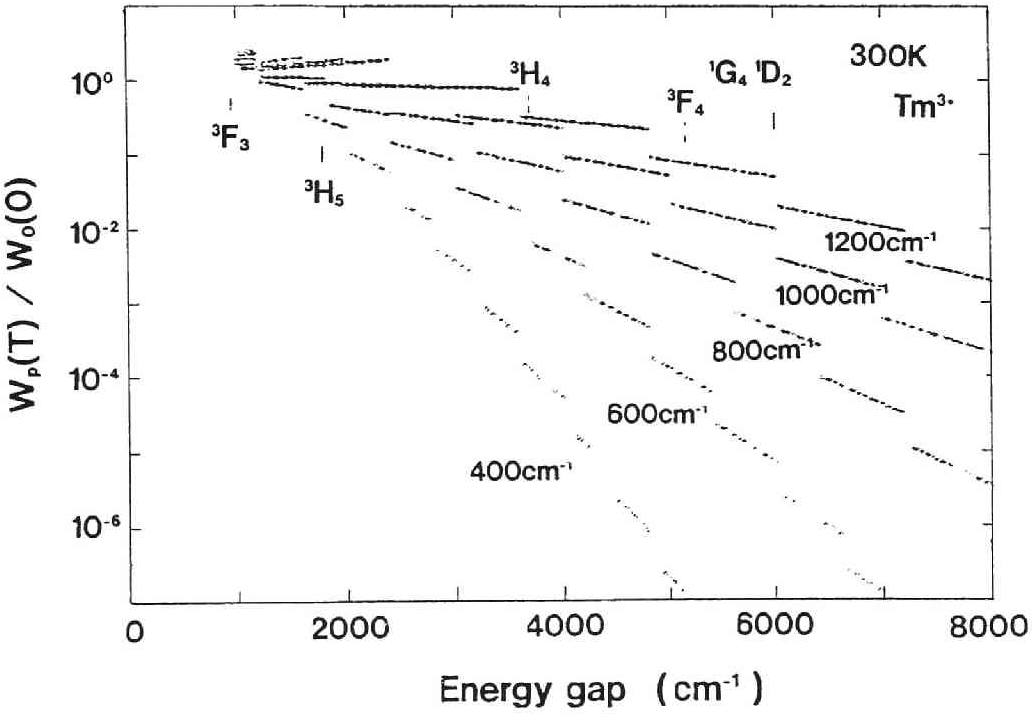

FIG.10. Multiphonon decay rate as a function of the energy gap for various phonon energies. The corresponding Tm^{3+}-levels are indicated.

The lifetime of $^3H_4$ level dominates the ratio of total electronic transition rate (including *ESA*) to the nonradiative decay rate. This ratio is responsible for the intensity ratio of upconversion emissions from $^1D_2$ and $^1G_4$ levels, to which ESA occur from $^3H_4$ and $^3F_4$, respectively. Because both emissions are observed by suitable pumping conditions, the quantum efficiency of $^3H_4$ can not be near zero nor unity. For this reason, it is possible to change the ratio of 450nm to 480nm emission intensities, by controlling the W_p of $^3H_4$ level (Fig.11) as well as by tuning the pumping wavelength.

V. CONCLUSIONS

In contrast to Er^{3+}, clarified are the evidence of the excited state absorption mechanisms of UV- and blue-upconversion fluorescences in Tm^{3+}-doped fluoride glass by using a tunable DCM-dye laser for a single wavelength pumping. It was found that the dependences of fluorescence intensity on the incident excitation power were quadratic both for 0.36 and 0.45μm emissions, which originate from $^1D_2$, and also for 0.48μm emission from $^1G_4$, indicating two step excitation mechanisms. To investigate the upconversion mechanisms, the excitation efficiencies were monitored for these upconversion emissions and for the normal one-step emission at 0.79μm by tuning the pumping wavelength. It was found that the excitation profile for the normal emission was varied in the same way as that of the absorption spectra of $^3F_{2,3} \leftarrow {}^3H_6$ transition, while those for upconversion emissions shifted to higher energy side. Moreover, the excitation process to $^1G_4$ was found to be different from that to $^1D_2$ level. It was

concluded that the mechanisms leading to these upconversion emissions are *ESA* for both levels and the process to $^1D_2$ level is that from $^3H_4$, while that to $^1G_4$ is from $^3F_4$ after nonradiative decay from the upper levels. The slow multiphonon decay rate from $^1D_2$ to $^1G_4$ level was shown in this glass with the phonon energy of $600cm^{-1}$.

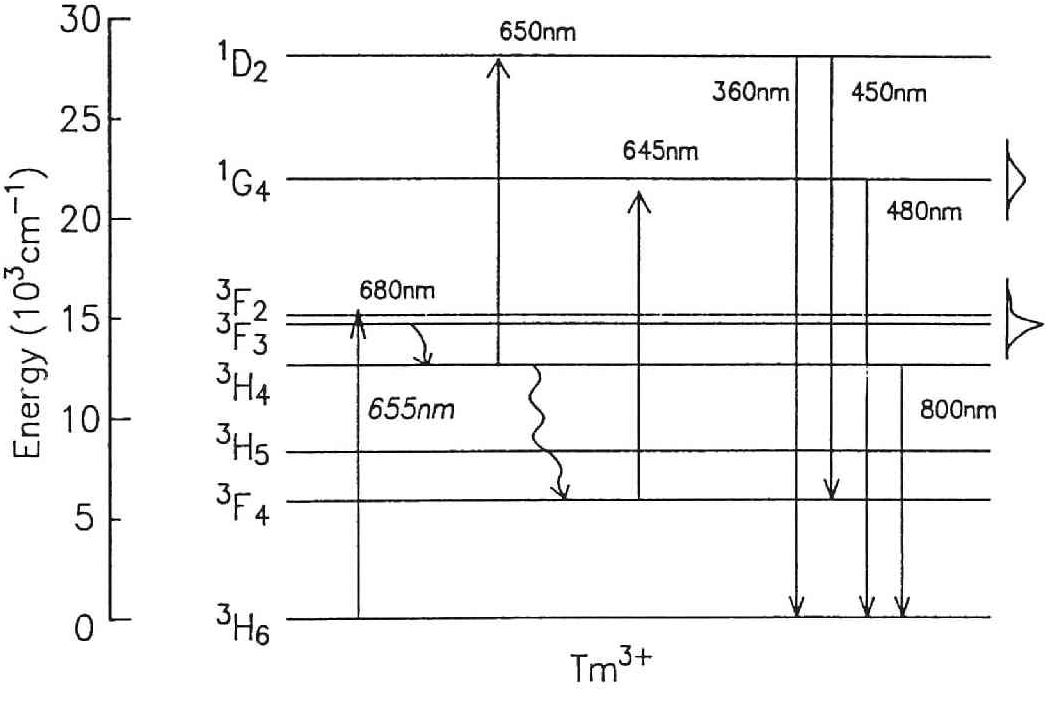

FIG.11. Upconversion mechanism of the present glass.

REFERENCES

[1] J.P. van der Ziel, L.G. Van Uitert, W.H. Grokiewicz and R.M. Mikuljak, *J.Appl. Phys.* **60**(12), (1986) 4262-67.

[2] D.C. Yeh, W.A. Sibley, M. Suscavage and M.G. Drexhage, *J. Appl. Phys.* 62(1), (1987) 266-275.

[3] S. Tanabe, K. Hirao, N. Soga and T. Hanada, *SPIE 1513 Proc. Int. Cong. Opt. Sci. Eng.* (1991) 340-348.

[4] S. Tanabe, S. Todoroki, K. Hirao and N. Soga, *J. Non-Cryst. Solids* 122 (1990) 59-65.

[5] R.D. Peacock, in "*Structure and Bonding*, vol.22," (ed. J.D. Dunitz, Springer-Verlag, Berlin, 1975) pp.83-122.

[6] M.J. Weber, Phys. Rev. **157**(2), (1967) 262-272.

[7] M.J. Weber, *Ceram. Bull.* **64**(11), (1985) 1439-43.

[8] S. Zemon, G. Lambert, W.J. Miniscalco, L.J. Andrews and B.T. Hall, *Proc. SPIE 1171*, (1989) 219.

[9] Y. Kawamoto and A. Kono, *J. Non-Cryst. Solids* **85**, (1986) 335-345.

[10] T. Tanaka, H. Yanagisawa, H. Kakibayashi, S. Minagawa and T. Kajimura, *Appl. Phys. Lett.* **59**, (1991) 1943-46.

[11] S. Tanabe, K. Hirao and N. Soga, *J. Non-Cryst. Solids* **122**, (1990) 79-82.

[12] J.Y. Allain, M. Monerie and H. Poignant, *Electron. Lett.* **26**(4), (1990) 261-63.

[13] C.B. Layne and M.J. Weber, *Phys. Rev. B* **16**(7), (1977) 3259-61.

[14] J.Y. Allain, M. Monerie and H. Poignant, *Electron. Lett.* **26**(3), (1990) 166-68.

[15] M. Ikeda, A. Toda, K. Nakano, Y. Mori and N. Watanabe, *Appl. Phys. Lett.* **50**, (1987) 1033-36.

[16] S. Tanabe, S. Yoshii, K. Hirao and N. Soga, *"Science and Technology of New Glasses,"* (ed. S.Sakka and N.Soga, Ceram. Soc. Japan, 1991) pp.193-198.

[17] B.R. Judd, *Phys. Rev.* **127**, (1962) 750-761.

[18] G.S. Ofelt, *J. Chem. Phys.* **37**, (1962) 511-520.

[19] N. Spector, R. Reisfeld and L. Boehm, *Chem. Phys. Lett.* **49**(1), (1977) 49-53.

[20] D.C. Hanna, R.M. Percival, I.R. Perry, R.G. Smart, J.E. Townsend and A.C. Tropper, *Opt. Commun.* **78**(2), (1990) 187-194.

[21] R. Reisfeld, in *"Structure and Bonding, vol.22"*, (ed. J.D.Dunitz, Springer Verlag, Berlin 1975) pp.123-175.

[22] C.K. Jørgensen and B.R. Judd, *Mol. Phys.* **8**, (1964) 281-290.

[23] S. Tanabe, T. Ohyagi, N. Soga and T. Hanada, *Phys. Rev. B* **46**, (1992) 3305-10.

[24] S. Tanabe, K. Hirao and N. Soga, *J. Non-Cryst. Solids* **142**, (1992) 148-154.

[25] J.R. Morgan, E.P. Chock, H.D. Hopewell, M.A. El-Sayed and R. Orbach, *J. Phys. Chem.* **85**, (1981) 747-751.

[26] J.M. Pellegrino, W.M. Yen and M.J. Weber, *J. Appl. Phys.* **51**(12), (1980) 6332.

[27] T. Miyakawa and D.L. Dexter, *Phys. Rev. B* **1**(7), (1970) 2961-69.

[28] C. Kittel, *"Introduction to Solid State Physics"*, (6th ed. John Wiley & Sons, Inc. NY, 1986) p.101.

[29] C.B. Layne, W.H. Lowdermilk and M.J. Weber, *Phys. Rev. B* **16**(1), (1977) 10-20.

SUMMARY

In the present thesis, the structure and optical properties of rare earth containing glasses are investigated.

In Chapter 1, the fundamental background for rare earth research was reviewed. The theories of radiative and nonradiative transition of trivalent rare earth ions are shown. These relaxation phenomena dominate the optical characteristics. Also the background for the Mössbauer spectroscopy on rare earth elements is revealed. The applicability of this spectroscopy to the local structure of rare earth ions in solids was discussed.

In Chapter 2, the results of ^{151}Eu Mössbauer spectroscopy for several oxides have been shown. The relationship between the isomer shift and the coordination number of Eu^{3+} ions or Eu-O bond length in several oxide crystals are clarified, where Eu^{3+} ions take 6- to 12-fold coordination. On these bases, this spectroscopy was applied to europium containing aluminosilicate glasses, in which the coordination number change from 8 to 12 with decreasing optical basicity of the host composition. In order to investigate the structure and lattice dynamic properties of europium aluminosilicate glasses, the compositional dependences of molar volume and sound velocities were obtained. From the chemical shift of Al$K\alpha$ band emission spectra and the isomer shift of ^{151}Eu by Mössbauer spectroscopy, it was found that the coordination number of Eu^{3+} ions was twelve, while the average coordination number of Al^{3+} ions was almost five in these glasses. By introducing Eu_2O_3, the packing of constituent ions was strongly enhanced and the elastic moduli increased in this sys-

tem. The compositional dependence of the molar volume and elastic moduli were explained by these states of high CN for Eu^{3+} and low CN for Al^{3+} ions compared with those in the corresponding M_2O_3 crystals.

In Chapter 3, the local structure and multiphonon relaxation mechanisms of Eu^{3+} ions in several oxide, fluoride and fluorophosphate glasses were discussed. The phonon sideband measurements have been revealed to be effective to get the information about the local vibrational mode contributing to the multiphonon relaxation of rare earth ions in glass.

The phonon sideband of Eu^{3+} associated with the $^5D_2$<-$^7F_0$ transition was investigated for the B_2O_3-Na_2O glasses doped with 1 mol% Eu_2O_3. The phonon mode coupled with Eu^{3+} ions in the glasses, assigned to those in IR or Raman spectra, was almost consisting of $B\text{-}O^-$ or B-O stretching vibration of BO_3 units and vibrations of BO_4^- units in tetra- and diborate groups. Moreover, the electron-phonon coupling strength of each borate group was found to be influenced not only by its fraction present in glasses but also by the site selectivity of Eu^{3+} ion to them. This discrepancy could be interpreted in terms of the different chemical affinity of groups and site-preference of Eu^{3+} ion.

In addition to the glasses, a single crystal and an amorphous solid of $EuAl_3(BO_3)_4$ were prepared and their fluorescence properties were compared each other. The $^5D_0$ -> $^7F_0$ transition in the amorphous state, which is forbidden for Eu^{3+} ions at D_{3h} symmetry in the huntite crystal structure, became allowed and a decrease of the ligand field symmetry around Eu^{3+} ion was suggested with the glass formation. The results of ^{151}Eu Mössbauer

effect and Al$K\alpha$ emission spectroscopy showed that the coordination number of Eu^{3+} ions increased from 9 to 12 and that of Al^{3+} ions decreased from 6 to 4 by glassification. The increase of the linewidth of both the fluorescence and Mössbauer spectra could be attributed to the site variation and ligand asymmetry of Eu^{3+} ions in the glass of this system.

As a typical host of laser materials, fluorophosphate glasses were prepared in the system of AlF_3-$AlPO_4$-EuF_3-MF_2 (M = Ca,Ba) and the compositional dependences of Eu^{3+}-fluorescence properties were investigated. It was found that with an increase of $AlPO_4$ content, the fluorescence intensities from Eu^{3+}:^5D_J(J=1,2,3) levels were decreased and the intensity ratio of ($^5D_0$ -> $^7F_2$) / ($^5D_0$ -> $^7F_1$) was increased. The local structure and multiphonon relaxation mechanisms were investigated by measuring the ^{151}Eu Mössbauer effect and phonon sideband spectra associated with the $^5D_2$<-$^7F_0$ transition. It was concluded that the P-O^- stretching mode with the highest phonon energy contributes to the rapid multiphonon relaxation of ^5D_J states and that the covalency and asymmetry of Eu^{3+}-ligand field were increased by the addition of $AlPO_4$ to the present glasses.

In Chapter 4, the upconversion characteristics of Er^{3+} ions in several glasses were discussed in terms of the nonradiative loss due to the multiphonon relaxation. The upconversion efficiency of fluorophosphate glasses are found to be lower than that of fluoride glasses owing to the coupling of P-O stretching vibration with high phonon energy. The temperature dependence of upconversion intensity was large for the fluoride system, while it was small for the fluorophosphate system. These tenden-

cies could be well explained by considering the multiphonon decay rate of the Er^{3+} intermediate level and its temperature dependence, which are functions of the phonon energy of the host and the energy gap to the next-lower level of Er^{3+}. These differences in local structure and multiphonon mechanisms were confirmed by the results of ^{151}Eu Mössbauer spectroscopy. It is concluded that the the efficiency of the upconversion process is dominated by the lifetime of the intermediate level, which is influenced by the phonon mode locally coupled to the rare earth ion in the glass.

Owing to their low phonon energy, the efficient upconversion phenomena of Er^{3+} have been also reported for the first time in heavy metal oxide glasses with the AlGaAs/GaAs semiconductor laser pumping. The possibility was shown that these oxide glasses can become one candidate for a high temperature upconversion device.

In Chapter 5, the upconversion mechanisms of Er^{3+} doped and Tm^{3+} doped fluoride glasses were investigated by using tunable dye laser. In the Er^{3+} doped glass, the energy transfer between the $^4I_{11/2}$ levels is found to be the controlling mechanism for the green upconversion. The upconversion characteristics were investigated in the excitation wavelength range of 0.62~0.69μm. The power dependence of 0.55μm emission due to $^4S_{3/2} \rightarrow {}^4I_{15/2}$ obeyed quadratic law, indicating two-step process. The excitation spectra of upconversion and infrared Stokes emissions were compared and both of them had a similar profile to that of $^4F_{9/2} \leftarrow {}^4I_{15/2}$ absorption. It was concluded that the excited state absorption from any ^4I_J level (J = 9/2, 11/2, 13/2) was not

the main mechanism. From the temperature dependence of efficiency, the energy transfer between $^4I_{11/2}$ excited Er^{3+} ions was found to be the controlling process to upconversion of this glass.

On the other hand, in the Tm^{3+} doped glass, the excited state absorption was found to be the main process leading to UV and blue upconversions. The dependences of fluorescence intensity on the incident excitation power were found to be quadratic both for 0.36 and 0.45μm emissions, which originate from $^1D_2$, and also for 0.48μm emission from $^1G_4$, indicating two step excitation mechanisms. While the excitation profile for Stokes emission was varied in the same way as that of the absorption spectra of $^3F_{2,3}$ <- $^3H_6$ transition, those for upconversion emissions shifted to higher energy side. The mechanisms leading to these upconversion emissions are clarified to be *ESA* for both levels and the process to $^1D_2$ level is that from $^3H_4$, while that to $^1G_4$ is from $^3F_4$ after nonradiative decay from the upper levels.

ACKNOWLEDGMENTS

The present work has been carried out under the direction of Professor Naohiro Soga, at Faculty of Engineering in Kyoto University.

The author expresses his sincere gratitude to Prof. N. Soga for his continuous guidance, valuable advice and encouragement throughout this work. Also helpful advice, discussion and encouragement by Prof. T. Hanada and Prof. K. Hirao is gratefully appreciated.

He is grateful to Prof. S. Sakka and Prof. T. Kokubo for their guidance and discussion in preparing the present thesis.

Continuous cooperation and helpful discussion by Prof. Y. Isozumi at Radioisotope Research Center in Mössbauer effect measurement is appreciated.

He also thanks Dr. K. Nakanishi, Dr. K. Tanaka and all the students in Soga laboratory for their helpful discussion and assistance in the present work.

Finally hearty thanks are made to his parents and wife for their cooperation and encouragement.

Setsuhisa TANABE